PhD Program in Translational and Molecular Medicine

DIMET
(XXVIII cycle)

University of Milano-Bicocca

School of Medicine and School of Science

Cell signaling in high risk childhood B cell precursor acute lymphoblastic leukemia: high-throughput dissection and targeting strategies

Coordinator: Prof. Andrea Biondi

Tutor: Prof. Andrea Biondi

Co-tutor: Dr. Giuseppe Gaipa

Jolanda Sarno

Matr. 744675

TABLE OF CONTENTS

Chapter 1

General introduction

1. Childhood acute lymphoblastic leukemia

1.1 Molecular basis of leukemia

Leukemia is a malignant disease arising from a clone of over-proliferating cells, arrested at some stage of lymphoid or myeloid differentiation, that occupy and replace the normal bone marrow cells. This results in a dysfunction of the bone marrow in the production of erythrocytes, neutrophils and platelets responsible for anemia, frequent infections, fatigue, weakness and bleeding that represent the most warning signs of leukemia.

Leukemias are classified as lymphoid versus myeloid depending on the lineage of origin of the malignant cell clone (commonly called as blasts) and acute versus chronic in accordance to the velocity of proliferation and invasion of blast cells. The majority of childhood leukemia cases are acute and the most common subtype is the acute lymphoblastic leukemia (ALL) accounting for 25% of all childhood cancers with a peak incidence in patients aged 2-5 years[1,2].

ALL, like cancer in general, probably arises from interactions between exogenous or endogenous exposures, genetic susceptibility and chance. Nowadays the challenge remains to identify the most relevant exposure and inherited genetic variants and understand in which way these factors contribute to the multistep natural history of ALL[3].

ALL is a heterogeneous disease with biologically and clinically distinct subsets identified by morphological, immunophenotypic and cytogenetic and molecular biology analysis. Based on the presence of immunological lineage associated markers (cluster differentiation or CD markers) ALL is distinct in two main subgroups: B-lineage and T-lineage ALL.

Approximately 85% of childhood ALL arise from precursor of B-cell lineage (BCP-ALL) that is further classified according to the corresponding differentiation markers expressed by the leukemic clone in:

- Early pre-B precursor ALL or pro-B ALL (B-I): CD19+/CD10-/HLA-DR+/SmIg-
- Common ALL (cALL) (B-II): CD19+/CD10+/HLA-DR+/SmIg-
- Pre-B ALL (B-III): CD19+/CD10+/HLA-DR+/SmIg+ (κ- e λ-)
- Mature B ALL (B-IV): CD19+/CD10+ or CD10-/HLA-DR+/SmIg+ (κ+ o λ+)

However, around 15% of childhood ALL have a T-cell origin and they are classified, based on maturation states of T lymphoblasts, as:

- Pro-T ALL (T-I): cyCD3+/CD7+
- Pre-T ALL (T-II): cyCD3+/CD7+/CD2+ e/o CD+ e/o CD8+
- Intermediate T-ALL (T-III): cyCD3+/CD7+/CD2+/CD1a+
- Mature T ALL (T-IV): CD3+/CD7+/CD2+/CD1a

Seventy-five percent of BCP-ALL cases harbor genetic alterations abnormalities detectable by conventional cytogenetic approach that are divided into numerical alterations, such as hyperdiploidy or hypodiploidy, and structural alterations including chromosomal rearrangements resulting in translocations and/or deletion and aberrant expression of proto-oncogenes[4,5]. The frequencies of these alterations differ in children compared to adults and they have been shown to influence aggressiveness of leukemic cells and response to therapy[1,3]. Chromosomal alterations are acquired early in the leukemogenesis driving transcriptional and epigenetic deregulation and aberrant self-renewal. These lesions together with secondary lesions are able to disrupt the normal lymphoid development resulting in the arrest of lymphoid maturation.

Additional genetic alterations target multiple cellular pathways, including cell-cycle regulation, tumor suppression, and chromatin modification. Together, these events result in the proliferation and establishment of the leukemic clone. At diagnosis ALL samples are commonly clonally heterogeneous, and genetic alterations in minor clones may confer resistance to therapy and promote disease relapse[6].

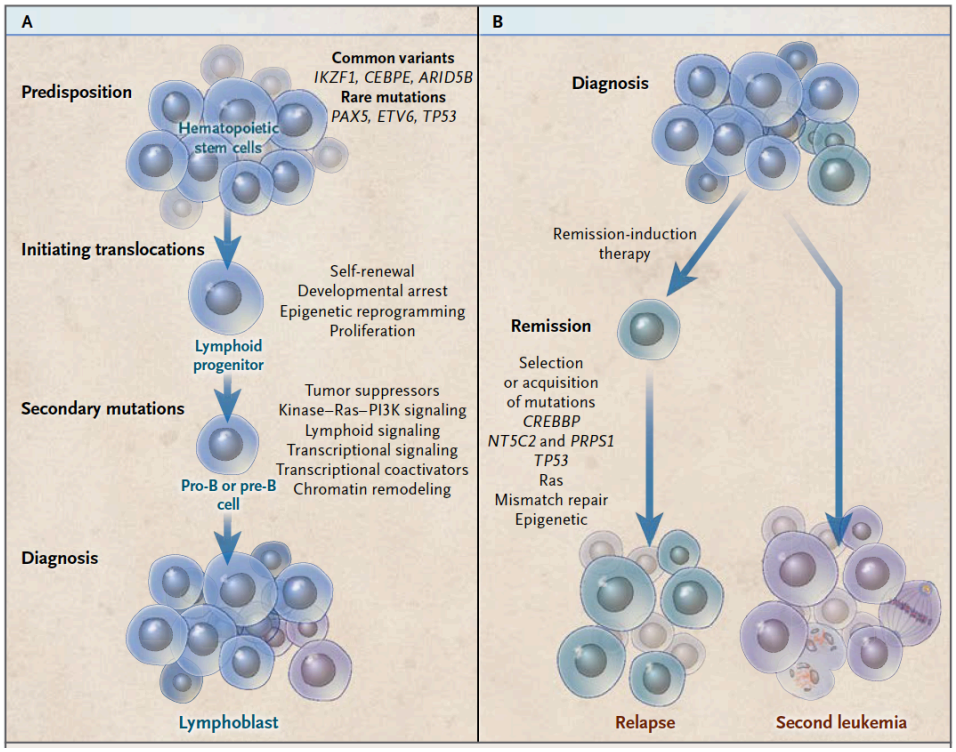

Figure 1. **Proposed sequential acquisition of genetic alterations contributing to the pathogenesis and relapse of ALL**. In panel A is shown how either common variants or rare mutations can confer a predisposition to ALL. Initiating translocation occurs in lymphoid progenitor; when cells acquire also secondary mutations in specific regulatory pathways the leukemia is clinically evident. As shown in panel B, although the remission-induction therapy induce a massive cell death, in same cases leaving sub-clones harbor or acquire mutations conferring resistance to therapy and relapse of disease. Less commonly, relapses clones did not share the same genetic background of the diagnosis, giving a second leukemia genetically different from the first one[7].

1.2 Genetic alterations in B-cell leukemia

Recurring chromosomal rearrangements involve genes that regulate normal hematopoiesis and lymphoid development. The most common translocations are listed below:

- t(12;21)(p13;q22) is present in about 25% of BCP-ALL and results in *TEL-AML1* fusion gene. *TEL*, a member of the *ETS* family of transcription factor genes, is required for the homing of hematopoietic progenitor cells to the bone marrow; *AML1*, encode for the α subunit of core binding factor, a master regulator of the formation of the hematopoietic stem cell[1]. The effect of the *TEL-AML1* gene fusion is the inhibition of the transcriptional activity that is normally initiated when AML1 binds DNA, resulting in an alteration of the self-renewal and differentiation capacity of hematopoietic stem cells. Nevertheless this alteration is associated with a favorable outcome.
- t(1;19)(q23;p13) is present in about 5% of patients and consist in the fusion of *TCF3* (E2A) gene with *PBX1* gene. *TCF3* encodes two transcription factors, E12 and E47, and PBX1 encodes a member of homeodomain proteins. Since both of them are required for lymphoid development, the *TCF3-PBX1* fusion protein interferes with the hematopoietic differentiation. This alteration in pre-B ALL seems not to have a prognostic impact[5].

- t(9;22)(q34;q11) occurs in about 3-5% of childhood BCP-ALL and generates the *BCR-ABL1* fusion gene, also known as Philadelphia (Ph) chromosome. The resulting *BCR-ABL1* fusion has two variants due to two breakpoints areas on *BCR* gene. In both cases the fusion of the BCR signaling protein with the ABL tyrosine kinase results in a constitutive tyrosine kinase activity activating multiple signaling pathways, increasing cell proliferation and deregulating cell differentiation and adhesion[5,8]. Prognosis for this subtype of patients with standard chemotherapy is really poor[9] but, thank to recently advance in this field, the administration of specific tyrosine kinase inhibitors (TKIs) has strongly improved the outcome of Ph-positive leukemia patients to a 4-year event free survival (EFS) rate up to 80%[10].
- t(4;11)(q21;q23) is the most common translocation of the *MLL* gene that generate the *MLL-AF4* fusion gene. In general rearrangements of the *MLL* gene at 11q23 are found in 75% infant ALL (patients younger than one year), 3% of childhood ALL and 7% of adult ALL. More than 70 different translocations involved the *MLL* gene, that encode for a histone methyltransferase involved in the epigenetic regulation of blood-cell development. For this reason the resulting fusion proteins mediate an aberrant self-renewal of hematopoietic

progenitors[5,7]. The *MLL* prognosis is poor in infant patients, but better in childhood ALL[11].

The advent of genome-wide profiling of DNA and RNA and next-generation sequencing (NGS) technologies have greatly increased the knowledge of the genetic alterations present in leukemic cells helping to identify new molecular subtypes that can be used to refine risk stratification schemes in the near future.

In this contest deletions of the *IKFZ1* gene, that encodes for the transcription factor Ikaros, was found deleted in 76% of childhood Ph+ BCP-ALL and it is correlated with a poor prognosis[12]. Furthermore the *PAX5* gene, located on the chromosome 9, is also mutated in about 30% of BCP-ALL even though is not associated with an adverse outcome[13]. *PAX5* (9q13), a member of the paired box gene family, encodes a transcription factor necessary for the normal hematopoietic development. This gene is the target of broad or focal deletions, sequence mutations and translocations, which results in haploinsufficiency, expression of truncated transcripts and chimeric fusion proteins.

Patients bearing deletion of *ERG* gene, located at 21q22, represent a recently recognized BCP-ALL subtype. This alteration is present in about 5% of patients and it is associated with a favorable outcome suggesting the possibility to use it as a good prognostic marker. Moreover, *ERG*

deletions are able to neutralize the negative prognostic impact of *IKZF1* alterations[14].

Noteworthy are also alterations in the *CRLF2* gene that are responsible of its overespression, present in about 7% of BCP-ALL cases, 14% of high-risk patients and at least 50% of Down syndrome-associated ALL patients[15]. *CRLF2*, also known as thymic stromal lymphopoietin protein receptor (TSLPR), is located in the pseudoautosomal region 1 (*PAR1*) of chromosome Xp22.3/Yp11.3 and encodes for one subunit of the heterodimeric receptor of the cytokine TSLP.

Recently a new subgroup of BCP-ALL has been described as *BCR-ABL1*-like, or Philadelphia chromosome-like ALL (Ph-like) ALL. It accounts for about 10-15% of childhood ALL and about 30% of adolescent and young BCP-ALL. Patients with Ph-like ALL even though they do not have *BCR-ABL1* fusion protein expressed from the translocation t(9;22), they have a gene-expression profile similar to that of patients with BCR-ABL1 ALL[16]. In particular this subtype is characterized by abnormalities in B-cell development genes suggesting a defective pre B cell receptor (pre-BCR) signaling pathway. As for Ph+ ALL, Ph-like ALL patients have a high prevalence of *IKZF1* alterations as well as abnormalities in B-cell development genes as *TCF3, EBF1, PAX5* and the pre-BCR surrogate light chain VPREB1[16]. In addition also the amplification of chromosome 21q21-q22 (iAMP21), which is known to be associated with poor outcome, have been reported in these patients although at lower

incidence. Roberts et al. recently identified other genetic alterations, which lead to activated kinase and pre-BCR signaling, including overexpression of *CRLF2* (present in about 50% of Ph-like ALL), mutations in *JAK1/2* genes[17], rearrangements of erythropoietin receptor (*EPOR*), activating mutation of interleukin 7 Receptor (*IL-7R*) and *FLT3*, a receptor tyrosine kinase required for the hematopoietic stem cell development[17]. Overall these aberrations cause, by different mechanisms, aberrant activations of several signaling pathways, such as RAS and JAK/STAT, involved in the leukemic transformation of the normal bone marrow cells, suggesting the possibly use of specific TKIs in addition to the conventional chemotherapy for this subgroup of high-risk patients.

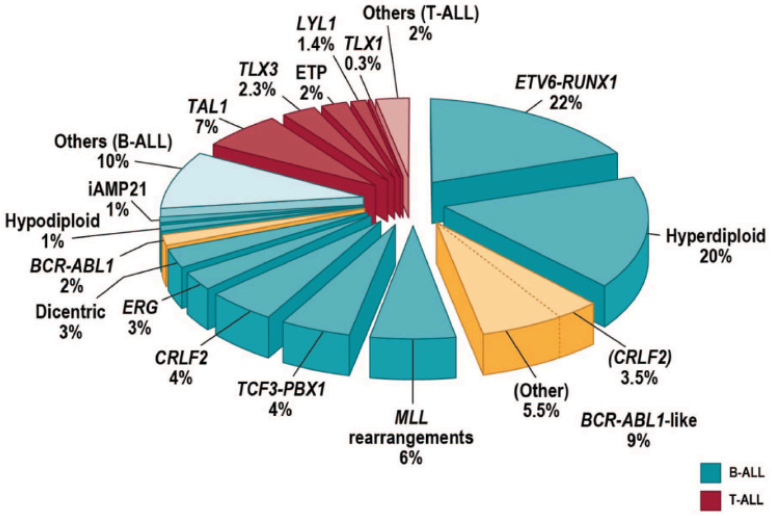

Figure 2. Frequencies of cytogenetic subtypes of pediatric ALL

1.3 Signaling pathways in precursor B-cell

B-cell development

Pluripotent stem cells in the bone marrow (and fetal liver), generally called hematopoietic stem cells (HSCs), give rise to all lineages of blood cells, including cells of the lymphocyte lineage. HSCs mature into common lymphoid progenitors (CLPs) that can give rise to B cells, T cells, natural killer (NK) cells and some dendritic cells (DCs). During their maturation, cells of the B lymphocyte lineage go through distinguishable stages, each characterized by distinct cell surface markers and a specific pattern of Ig gene expression.

The earliest B-lineage cells are known as pro-B cells, progenitors cells with limited self-renewal capacity. Pro-B cells do not produce Ig, but they can be distinguished from other immature cells by the expression of B lineage-restricted surface molecules such as CD19 and CD10. Recombination-activating (*RAG*) gene are first expressed at this stage and the first recombination of Ig genes occurs at the heavy chain locus: D_H to J_H joining at the early pro-B cell stage is followed by V_H to DJ_H joining at the late pro-B cell stage. Productive VDJ_H joining leads to the expression of an intact μ chain, which is the hallmark of the next main stage of development, the pre-B cell stage. The μ chain in large pre-B cell is expressed in small amount at the cell surface in combination with a surrogate light chain as part of a pre-B cell receptor (pre-BCR); this permit to the large pre-B cells to divide further before giving rise to small

pre-B cells, in which light-chain rearrangements proceed.

Once a light-chain gene is assembled and a complete IgM molecule is expressed on the cell surface, the cell is defined as an immature pre-B cell. All development up to this point has taken place in the bone marrow and is independent of antigen. At this stage cells are subject to selection for self-tolerance and ability to survive in the periphery and cells that pass this step undergo further differentiation to become mature B cells expressing IgD in addition to IgM.

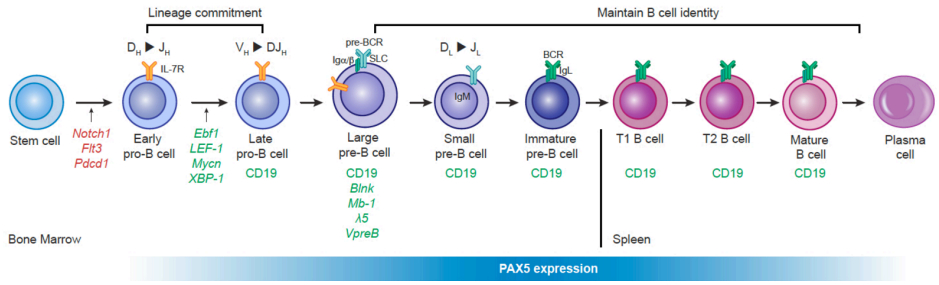

Figure 3. B-cell differentiation and *PAX5* expression. In the bone marrow development progresses from stem cells through the pro-B cell, pre-B cell and immature pre-B stages. During these stages VDJ rearrangements at the Ig locus result in the generation and surface expression of the pre-BCR and its signaling is necessary for proliferation and further differentiation, resulting in a mature BCR. Cells that complete successfully this checkpoint leave the bone marrow and proceed through two transitional stages (T1 and T2) before becoming a mature follicular B-cell or marginal-zone B cell. D, diversity; J, joining; V, variable; SLC, surrogate light chain. Factors activated by PAX5 are listed in green, while factors inhibited are in red[18].

Signaling pathway in normal and malignant B-cell

During B cell development, the cell fate is controlled by two different signaling pathways involved in the control of survival, proliferation and differentiation of B-cell that are the ones downstream the IL-7 receptor and the pre-B cell receptor.

IL-7R is composed by the common-γ chain (γc) and IL-7Rα chain, which confers specificity for IL-7; the latter is also a component of the thymic-stromal lymphopoietin receptor (TSLPR). The increased expression of the α chain of the IL-7R demarks the passage from CLPs to the lymphoid-primed multipotent progenitors (LMMPs). Has been demonstrated in mice that mutation of the gene encoding IL-7Rα severely impairs B cell lymphopoiesis[19]; in this mice only few B cells mature and populate the periphery, supporting the hypothesis that IL-7 is required for proper cell proliferation during early B cell development. Of note, most of the mice that have enhanced IL-7R signaling develop pro and pre-B cell tumors. The IL-7R pathway begins by the binding of the IL-7 to its cognate receptor, which basally is completely inactive. Cytokine binding induces a conformational change that induces receptor dimerization. As a consequence, JAK3, pre-bound to the cytoplasmic region of the receptor, become activated, leading to cross-phosphorylation and receptor tyrosine phosphorylation, thus creating binding sites for STAT5. Phosphorylation leads to STAT5 homodimerization, translocation and retention in the nucleus where it acts as transcription factor.

This pathway has a central role in the signaling of cytokines by regulating cell proliferation, survival, differentiation and immune response. Constitutively active cytokine receptors lead to permanent signaling. Thus, constitutively active STAT5 in the nucleus overcomes negative regulatory mechanisms, eventually leading to oncogenesis[20].

Several experiments indicate that there is intensive crosstalk between the signaling pathways that are triggered by the pre-BCR and IL-7R. Expression of the pre-BCR by pro-B cells upregulates IL-7R expression on the cell surface, thereby increasing the responsiveness of these cells to IL-7. This results in the selective expansion of pre-BCR positive cells in conditions in which IL-7 concentration is low. At the same time, however, the pre-BCR also induces the differentiation of pre-B cells into a state in which they have reduced IL-7 responsiveness, which probably limits the expansion of pre-B cells during B-cell development *in vivo* [21,22].

The pre-BCR is formed by the coupling of μ heavy chain with surrogate light chain components VpreB (Vpreb1) and λ5 (Igll1). The pre-BCR is present on the surface of the pre-BI cells. The extracellular part of the pre-BCR is linked to two signaling chains, Igα (CD79a) and Igβ (CD79b), which contain immunoreceptor tyrosyne-based activation motifs (ITAM). The pre-BCR serves as an immunological synapse where the Igα and Igβ signaling chains serve as docking sites to assemble and activate the components of the pre-BCR signaling cascade. The pre-BCR has a dual function: it is responsible for both proliferation and survival, and growth

arrest and differentiation. Therefore, it serves as a checkpoint in early B cell development, it decides whether the cell should survive for further differentiation or undergo apoptosis. If the pre-BCR does not carry a functional heavy chain rearrangement, it is eliminated by apoptosis and this phenomenon is termed as negative selection. If the rearrangement is functional, the cell survives and the pre-BCR signals for proliferation and differentiation[23]. As shown in Figure 4 (panel A) one of the main proteins that docks at the immunological synapse and mediates the dual function of the pre-BCR is the spleen tyrosine kinase (SYK). SYK and Bruton tyrosine kinase (BTK), which is activated downstream of PI3K, phosphorylate the B cell linker protein BLNK, which can regulate the cell cycle both positively (through the activation of the RAS-ERK pathway) and negatively. In the case of negative regulation, BLNK inhibits the activation of AKT, thereby promoting the nuclear translocation of forkhead box protein O1 (FOXO1). FOXO1 targets the transcriptional repressor B cell lymphoma (BCL-6), which inhibits the transcription of cyclin2 (CCND2) and MYC or can directly inhibit STAT5.

Taken together, the signaling molecules at the pre-BCR checkpoint maintain the balance between negative selection of non-functional B cells (apoptosis) and leukemic transformation. As shown in Figure 4 (panel B), in the pre-B cells from patients with B-ALL, increased paracrine and autocrine IL-7 stimulation enhances the activation of PI3K and JAK3-STAT5, which leads to the survival and the proliferation of these cells.

Moreover inactivating BLNK mutations release the inhibition of JAK3 and AKT leading to a survival and proliferation of the leukemic cells. Hyperactivation of the RAS-ERK pathway can occur as a result of gain-of-function mutations in RAS or SHP2 proteins [23].

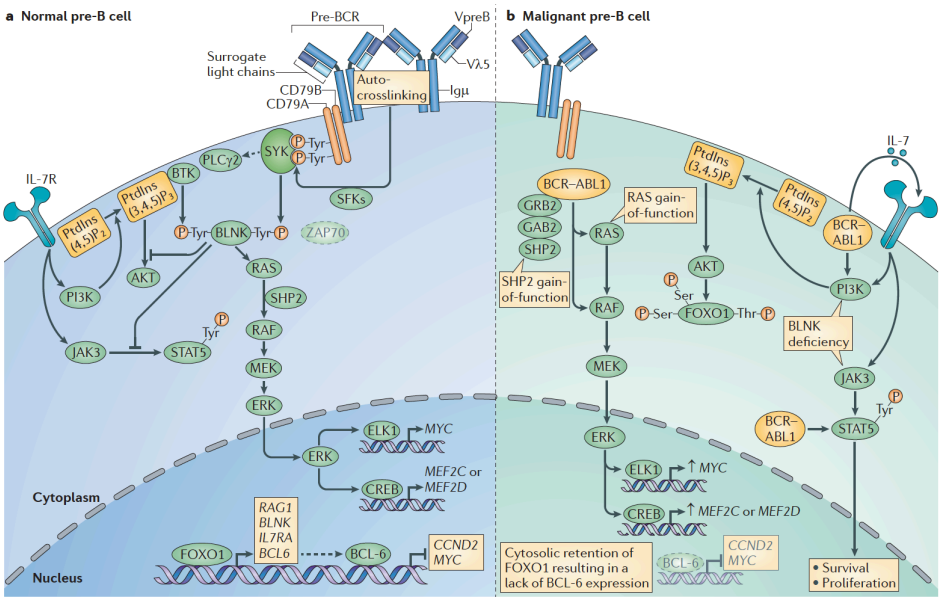

Figure 4. Pre-BCR signaling in normal and malignant B-cell[23]

In the panel A is shown the early pre-B cell proliferation and survival pathway in a normal pre-B cell. It is initially driven by IL-7R signaling, which includes the activation of PI3K/JAK3/STAT5 pathways. In the panel B are represented the mechanisms arising in pre-B cells from patients with B-ALL.

2. Prognostic markers and patients stratification

Current clinical trials for children with BCP-ALL are based on risk stratification of patients using several parameters such as clinical features, cytogenetics and individual response to treatment.

2.1 Clinical features

The patient's age and initial white blood cells (WBC) count are predictive of outcome, with older age or higher WBC portending a worse prognosis. In general patients are defined as "standard risk" whether the patient's age is between 1 and 10 and the WBC is lower than 50.000 mm^3; in the other hand "high risk" defined patients are older than 10 years and/or initial WBC ≥ 50.000 mm^3. Infants younger than 1 year are a special subgroup with worse outcome.

2.2 Biologic and genetic features

As described before several genetic alterations are associated with the outcome in children with ALL. In particular high hyperdiploidy and the translocation t(12;21) (*ETV6-RUNX1*) are associated with a favorable outcome. Hypodiploidy with less than 44 chromosomes[24], *MLL* rearrangements[11,25], *BCR-ABL1* ALL[26], Ph-like ALL[17], *CRLF2* rearrangement[15] and intrachromosomal amplification of chromosome 21[27] are associated with high risk clinical features and poor outcome.

2.3 Response to therapy

The time required to eliminate the bulk leukemic population to undetectable levels is the single most powerful prognostic factor in ALL in children[28]. The blast clearance can be monitored by the assessment of the Minimal Residual Disease (MRD) measured by using real-time quantitative polymerase chain reaction (RQ-PCR) amplification of fusion transcript, Immunoglobulin (Ig) and T-cell receptor (TCR) gene rearrangements (that are unique to an individual patient) or by flow cytometric (FCM) detection of leukemia-associated immunophenotypes.

Clonal rearrangements of immunoglobulin and TCR genes occur in about 90% of patients with ALL and result in junctional regions that can be considered as fingerprint clone-specific sequences[29]. Although rearrangements of Ig and TCR genes are clone-specific, they are not directly linked to the oncogenic process; for this reason to prevent false-negative results the monitoring of MRD is done by using two or more independent Ig/TCR targets. PCR-based MRD monitoring has a high sensitivity allowing the detection of one leukemic cell in 100.000 normal bone marrow cells (or 0.001%) [30].

Leukemia-associated immunophenotypes can be assessed and quantified by using multiparametric flow cytometry in order to distinguish leukemic lymphoblasts from their normal counterpart[31]. Has been widely demonstrated that the MRD detection by flow cytometry is feasible, predictive of the outcome[32,33] and sensitive allowing the

detection of one leukemic cell in 10.000 normal bone marrow cells (or 0.01%). The major challenge nowadays is to reach the same sensitivity of the PCR-based technologies and a large number of centers are moving in this direction. Attempts to automate the interpretation of FCM-MRD data are now being made by different multicentric studies[33,34] (i.e. Euroflow Consortium) in order to find the best combination of markers that would make ALL cells more distinct from the normal bone marrow cells and also set up standardized protocols focused to the acquisition of a larger number of cells.

In the Associazione Italiana Ematologia Oncologia Pediatrica and Berlin-Frankfurt-Münster (AIEOP-BFM) clinical trials patients are stratified in 3 different risk groups: high, intermediate and standard. Patients are assigned to each specific risk group based on the prednisone response at Day 7, complete remission at Day 33, MRD levels at Day 33 and Day 78 and the presence of *BCR/ABL* or *MLL/AF4* fusion transcripts[35,36].

Standard risk (SR): Patients MRD negative at day 33 and day 78 time-points, evaluated by PCR on at least 2 markers. In case of unavailability of the PCR-MRD data, are considered SR patients with a FCM-MRD <0.1% at Day 15;

Intermediate risk (IR): Patients not classified as SR, and MRD < 10^{-3} at day 78;

High risk (HR): Patients with the following features: prednisone poor-responder (PPR), FCM-MRD ≥ 10% at day 15, PCR-MRD > 10^{-3} at Day 78, MLL/AF4 positive, hypodiploidy (<45 chromosomes).

Thereby patients with unfavorable risk receive more intense chemotherapy whereas those with good prognosis receive less or modified versions of the intensive treatment.

3. A new prognostic marker in precursor B-cell ALL

In the last decades steady progress in development of effective treatments has led to an elevated rate of success in treating this disease. To date, even thought about 75-80% of patients are cured, 25% of cases having a relapse has a survival probability of only 30%. Of note, more than 50% of relapses concern patients not classified in high-risk groups based on assessment of prognostic factors at diagnosis or on measurement of Minimal Residual Disease (MRD) emphasizing the need to identify new molecular prognosis factors able to recognize patients with high risk of relapse.

Recent studies indicated that the Cytokine Receptor Like Factor 2 (*CRLF2*) aberrations is one of the several abnormalities that characterize a high risk group of childhood leukemia amenable to targeted therapy[37].

3.1 The Cytokine Receptor Like Factor 2 (*CRLF2*) gene

CRLF2 gene is localized at the end of the petit arm of the chromosome X or Y (ChrX-1,314,890-1,331,616; ChrY-1,264,890-1,281,616; ENSG00000205755) in the Pseudoautosomal Region 1 (PAR1)[38]. Binding and cross-linking experiments demonstrated that the protein encoded by the *CRLF2* gene is the receptor for a recently described interleukin 7 (IL-7)-like factor, Thymic Stromal Lymphopoietin (TSLP)[39]. Most of type I cytokine receptor systems, require at least two distinct receptor chains for high affinity binding with the ligands and subsequent signal transduction. The heterodimeric complex formed by the CRLF2 subunit and IL-7Rα was demonstrated to be a functional receptor for TSLP[40]. CRLF2 itself has low affinity for TSLP but in combination with IL-7Rα generates high affinity binding for TSLP, called TSLPR, which triggers signaling transduction[39].

Expression and physiological role of TSLP

The TSLP gene is localized on chromosome 5q22.1 and encodes a 159 amino acid protein that shares only 43 % similarity between human and mouse[41]. TSLP was originally identified in the conditioned medium of a murine medullary thymic cell line; hence its name[42]. Its major sites of production are the lung, bronchial tree, intestine, and the skin[41] where TSLP mediates inflammatory and allergic reactions, and its main physiological role is thought to be protection from helminthic infections.

Increased TSLP levels are associated with airway inflammatory disease and atopic dermatitis[43]. Moreover, TSLP cytokine mediates also B-cell precursor proliferation and survival[40]. Demehri et al. showed that endogenously overexpressed or exogenous TSLP supplemented during neonatal hematopoiesis results in drastic expansion of peripheral pre-B and immature B cells, thus causing B-cell lymphoproliferative disorders[44]. Yet a potential secondary role for TSLP in lymphoid development was revealed by also analyzing its redundancy with IL-7. Another support for these findings came from Chappaz et al., who showed that transgenic expression of high levels of TSLP restored T and B lymphopoiesis in IL-7-deficient mice[45].

TSLP can execute its biological functions through its action on many different types of cells. TSLP can activate CD4+ T cells and CD8+ T cells in mice and induces B-cell proliferation and differentiation in humans[43,46].

It also enhances maturation and proliferation of dendritic cells and naive T-cells, respectively. It has also been shown to induce the release of T-cell attracting chemokines from monocytes. In combination with interleukin-1 and tumor necrosis factor, TSLP can stimulate the production of Th2 cytokines by human mast cells[47].

TSLPR signaling

The TSLP receptor is a heterodimer composed by the IL-7Rα and CRLF2 (or TSLPR) subunits. Studies have shown that stimulation of IL7R/TSLPR

complex by TSLP induces the phosphorylation and activation of Janus kinases (JAKs) proteins. Activated JAKs, in turn, by using their kinase activity are able to phosphorylate and regulate the activity of signal transducers and activators of transcription (STAT) proteins, mainly STAT5a/b. The activated STATs dimerize and translocate into the nucleus where they act as transcription factor regulating genes involved in proliferation, development and apoptosis[43,48]. Together with this canonical pathway, several other proteins such as AKT1, ERK1/2, JNKs, ribosomal protein S6 kinase and 4E-BP1 have also been shown to be activated on TSLP stimulation[49]. A recent proteomic study demonstrated that TSLP also signals through TEC and SRC family of non-receptor tyrosine kinases promoting in general the activation of dendritic cells, the stimulations of Th2 inflammatory responses and T cell lymphopoiesis and homeostasis[49,50].

Recent studies also show the involvement of the TSLPR signaling in the leukemogenesis caused by the inhibition of death-inducing factors (like BAX and BAD) and the activation of life-promoting factors (like MCL-1, BCL-2 and BCL-X_L)[51].

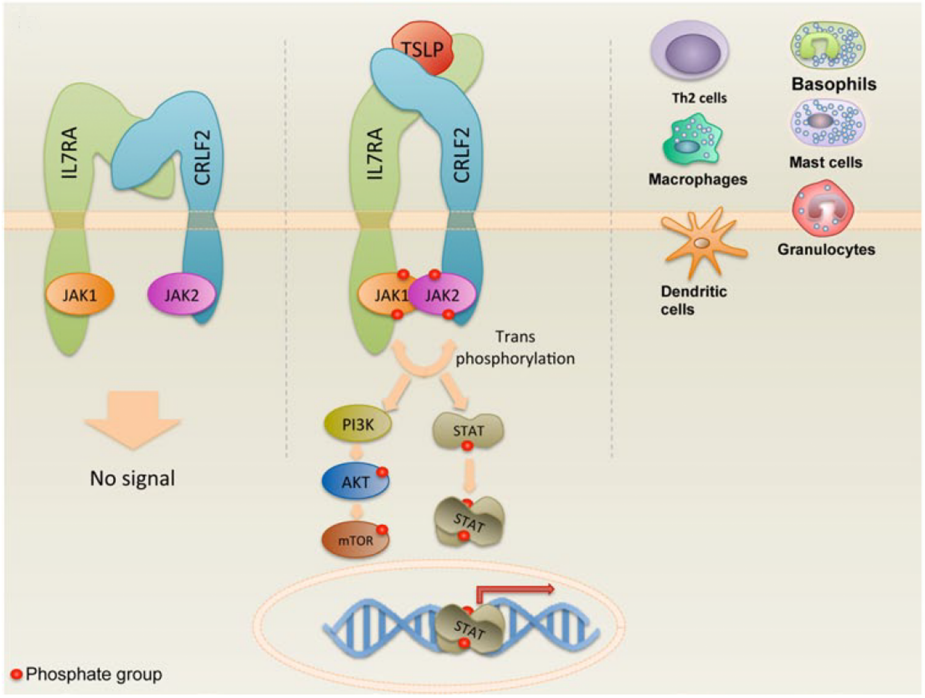

Figure 5. Signaling pathway of TSLP. Ligand binding of TSLP to the heterodimeric receptor IL-7Rα/CRLF2 induce the dimerization of the receptor subunits leading to phosphorylation of JAK1 and JAK2. Activated JAK1/2 kinases can both create a docking site for STAT proteins that dimerize and translocates to the nucleus where act as transcription factor or activate other pathways, like PI3K/mTOR pathway[51].

<u>*CRLF2* rearrangements (r) in BCP-ALL</u>

In the last years, four research group independently discovered the aberrant expression of *CRLF2* in BCP-ALL by using different methodologies[38,52–54].

Overexpression of *CRLF2* is present at different extent in several paediatric BCP-ALL patient's subgroups: up to 7% and 14% in standard-

risk and high-risk patients respectively[5], up to 50-60% in Down Syndrome-associated ALL (DS-ALL) patients[55] and up to 50% of BCR-ABL1–like (Ph-like) BCP-ALL[17].

It has been demonstrated that the overexpression of the *CRLF2* gene can occurs through different molecular alterations:

- Translocation of the Immunoglobulin Heavy Chain (*IGH@*) locus of chromosome 14 with the pseudoautosomal region 1 (*PAR1*) of chromosome X.

  The *IGH@* is a locus involved in several common translocations and rearrangements involving *IGH@* locus have been identified as a new cytogenetic subgroup in BCP-ALL, occurring predominantly among older children and young adults. Translocation of *CRLF2* with the IGH@ locus leads to expression of *CRLF2* via *IGH@* enhancer elements as the entire *CRLF2* gene has relocated to the chromosome 14[38,52].

- Interstitial deletion of the *PAR1* locus at Xp 22.3 or Yp 11.3. The region of the *PAR1* deletion involved at least five genes (*P2RY8, ASMTL, SLC25A6, IL3RA* and *CSF2RA*). The deletion juxtaposes the first non-coding exon of *P2RY8* gene to the first exon of *CRLF2*. *P2RY8* encodes a purigenic receptor (P2Y, G protein coupled, 8) that is expressed at high levels in many tissues, including leukemic cells. A single case of rearrangement of *P2RY8* to *SOX5* has been reported in primary splenic follicular lymphoma[56].

CRLF2 expression from this chimeric locus is driven by the constitutively active *P2RY8* promoter resulting in high expression of the chimeric transcripts *P2RY8-CRLF2*.

The frequency of translocations and deletions involving *CRLF2* that lead to *CRLF2* overexpression seems to be dependent on the cohort of samples studied. In unselected B-progenitor ALL cases, *PAR1* deletions are more common than *CRLF2* translocations (approximately 2:1). In contrast, the *IGH@CRLF2* alteration is much more frequent than *PAR1* deletions in a cohort composed of high-risk B-precursor ALL[15].

Recently, it has been reported that aberrant expression or activating mutations of a heterodimeric receptor components, may induce homodimer formation. Sequencing of *CRLF2* in childhood B-ALL specimens, including over-expressing cases, identified in some cases a point mutation changing the phenylalanine 232 to cysteine (also known as Phe232Cys or F232C). This mutation was also detected in several adult B-ALL patients that showed overexpression of *CRLF2*.

The *CRLF2* Phe232 residue is near the junction of the extracellular and trans-membrane domains. Mutations that introduce cysteine residues in this region of other receptors can activate signal transduction through intermolecular disulfide-bonded dimers. To confirm that *CRLF2* Phe232Cys promotes constitutive dimerization, Yoda and colleagues performed immunoblots in BaF3 cells expressing wild type (WT) *CRLF2* or

CRLF2 Phe232Cys. Under non-reducing conditions, the molecular weight of *CRLF2* Phe232Cys band, but not the WT band, was doubled, consistent with constitutive dimerization through the cysteine residues[53].

Moreover, it has been demonstrated that, CRLF2 may signal independently of TSLP as a homodimer when harboring the F232C mutation inducing a strong constitutive STAT5 phosphorylation. Anyway, cells expressing *CRLF2* Phe232Cys are still sensitive to enzymatic JAK inhibitors arguing that JAKs are involved in signaling even when *CRLF2* is mutated[53]. It is reasonable to hypothesize that *CRLF2* Phe232Cys could also interact with unknown partners to create a mutant heterodimer, leading to activation of signal transduction in absence of TSLP.

CRLF2 targeting in BCP-ALL

The JAK/STAT pathway represents one of the main pathway mediating cytokine receptor signaling and plays an important role in hematopoietic cell growth, proliferation, differentiation and survival[57]. A variety of hematologic malignancies are characterized by deregulated JAK/STAT signaling through several mechanisms, including JAK activating mutations, fusions and repression of negative regulators[58]. *CRLF2* gene rearrangements are responsible for a relevant part of these deregulations and although the role of *CRLF2* aberrations in the leukemic transformation are not clearly understood, in the last few years several groups hypothesized TSLPR targeting as a therapeutic strategy for this

subgroup of BCP-ALL.

Recently, several studies demonstrated an *in vitro* and *in vivo* efficacy of JAK1/2 inhibitor, Ruxolitinib, in *CRLF2* rearranged (*CRLF2r*) primary samples and cell lines[59,60] promoting the use of this specific kinase inhibitor (KI) to treat patients bearing an hyper-activation of the JAK/STAT pathway. Starting from these evidences, Ruxolitinib has been recently approved in a phase 2 study to treat patients with Ph-like ALL (ClinicalTrials.gov identifier NCT02420717), thus including also the *CRLF2r* ALLs.

Nevertheless, growing evidence of new resistance mechanisms to JAK inhibitors impairing their efficacy underline the need for innovative therapeutic strategies[61,62]. In this contest a type II JAK inhibitor, able to stabilize the kinase domain in an inactive conformation, has been recently investigated both *in vitro* and *in vivo* showing a strong anti-leukemic effect and also a synergic activity with dexamethasone, suggesting a promising combination strategy[62].

Meanwhile, other therapeutic approaches have been also investigated. Qin et al. developed T cells engineered with a Chimeric Antigen Receptor (CAR) targeting the TSLPR protein able to completely eradicate human *CRLF2* rearranged (TSLPR-overexpressing) ALL in multiple model systems including both cell lines and patient-derived xenografts (PDX)[63]. Vetter et al. developed and tested an inhibitory antibody directed against the TSLPR receptor in 10 different BCP-ALL primary samples demonstrating

an inhibition of TSLP-triggered cell proliferation and STAT transcription factor activation in one patient that showed a strong overexpression of the receptor[64]. Finally Raghunatan et al. investigated the possibility to use anti-CRLF2 antibody-armored biodegradable nanoparticles by setting the conditions necessary to the internalization of the nanoparticles that in future could be use for the treatment of CRLF2r ALLs[65].

3.2 JAK2 and IL7Rα: *CRLF2*-related partners in BCP-ALL

Russell and colleagues demonstrated the *CRLF2* overexpression was able to enhance the growth of pre-B cell *in vitro*, but when they silenced *CRLF2*, by using a short hairpin RNA (shRNA), the cells growth was only partially inhibited. These findings suggested that the *CRLF2* overexpression was not sufficient per se to transform cells, hypothesizing that cooperating mutations may be involved in the leukemic process[38].

Although *JAK2* mutations are most common in myeloproliferative neoplasms (MPNs), recently genetic and functional studies described a dysregulated JAK/STAT signaling in about 10% of patients with high-risk ALL and about 20% of DS-ALL patients[66,67]. In particular, an association of *JAK2* mutations (mostly the R683G mutation) with *CRLF2* rearrangements was described in about half of cases of DS-ALL[52,55].

A deletion in pseudokinase domain of *JAK2* called JAK2ΔIREED including R683 was initially discovered in a patient with DS and BCP-ALL[68].

Expression of JAK2ΔIREED in BaF3 cells induced constitutive activation of JAK/STAT pathway and growth factor-independent cell proliferation[68]. These *JAK2* mutants are associated with *CRLF2* rearrangements leading to overexpression of this receptor[52]. Mullighan and colleagues showed co-immunoprecipitation of human *CRLF2* and phosphorylated mutant *JAK2*, suggesting that these proteins physically interact[52]. Consequently, *JAK* gain-of-function mutants do not confer a transformed phenotype in the absence of a compatible cytokine receptor. This situation would be analogous to *JAK2* interaction with cytokine receptors in myeloproliferative neoplasms (MPN), in which MPN associated with *JAK2* mutants requires expression and interaction with a cytokine receptor to induce transforming signals[69]. To test this idea, several groups expressed *CRLF2* and *JAK2* Arg683 mutants in combination and alone in BaF3 cells, and determined the ability of these proteins to transform cells to cytokine independence. The combination of WT *CRLF2* and WT *JAK2* provided a growth advantage versus *JAK2* alone, and *JAK2* Arg683 mutation alone was insufficient to confer IL-3 independence[52,53]. Cells overexpressing *CRLF2* and expressing *JAK2* Arg683 mutants had constitutively phosphorylated JAK2 and induced activation of transforming signals in the presence or absence of IL-7R[52]. The reason why most *JAK2* Arg683 mutations are not transforming in absence of *CRLF2* overexpression is still unclear[52].

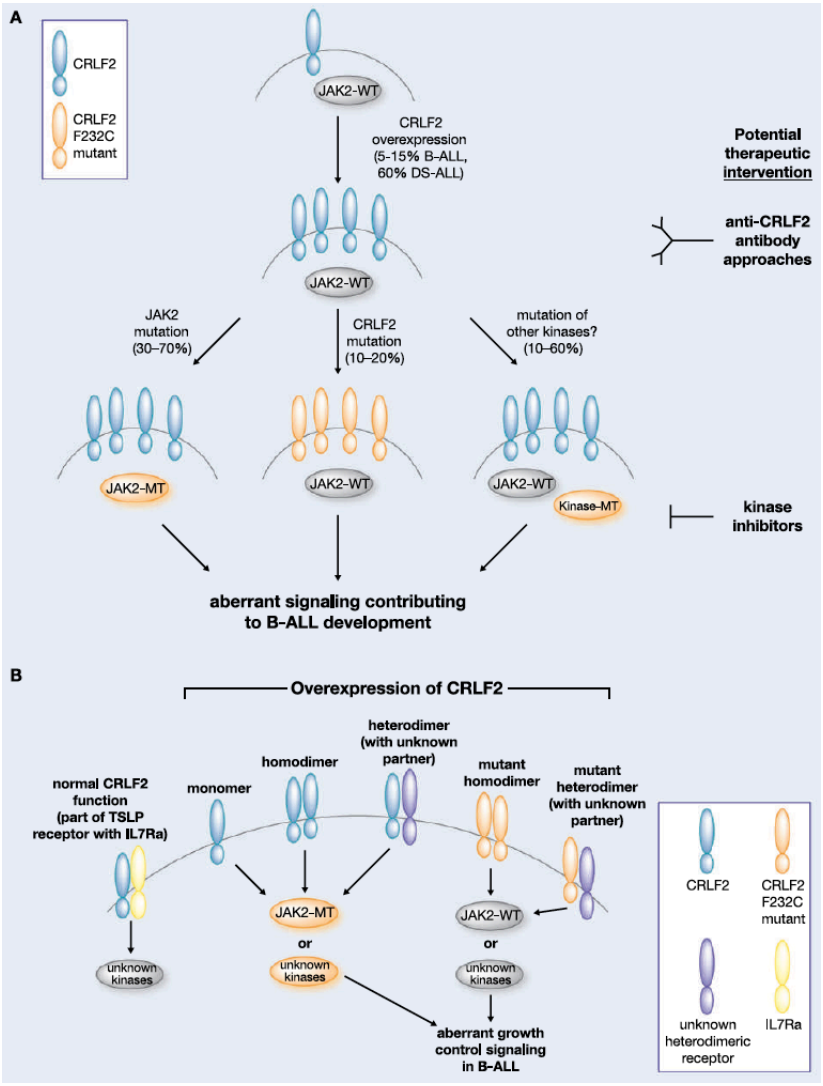

Figure 6. Aberrant CRLF2/JAK2 signaling in BCP-ALL. As shown in panel A, CRLF2 overexpression may lead to aberrant signaling through mechanisms involving alterations in JAK2, CRLF2 or other unknown kinases. In panel B is showed as the overexpression of CRLF2 may lead to aberrant signaling through monomeric, homodimeric or heterodimeric receptor configurations of wild-type (blue) or mutated (orange) CRLF2 protein, via activation of mutant (orange) or wild-type (grey) JAK2 or other kinases[40].

The overexpression of *CRLF2* can be associated with mutations in other genes such as IL7Rα[70]. CRLF2 dimerizes with IL-7Rα to form the receptor for TSLP. The IL-7Rα is a component of both the IL-7 and TSLP receptors and this suggests that the activation of these two receptors may trigger a common signaling pathway. Human IL-7 and TSLP use two different but complementary mechanisms to regulate peripheral T cell homeostasis. IL-7 has a potent and direct effect on T cells activation and displays a limited effect on dendritic cells, whereas TSLP predominantly acts on dendritic cells and has a moderate direct effect on T cells[71]. A dominant role of TSLP in human B-lymphoid development has been highlighted by a recent study showing that *CRLF2* and not IL-7R signaling induces proliferation of human fetal liver-derived multi-lineage progenitors, pro-B and pre-B cells. The authors observed that human CD34+CD38-HSCs display a short wave of precursor B-cell expansion with IL-7, followed by extended CRLF2 signaling that increases the absolute numbers of mature human B cells[46]. Both receptors activate STAT5, but they use two distinct mechanisms of activation since signaling from the IL-7 receptor is known to involve JAK1 and JAK3 and not JAK2, as happen with the TSLPR signaling. Somatic gain-of-function IL7Rα exon 6 mutations have been found in B and T-ALL. In most cases, these mutations introduce an unpaired cysteine in the extracellular juxtamembrane-transmembrane region and promote dimerization of the receptor, inducing constitutive JAK1 activation. In B-ALL these mutations are sometimes associated with

an overexpression of CRLF2 forming a functional, spontaneously activated receptor for TSLP[72] .

4. Novel therapeutic approaches in ALL

4.1 Tyrosine Kinase Inhibitors (TKIs)

The idea that "driver" lesions are correlated with the leukemogenesis, such as the aberrant activation of signaling pathways and various epigenetic modifications, have led to the discovery of novel agents that specifically target the mechanism of transformation. Recent discoveries in this field completely changed the story of specific subtypes of leukemia, as happened for the success of the "magic bullet" Imatinib in the treatment of chronic myeloid leukemia (CML) in adults[73–75].

Targeted therapies in pediatric leukemia are largely unproven to date[76], with some clear exceptions, like the tyrosine kinase inhibitors (TKIs) in BCR-ABL positive leukemia[77], and all-trans retinoic acid (ATRA) in acute promyelocytic leukemia (APML) with *PML-RARα* fusions[78].

Among the successful stories of targeted therapies in pediatric acute leukemia, noteworthy is the introduction of the TKI imatinib into upfront therapy for Philadelphia chromosome positive (Ph+) ALL patients. The Children's Oncology Group (COG) trial AALL0031 (2002–2006) incorporated imatinib into an upfront, intensive chemotherapy backbone for Ph+ ALL pediatric patients. Initial results from this trial

demonstrated a 3-year event-free survival (EFS) of 88%, doubling that of historical controls[77]. Retrospective analysis of patients who relapsed after treatment demonstrated remission reinduction rates similar to other high-risk non-Ph+ ALL patients treated on contemporaneous trials, allowing these patients to proceed to HSCT as salvage therapy[79]. Imatinib was FDA-approved for the treatment of Ph+ ALL in children in 2013. However, a well-known mechanism of resistance to TKI therapy is the outgrowth of resistant clones, often mediated through the development of point mutations in the kinase domain of ABL. In a recent review of 272 adult patients with relapsed Ph+ ALL, 70% harbored a kinase domain point mutation, including T315I, E255K and Y253H[80].

Dasatinib, a second-generation TKI, replaced imatinib in the most recent COG trial AALL1122 for Ph+ ALL patients, after COG phase I/II trial AALL0622 demonstrated good tolerability and rapid efficacy of dasatinib in combination with chemotherapy. There is in vitro evidence that dasatinib has superior central nervous system (CNS) penetration compared with imatinib[81], but although dasatinib is effective against many resistant mutations, there are still some exceptions, as the point mutation T315I[82]. For this reason has been developed also a third-generation TKI, ponatinib, that is clinically active against the T351I mutation even though toxicities of arterial thrombosis risk were documented[83], temporarily halting its development in clinical trials.

4.2 JAK/STAT inhibitors

Other classes of kinase inhibitors are being explored in adult Ph+ leukemia in an attempt to prevent the development of resistance, such as the Janus-associated kinase (JAK) inhibitor, ruxolitinib, in combination with nilotinib [ClinicalTrials.gov identifiers: NCT01702064 and NCT01914484].

The therapeutic use of Ruxolitinib could be expanded to all the diseases with aberrant activation of JAK signaling that have been widely described in the ALLs[84] and AML[85]. As demonstrated by Maude et al. xenograft models of eight cases of Ph-like ALL demonstrated decreased leukemic burden when treated with a selective JAK1/2 inhibitor, ruxolitinib, and six of these xenograft models harbored either a *JAK2* mutation or *CRLF2* rearrangement[86]. The remaining two Ph-like ALL patient samples contained some other activating signature of hyperactive JAK/STAT signaling, despite lacking a point mutation. This suggests that a JAK2 activation footprint may be more significant than the presence of a mutation, in terms of predicting response to JAK2 inhibition[76]. Interestingly, the mTOR pathway is also often aberrantly activated in Ph-like pre-B ALL patients, and single agent rapamycin demonstrated activity in all eight of these xenograft models[86]. Combining mTOR inhibitors with JAK2 inhibition, or combining JAK2 inhibition with cytotoxic chemotherapy, has not yet been studied in pediatric leukemia. The phase I COG study ADVL1011 recently investigated the safety and

dosing of single-agent ruxolitinib in children with relapsed/refractory hematologic malignancies and solid tumors, but results are still pending.
Although the in vitro and in vivo studies are promising trials are needed to determine whether identifying Ph-like patients and incorporating targeted TKIs into therapy will improve outcomes in this patient population.
However, as for Imatinib, also Ruxolitinib resistance mechanisms have been investigated[62]. This led several groups to pursue alternative strategies, such as HSP90 inhibitors[87] or combination of type I JAK2 inhibitor with additional agents[88]. Drug discovery efforts led to the identification of CHZ868, a type II JAK2 inhibitor that potently blocks JAK2 signaling in vitro and in vivo without induce toxicity in mice[62]. This new agent is able to stabilizes and locks JAK2 in the inactive conformation, preventing an hyper-phosphorylation (responsible for the Ruxolitinib resistance) and blocking downstream signaling in CRLF2/JAK2-dependent leukemia[89]. Wu et al also demonstrated a synergic activity of CHZ868 with dexamethasone in human CRLF2r cell lines and PDXs suggesting their possible use also into human trials.

4.3 PI3K/mTOR inhibitors

Mammalian target of rapamycin (mTOR) is a serine/threonine kinase, and is centrally integrated in several key signal transduction pathways critical to cell growth and proliferation. Aberrant activation of the mTOR

pathway has been demonstrated in multiple tumor types, and inhibition of mTOR by the macrolide rapamycin (sirolimus) or one of its analogs (temsirolimus, everolimus) has shown antitumor activity in preclinical models and in early phase clinical trials. Constitutive activation of the mTOR pathway has been demonstrated in the majority of cases of AML[90]. Rapamycin treatment causes G0/G1 cell cycle arrest in AML cell lines, and inhibits the clonogenic properties of AML patient samples without significantly affecting healthy donor CD34+ bone marrow (BM) cells[91]. Rapamycin has also been shown to have activity in pre-B cell ALL cell lines, primary patient samples, and a xenograft model[86]. Different studies provide strong rationale to pursue mTOR inhibition in combination with chemotherapy in pediatric ALL, and there are multiple ongoing early phase clinical trials investigating these agents[92].

A new agent recently investigated is the imidazoquiline derivatine NVP-BEZ235 that inhibits class I PI3K catalytic activity, as well as mTOR kinase activity, by capturing its ATP-binding site[93]. NVP-BEZ235 is able to block the growth and proliferation of different cancer cell types including, multiple myeloma, T-ALL and B-ALL[94–96] and is being investigated also in phase I clinical trials for therapy of solid tumors. As demonstrated by Schult C et al., NVP-BEZ235 blocks cell proliferation and induces cell cycle arrest by inhibiting cyclin D3 and CDK4 protein expression. Is also able to synergizes with conventional cytotoxic drugs and overcomes glucocorticoid resistance in T-ALL cells.

4.4 Monoclonal antibodies

Antibody-based therapy for cancer has become established over the past 15 years and is now the most successful and important strategies for treating patients with hematological malignancies and solid tumors[97]. The fundamental basis of antibody-based therapy of tumors dates back to the original observations of antigen expression by tumor cell through serological techniques in the 1960s[98].

Clinically useful mAbs can function through several different mechanisms, including inhibition of tumor-related signaling, induction of apoptosis, inhibition of angiogenesis, enhancing host immune response against cancer and targeted drug to the tumor site. The antibody-dependent cytoxicity (ADCC) and complement-dependent cytoxicity (CDC) are thought to be particularly important. ADCC involves destruction of the antibody-coated cell by recruitment of effector cells (such as NK cells, macrophages and neutrophils) whereas CDC involves destruction through complement activation.

The increasing knowledge of key molecules and cellular pathways involved in tumor pathogenesis has led to a rise in the proportion of therapeutic mAbs entering in clinical trials[99].

Different categories of mAbs have been develop for therapeutic use:

- **Murine monoclonal antibodies**: they are derived entirely from mice using hybridoma technology, which involves the fusion of immortalized myeloma cells with B-cells from immunized mice.

Their efficacy in humans is often limited due to short circulating half-lives, immunogenic issues and difficult to induce an immune effector response. They are mainly used as targeting agents for radioisotopes or cytotoxins that kill targeted tumor cells.

- **Chimeric monoclonal antibodies**: they are constructed by fusing the murine variable regions onto human constant regions in order to increase the immunologic efficiency. However, they often have poorer affinity than the parent murine mAb and they require also further manipulation to restore affinity and specificity of the original murine mAb.
- **Fully human monoclonal antibodies**: they were developed to further reduce immunogenicity associated with chimeric mAb. Human mAbs have been produced using either transgenic mice or phage display technology.

There have been a number of monoclonal antibodies and monoclonal antibody conjugates approved for the treatment of hematologic malignancies. One of the most successful monoclonal antibodies in this field is the anti-CD20 Rituximab. It is a chimeric murine-human monoclonal antibody produced by recombinant technology, from the parent murine monoclonal antibody, ibritumomab. Rituximab targets the CD20 surface antigen, which is found on about 95% of B cell lymphomas. Anti-CD20 antibodies have an effect on regulation of the cell cycle and

induce a number of signaling events, which lead to the induction of apoptosis. In vitro studies indicate that rituximab induces CDC as well as, ADCC[100] and in chemotherapy-resistant cell lines, chemo sensitivity may be restored by treatment with rituximab. Rituximab was approved by the US FDA for the second line treatment of CD20 + low grade lymphoma in 1997[101,102]. Aside from stand-alone efficacy, rituximab can improve the clinical activity of standard CHOP (cyclophosphamide, doxorubicin, vincristine and prednisone) treatment for patient with diffuse large B cell lymphoma[103].

4.5 Histone deacetylase inhibitors (HDACi)

Acetylation and deacetylation of histones help to regulate gene expression with remodeling of chromatin, allowing the binding of transcription factors. The acetylation of histones is regulated by two classes of enzymes: histone acetyltransferases and histone deacetylases (HDACs)[104,105]. Whereas the base pair sequence of DNA provides the fundamental code for proteins, post-translational modification of proteins plays a major role in the control of gene transcription. The development of HDACi's for treatment of cancer is based on de-repression of genes that participate in endogenous pro-apoptotic pathways and bring about a selective death of malignant cells while sparing healthy cells[105]. With hyperacetylation of nuclear histones, chromatin unravels and transcription factors can now bind to DNA and

initiate the synthesis of RNA coding for pro-apoptotic genes. By use of this mechanism, HDACi's would avoid the toxic effects of many chemotherapeutic drugs. Presently, HDAC inhibitors are used to treat patients with advanced solid and hematological tumors[106]. In general, HDAC inhibition selectively alters the transcription of few of the expressed genes (approximately 2% to 10% of expressed genes are increased or decreased in their rate of transcription)[107] . The attractive aspect of HDACi's is that they are orally active, and low concentrations are effective in reducing inflammation in humans[108] and animal models[109]. One unifying property of all HDAC inhibitors is the reduction in cytokine production as well as inhibition of cytokine signaling.

Among the new synthetic HDAC inhibitors, the class I/II orally active Givinostat (ITF2357) is widely used for a broad spectrum of diseases. As demonstrated by Leoni et al., Givinostat is effective in reducing inflammatory cytokines in vitro and in vivo models[110] having a potential and important role in treatment of chronic inflammatory and degenerative diseases.

There are evidences of an efficacy of Givinostat also in myeloproliferative disorders, in particular in patients with polycythemia vera (PV) and with myelofibrosis, bearing the JAK2V617F mutation (109). Givinostat was well tolerated and could induce hematological response in most PV patients alone or in combination with hydroxycarbamide, expecially in patients unresponsive to hydroxycarbamide

monotherapy[111]. As recently described by Pinazza et al. Givinostat has also effects in T-ALL setting where has been demonstrated to reduce engraftment in patient-derived models (PDX) and induce apoptosis of leukemic cells *in vivo* both in good responder and poor responder patients[112].

5. High-dimensional single cell analysis: mass cytometry

Acute leukemia is a strongly heterogeneous disease in which cancer-associated signaling phenotypes can be identified based on the study of abnormal signal transduction mechanisms. Knowledge of signaling pathways can predict features of cancer cell such as sensitivity to drug treatments, and consequently patient's prognosis. Single-cell approaches reveal the heterogeneity inherent in primary tumors and provide the means to characterize complex phenotypes, isolate rare populations, and dissect underlying mechanisms. A major advantage of a multidimensional, single-cell approach is that it allows determination of whether an abnormal trait in cancer, such as oncogenic signaling or a gene mutation, exists in all cells or is restricted to a cell subset[113]. The creation of single-cell network profiling techniques has led to important breakthroughs in blood cancer, where flow cytometry techniques are straightforward to apply[114].

5.1 The CyTOF: Cytometry by Time Of Flight

The mass spectrometer has been one of the signature tools of 'proteomics' over the past decade. Scott Tanner at the University of Toronto saw an opportunity to adapt a form of mass spectrometry termed inductively coupled plasma (ICP) to the measurement of events on and within cells[115] obtaining a flow-cytometer-mass spectrometer hybrid instrument. The idea was to tag antibodies with rare isotopes of elements not normally found in cells, stain cells with those tagged antibodies, nebulize those cells into a single-cell droplets and then are rapidly introduced them through a 7,500 K argon plasma[115,116]. There, the ions of what were once the individual cells pass into a time-of-flight (TOF) mass spectrometer tuned to the elemental weight range of the isotopes used to tag the antibodies bound to the cells. Every molecule within each individual cell is completely atomized and ionized and then those ions falling within a specific mass range are quantified by the CyTOF[115]. The summed levels of all isotopes from each cell are digitized and associated with that cell to create a spreadsheet of cell-by-cell information that is completely analogous to a flow cytometry data file. For a typical cell, the ion cloud has a lifetime of ≈ 300 μs over which it is measured (scanned) about 20 – 30 times by TOF-mass spectrometry. This lifetime precludes analysis of >1000 cell/s, as single cells cannot be resolved beyond this rate[117].

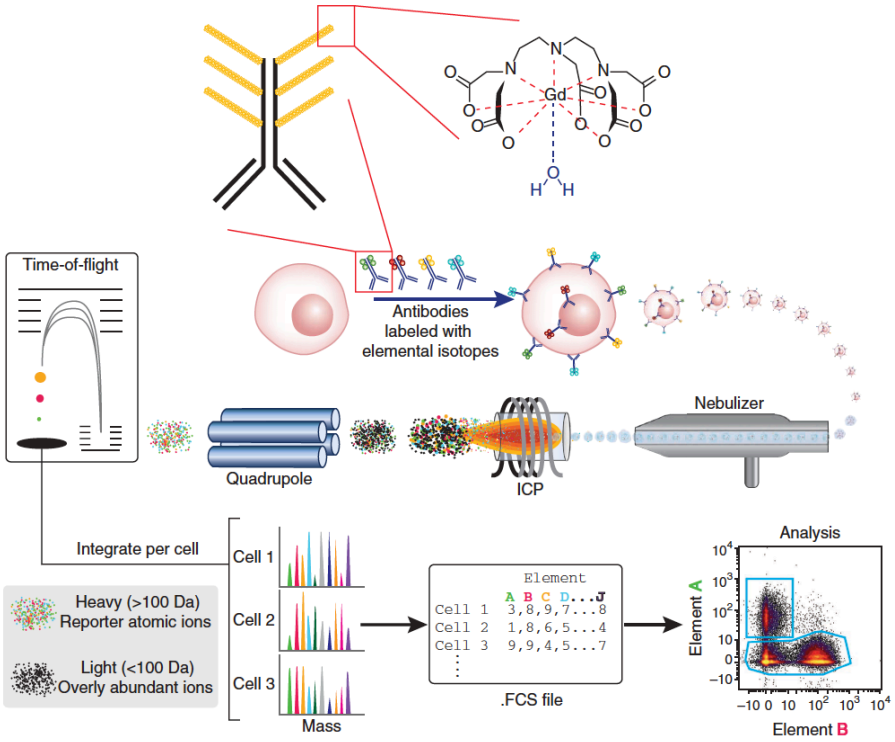

Figure 7. CyTOF working operation. First, a polymeric chelator is loaded with cations of a stable metal isotope. The loaded polymer is conjugated to the antibody of interest and cells are stained with these metal-conjugated antibodies. Cells are then injected into a nebulizer and passed through a ICP-TOF mass spectrometer where the single ions are counted and parsed into a flow cytometry file format[118].

5.2 Flow Cytometry versus Mass Cytometry

Although mass cytometry offers a number of unique features compared to Flow Cytometry (FCM) the technology is relatively new and encompasses unique hurdles. FCM has the unique capability to work on

live cells, and to be able to recover viable analyzed cells. Beyond this obvious difference, the two technologies are complementary although there is overlap, each is well-suited to addressing a particular set of questions[117].

The advent of mass cytometry allows researchers to account for complex features that would be much more difficult to study by fluorescent flow cytometry because of the limited number of non-conflicting fluorophore channels per experiment. Designing PFC panels becomes laborious, with a current limit of 18 markers measured simultaneously. In cases in which multiple intracellular events (pathways) must be tracked, FCM cannot simultaneously detail multiple pathways across multiple cell subsets. Therefore by mass cytometry is now possible to use about 50-60 different parameters per cell including surface markers, intracellular proteins, cell fate markers, transcription factors and epigenetic modifications. Interestingly, antibodies that recognize individual phosphorylated sites on signaling molecules, such as cytokine receptors and kinases (as well as their downstream effectors), can be used to measure the activities of intracellular signaling pathways based on the quantitative intensity of antibody labeling allowing a deep study of the aberrant signals present in the leukemic cells.

However there are a number of cellular qualities mass cytometry cannot yet measure. For example, forward and side scatter (FSC and SSC) are light-based measures of cell size and granularity commonly used in flow

cytometry to discriminate large granular leukocytes, lymphocytes, doublets of cells, and cellular debris. By contrast, there are also opportunities to measure novel metal parameters at the single-cell level including: platinum (cisplatin – a cancer drug), barium (magnetic resonance imaging contrast reagent), iodine (radioactive iodine therapy – for thyroid ablation), and gold (for experimental autoimmune therapy)[117].

The features of each technology are summarized in Table 1 [117]

Technology		Fluorescence flow cytometry	Mass cytometry
Measurement basis		Fluorescent probes	Stable mass isotope probes
Experimental design			
Max no. of measurements		20 (18 fluorescence)	37 (including DNA)
Theoretical no. of subsets[a]		2.6×10^5	1.4×10^{11}
Panel design complexity (no. of probes)	Easy	<8	37
	Moderate	8–12	
	Hard	12–18	
Sensitivity range for different probes[b]		0.1–10	1–2
Sample throughput			
Sampling efficiency		> 95%	< 30%
Measured cells/s		25 000	500–1000
Cells/h		25–60 million	2 million
Commercial reagent cost			
Per probe per test[c]		$2.00–$8.00	$1.50–$3.00

5.3 Analysis of the mass cytometry data

Rapid increases in the numbers of measurable single-cell parameters have brought a daunting increase in the complexity of the data. Analysis of flow cytometry data is typically manual, performed in one or two dimensions at a time by selecting subsets of interest from parent populations. This approach is not scalable, and suffers from individual user bias. The analysis of multidimensional data derived from mass cytometry has been enabled by the development of several bioinformatics tools.

The fcs file generated by the instrument can be uploaded and analyzed by using Cytobank (www.cytobank.org), a collaboration-centric, web-based analysis platform that that allow researchers to annotate, analyze and share results. Cytobank gives the possibility to, not only visualize the data by using the conventional 2D plots and histograms, but also analyze mass cytometry data with advanced tools (like heatmaps, 3D plots, histograms overlays) as well as use clustering and visualization software as SPADE and viSNE.

The SPADE (Spanning tree Progression of Density normalized Events) clustering algorithm groups cells stochastically based on shared immunophenotypic marker labeling, and can be used to compare cell signaling in selected cell populations across multiple experimental samples[119]. The more recently developed tool viSNE (Visualization of t-distributed Stochastic Neighbor Embedding algorithm) allows visualization of high-dimensional single cell data and is based on the t-Distributes Stochastic Neighbor Embedding (t-SNE) algorithm[120] viSNE finds the two dimensional representation of single-cell data that best preserves their local and global geometry[121]. The resulting viSNE map provides a visual representation of the single-cell data that is similar to a biaxial plot, but the positions of cells reflect their proximity in high-dimensional rather than two-dimensional space. For these reasons is a useful tool to study at single cell level the signaling in individual cells as well as detect with high resolution rare cell subset, like MRD cells[121].

6. Scope of the thesis

BCP-ALL is heterogeneous disease resulting from the accumulation of genetic alterations in B lymphoid precursor cells and represents the most common malignant disease in childhood[122]. Five-year survival rates now exceed 85% in children, however the survival following relapse is still poor[1]. Of note, more than a half of relapses concern patients not classified in high-risk groups by measurement of Minimal Residual Disease (MRD)[35], which is a surrogate parameter of individual response to therapy. Several genetic alterations have been demonstrated of clinical relevance for risk stratification and therapeutic approach. Approximately 75% of childhood ALL cases harbor a recurring chromosomal alterations detectable by karyotyping, FISH, or molecular techniques: these include hyperdiploidy, hypodiploidy, chromosomal rearrangements such as t(12;21) *TEL-AML1,* t(1;19) *E2A-PBX1*, t(9;22) *BCR-ABL1*, t(4;11) *MLL-AF4*, alterations in transcription factors required for B-lymphoid development like *PAX5*, *IKZF1* and rearrangements in proteins involved in signal transduction pathways like JAK1/2, CRLF2 and IL7R.

Several groups are currently focusing on genetic testing of individual lesions or on functional screening approaches to identify pathway deregulations and possibly new achievable targetable molecules.

In this setting we focused our research on a specific poor prognosis

subgroup of patients harboring alterations in *CRLF2* gene[54]. Herein we first refined the characterization and identifications of the *CRLF2* rearrangements and its overexpression, and then we dissected the signaling aberrant pathways focusing our research also on possible new therapeutic interventions for this particularly poor prognosis subgroup of patients. Specifically, three major lines of research have been investigated in this PhD thesis:

1. *Fine tuning of surface CRLF2 expression and its associated signaling profile in childhood BCP-ALL* (Chapter 2)

In this chapter we focused on refining the identification of patients with CRLF2 alterations. We aimed to demonstrate that screening of CRLF2 expression on surface of BCP-ALL patients can be successfully performed by standardized FCM protocols, allowing to identify also patients with weak or partial CRLF2 surface expression. We also investigated whether FCM data are concordant with CRLF2 transcript level performed by RQ-PCR and we studied the phospho-signaling profile associated with the overexpression of the TSLPR.

2. *Single-cell analysis uncovers functional targetable subpopulations in CRLF2 rearranged B-cell precursor acute lymphoblastic leukemia* (Chapter 3)

We then performed a high-throughput dissection of the TSLPR-related

signaling in order to better investigate the single cell heterogeneity of *CRLF2r* blasts. We aim also to test two monoclonal antibodies directed against the TSLPR receptor as a new possible therapeutic approach, comparing their efficacy *in vitro* with that of three different kinase inhibitors (Dasatinib, Ruxolitinib and NVP-BEZ235), either alone or in combination. We finally assessed the feasibility to use mass cytometry to study the features of chemo-resistant *CRLF2r* MRD cells and provide new evidences on the survival advantages of these cells for the identification new therapeutic strategies in this setting.

3. *Role of the hystone deacetylase inhibitor Givinostat (ITF2357) in treatment of CRLF2 rearranged BCP-ALL* (Chapter 4)

In this chapter we aim to investigate the efficacy of Givinostat, an hystone deacetylase inhibitor, in both *in vitro* and *in vivo* models of CRLF2r BCP-ALL, either alone or in combination with chemotherapeutic agents currently in use for clinical induction-remission therapy. Results from this study will provide the basis for the possible introduction of Givinostat in the current protocols, allowing combined therapies in patients, reducing doses and relative-associated toxicity thus maintaining therapeutic efficacy. This would provide particular benefits for those patients that particularly suffers of chemotherapy-related toxicity (i.e DS-ALL).

References

1. Pui C-H, Relling M V, Downing JR. Acute Lymphoblastic Leukemia — NEJM. *New Engl. J. …*. 2004;
2. Ward E, DeSantis C, Robbins A, Kohler B, Jemal A. Childhood and adolescent cancer statistics, 2014. *CA. Cancer J. Clin.* 2014;64(2):83–103.
3. Inaba H, Greaves M, Mullighan CG. Acute lymphoblastic leukaemia. *Lancet*. 2013;381(9881):1943–55.
4. Mullighan CG. Molecular genetics of B-precursor acute lymphoblastic leukemia. *J. Clin. Invest.* 2012;122(10):3407–15.
5. Ghazavi F, Lammens T, Van Roy N, et al. Molecular basis and clinical significance of genetic aberrations in B-cell precursor acute lymphoblastic leukemia. *Exp. Hematol.* 2015;43(8):640–653.
6. Mullighan CG. The molecular genetic makeup of acute lymphoblastic leukemia. *Hematology Am. Soc. Hematol. Educ. Program*. 2012;2012:389–96.
7. Longo DL, Hunger SP, Mullighan CG. Acute Lymphoblastic Leukemia in Children. *N. Engl. J. Med.* 2015;373(16):1541–1552.
8. Lugo TG, Pendergast AM, Muller AJ, Witte ON. Tyrosine kinase activity and transformation potency of bcr-abl oncogene products. *Science (80-.).* 1990;247(4946):1079–1082.
9. Ribeiro RC, Abromowitch M, Raimondi SC, et al. Clinical and biologic hallmarks of the Philadelphia chromosome in childhood acute lymphoblastic leukemia. *Blood*. 1987;70(4):948–53.
10. Jeha S, Coustan-Smith E, Pei D, et al. Impact of tyrosine kinase inhibitors on minimal residual disease and outcome in childhood Philadelphia chromosome-positive acute lymphoblastic leukemia. *Cancer*. 2014;120(10):1514–1519.
11. Andersson AK, Ma J, Wang J, et al. The landscape of somatic mutations in infant MLL-rearranged acute lymphoblastic leukemias. *Nat. Genet.* 2015;47(4):330–7.
12. Mullighan CG, Su X, Zhang J, et al. Deletion of IKZF1 and prognosis in acute lymphoblastic leukemia. *N. Engl. J. Med.* 2009;360(5):470–80.
13. Dang J, Wei L, De Ridder J, et al. PAX5 is a tumor suppressor in mouse mutagenesis models of acute lymphoblastic leukemia. *Blood*. 2015;125(23):3609–3617.
14. Clappier E, Auclerc MF, Rapion J, et al. An intragenic ERG deletion is a marker of an oncogenic subtype of B-cell precursor acute lymphoblastic leukemia with a favorable outcome despite frequent IKZF1 deletions. *Leukemia*. 2014;28(1):70–

7.
15. Harvey RC, Mullighan CG, Chen IM, et al. Rearrangement of CRLF2 is associated with mutation of JAK kinases, alteration of IKZF1, Hispanic/Latino ethnicity, and a poor outcome in pediatric B-progenitor acute lymphoblastic leukemia. *Blood*. 2010;115(26):5312–5321.
16. Den Boer ML, van Slegtenhorst M, De Menezes RX, et al. A subtype of childhood acute lymphoblastic leukaemia with poor treatment outcome: a genome-wide classification study. *Lancet Oncol.* 2009;10(2):125–134.
17. Roberts KG, Li Y, Payne-Turner D, et al. Targetable Kinase-Activating Lesions in Ph-like Acute Lymphoblastic Leukemia. *N. Engl. J. Med.* 2014;371(11):1005–1015.
18. Holmes ML, Pridans C, Nutt SL. The regulation of the B-cell gene expression programme by Pax5. *Immunol. Cell Biol.* 2008;86(1):47–53.
19. Peschon JJ, Morrissey PJ, Grabstein KH, et al. Early lymphocyte expansion is severely impaired in interleukin 7 receptor-deficient mice. *J. Exp. Med.* 1994;180(5):1955–1960.
20. Vainchenker W, Constantinescu SN. JAK/STAT signaling in hematological malignancies. *Oncogene*. 2012;32(May):1–13.
21. Herzog S, Reth M, Jumaa H. Regulation of B-cell proliferation and differentiation by pre-B-cell receptor signalling. *Nat. Rev. Immunol.* 2009;9(3):195–205.
22. Ochiai K, Maienschein-Cline M, Mandal M, et al. A self-reinforcing regulatory network triggered by limiting IL-7 activates pre-BCR signaling and differentiation. *Nat. Immunol.* 2012;13(3):300–307.
23. Rickert RC. New insights into pre-BCR and BCR signalling with relevance to B cell malignancies. *Nat. Rev. Immunol.* 2013;13(8):578–91.
24. Nachman JB, Heerema NA, Sather H, et al. Outcome of treatment in children with hypodiploid acute lymphoblastic leukemia. *Blood*. 2007;110(4):1112–1115.
25. Moorman A V., Ensor HM, Richards SM, et al. Prognostic effect of chromosomal abnormalities in childhood B-cell precursor acute lymphoblastic leukaemia: Results from the UK Medical Research Council ALL97/99 randomised trial. *Lancet Oncol.* 2010;11(5):429–438.
26. Aricò M, Schrappe M, Hunger SP, et al. Clinical outcome of children with newly diagnosed Philadelphia chromosome-positive acute lymphoblastic leukemia treated between 1995 and 2005. *J. Clin. Oncol.* 2010;28(31):4755–61.
27. Harrison CJ, Moorman A V, Schwab C, et al. An international study of intrachromosomal amplification of chromosome 21 (iAMP21): cytogenetic characterization and outcome. *Leukemia*. 2014;28(5):1015–21.

28. Coustan-Smith E, Sancho J, Hancock ML, et al. Clinical importance of minimal residual disease in childhood acute lymphoblastic leukemia. *Blood*. 2000;96(8):2691–2696.
29. van Dongen JJ, Seriu T, Panzer-Grumayer ER, et al. Prognostic value of minimal residual disease in acute lymphoblastic leukaemia in childhood. *Lancet*. 1998;352(9142):1731–1738.
30. Velden VHJ Van Der, Dongen JJM Van. MRD Detection in Acute Lymphoblastic Leukemia Patients Using Ig/TCR Gene Rearrangements as Targets for Real-Time Quantitative PCR. 2009.
31. Gaipa G, Basso G, Biondi A, Campana D. Detection of minimal residual disease in pediatric acute lymphoblastic leukemia. *Cytom. Part B - Clin. Cytom.* 2013;84(6):359–369.
32. Basso G, Veltroni M, Valsecchi MG, et al. Risk of relapse of childhood acute lymphoblastic leukemia is predicted by flow cytometric measurement of residual disease on day 15 bone marrow. *J. Clin. Oncol.* 2009;27(31):5168–5174.
33. Borowitz MJ, Wood BL, Devidas M, et al. Prognostic significance of minimal residual disease in high risk B-ALL: A report from Children's Oncology Group study AALL0232. *Blood*. 2015;126(8):964–971.
34. Kalina T, Flores-Montero J, Lecrevisse Q, et al. Quality assessment program for EuroFlow protocols: Summary results of four-year (2010-2013) quality assurance rounds. *Cytom. Part A*. 2015;87(2):145–156.
35. Conter V, Bartram CR, Valsecchi MG, et al. Molecular response to treatment redefines all prognostic factors in children and adolescents with B-cell precursor acute lymphoblastic leukemia: results in 3184 patients of the AIEOP-BFM ALL 2000 study. *Blood*. 2010;115(16):3206–3214.
36. Schrappe M, Valsecchi MG, Bartram CR, et al. Late MRD response determines relapse risk overall and in subsets of childhood T-cell ALL: Results of the AIEOP-BFM-ALL 2000 study. *Blood*. 2011;118(8):2077–2084.
37. Izraeli S, Shochat C, Tal N, Geron I. Towards precision medicine in childhood leukemia - Insights from mutationally activated cytokine receptor pathways in acute lymphoblastic leukemia. *Cancer Lett.* 2014;352(1):15–20.
38. Russell LJ, Capasso M, Vater I, et al. Deregulated expression of cytokine receptor gene, CRLF2, is involved in lymphoid transformation in B-cell precursor acute lymphoblastic leukemia. *Blood*. 2009;114(13):2688–2698.
39. He R, Geha RS. Thymic stromal lymphopoietin. *Ann. N. Y. Acad. Sci.* 2010;1183:13–24.
40. Roll JD, Reuther GW. CRLF2 and JAK2 in B-progenitor acute lymphoblastic

leukemia: A novel association in oncogenesis. *Cancer Res.* 2010;70(19):7347–7352.

41. Quentmeier H, Drexler HG, Fleckenstein D, et al. Cloning of human thymic stromal lymphopoietin (TSLP) and signaling mechanisms leading to proliferation. *Leukemia*. 2001;15(8):1286–1292.
42. Friend SL, Hosier S, Nelson A, et al. A thymic stromal cell line supports in vitro development of surface IgM+ B cells and produces a novel growth factor affecting B and T lineage cells. *Exp. Hematol.* 1994;22(3):321–8.
43. Rochman Y, Leonard WJ. Thymic stromal lymphopoietin: a new cytokine in asthma. *Curr. Opin. Pharmacol.* 2008;8(3):249–254.
44. Demehri S, Liu Z, Lee J, et al. Notch-deficient skin induces a lethal systemic B-lymphoproliferative disorder by secreting TSLP, a sentinel for epidermal integrity. *PLoS Biol.* 2008;6(5):0992–1005.
45. Chappaz S, Flueck L, Farr AG, Rolink AG, Finke D. Increased TSLP availability restores T- and B-cell compartments in adult IL-7-deficient mice. *Blood*. 2007;110(12):3862–3870.
46. Scheeren FA, Van Lent AU, Nagasawa M, et al. Thymic stromal lymphopoietin induces early human B-cell proliferation and differentiation. *Eur. J. Immunol.* 2010;40(4):955–965.
47. Allakhverdi Z, Comeau MR, Jessup HK, et al. Thymic stromal lymphopoietin is released by human epithelial cells in response to microbes, trauma, or inflammation and potently activates mast cells. *J. Exp. Med.* 2007;204(2):253–8.
48. Wohlmann A, Sebastian K, Borowski A, Krause S, Friedrich K. Signal transduction by the atopy-associated human thymic stromal lymphopoietin (TSLP) receptor depends on Janus kinase function. *Biol. Chem.* 2010;391(2-3):181–186.
49. Zhong J, Kim M-S, Chaerkady R, et al. TSLP signaling network revealed by SILAC-based phosphoproteomics. *Mol. Cell. Proteomics*. 2012;11(6):M112.017764.
50. Zhong J, Sharma J, Raju R, et al. TSLP signaling pathway map: a platform for analysis of TSLP-mediated signaling. *Database (Oxford).* 2014;2014:1–8.
51. Tal N, Shochat C, Geron I, Bercovich D, Izraeli S. Interleukin 7 and thymic stromal lymphopoietin: From immunity to leukemia. *Cell. Mol. Life Sci.* 2014;71(3):365–378.
52. Mullighan CG, Collins-underwood JR, Phillips LAA, et al. Rearrangement of CRLF2 in B-progenitor – and Down syndrome – associated acute lymphoblastic leukemia. *Nat. Genet.* 2009;41(11):1243–1246.
53. Yoda A, Yoda Y, Chiaretti S, et al. Functional screening identifies CRLF2 in precursor B-cell acute lymphoblastic leukemia. *Proc. Natl. Acad. Sci. U. S. A.*

2010;107(1):252–7.

54. Cario G, Zimmermann M, Romey R, et al. Presence of the P2RY8-CRLF2 rearrangement is associated with a poor prognosis in non-high-risk precursor B-cell acute lymphoblastic leukemia in children treated according to the ALL-BFM 2000 protocol. *Blood*. 2010;115(26):5393–5397.
55. Hertzberg L, Vendramini E, Ganmore I, et al. Down syndrome acute lymphoblastic leukemia, a highly heterogeneous disease in which aberrant expression of CRLF2 is associated with mutated JAK2: A report from the International BFM Study Group. *Blood*. 2010;115(5):1006–1017.
56. Storlazzi CT, Albano F, Lo Cunsolo C, et al. Upregulation of the SOX5 by promoter swapping with the P2RY8 gene in primary splenic follicular lymphoma. *Leukemia*. 2007;21(10):2221–5.
57. Heim MH. The Jak-STAT pathway: cytokine signalling from the receptor to the nucleus. *J. Recept. Signal Transduct. Res.* 1999;19(1-4):75–120.
58. Roberts KG, Morin RD, Zhang J, et al. Genetic Alterations Activating Kinase and Cytokine Receptor Signaling in High-Risk Acute Lymphoblastic Leukemia. *Cancer Cell*. 2012;22(2):153–166.
59. Tasian SK, Doral MY, Borowitz MJ, et al. Aberrant STAT5 and PI3K/mTOR pathway signaling occurs in human CRLF2-rearranged B-precursor acute lymphoblastic leukemia. *Blood*. 2012;120(4):833–842.
60. Maude SL, Tasian SK, Vincent T, et al. Targeting JAK1/2 and mTOR in murine xenograft models of Ph-like acute lymphoblastic leukemia. *Blood*. 2012;120(17):3510–3518.
61. Springuel L, Hornakova T, Losdyck E, et al. Cooperating JAK1 and JAK3 mutants increase resistance to JAK inhibitors. *Blood*. 2014;124(26):3924–3931.
62. Wu S, Li LS, Kopp N, et al. Activity of the Type II JAK2 Inhibitor CHZ868 in B Cell Acute Lymphoblastic Leukemia. *Cancer Cell*. 2015;29–41.
63. Qin H, Cho M, Haso W, et al. Eradication of B-ALL using chimeric antigen receptor-expressing T cells targeting the TSLPR oncoprotein. *Blood*. 2015;126(5):629–639.
64. Vetter T, Borowski A, Wohlmann A, et al. Blockade of thymic stromal lymphopoietin (TSLP) receptor inhibits TSLP-driven proliferation and signalling in lymphoblasts from a subset of B-precursor ALL patients. *Leuk. Res.* 2016;40:38–43.
65. Raghunathan R, Mahesula S, Kancharla K, et al. Anti-CRLF2 antibody-armored biodegradable nanoparticles for childhood B-ALL. *Part. Part. Syst. Charact.* 2013;30(4):355–364.

66. Flex E, Petrangeli V, Stella L, et al. Somatically acquired JAK1 mutations in adult acute lymphoblastic leukemia. *J. Exp. Med.* 2008;205(4):751–8.
67. Bercovich D, Ganmore I, Scott LM, et al. Mutations of JAK2 in acute lymphoblastic leukaemias associated with Down ' s syndrome. *Lancet*. 2008;372(9648):1484–1492.
68. Malinge S, Ben-Abdelali R, Settegrana C, et al. Novel activating JAK2 mutation in a patient with Down syndrome and B-cell precursor acute lymphoblastic leukemia. *Blood*. 2007;109(5):2202–2204.
69. Lu X, Levine R, Tong W, et al. Expression of a homodimeric type I cytokine receptor is required for JAK2V617F-mediated transformation. *Proc. Natl. Acad. Sci. U. S. A.* 2005;102(52):18962–18967.
70. Chen I-M, Harvey RC, Mullighan CG, et al. Outcome modeling with CRLF2, IKZF1, JAK, and minimal residual disease in pediatric acute lymphoblastic leukemia: a Children's Oncology Group study. *Blood*. 2012;119(15):3512–22.
71. Lu N, Wang Y-H, Wang Y-H, et al. TSLP and IL-7 use two different mechanisms to regulate human CD4+ T cell homeostasis. *J. Exp. Med.* 2009;206(10):2111–2119.
72. Shochat C, Tal N, Bandapalli OR, et al. Gain-of-function mutations in interleukin-7 receptor-α (IL7R) in childhood acute lymphoblastic leukemias. *J. Exp. Med.* 2011;208(5):901–908.
73. Gambacorti-Passerini C, Antolini L, Mahon F-X, et al. Multicenter independent assessment of outcomes in chronic myeloid leukemia patients treated with imatinib. *J. Natl. Cancer Inst.* 2011;103(7):553–61.
74. Smith BD. Imatinib for chronic myeloid leukemia: The impact of its effectiveness and long-term side effects. *J. Natl. Cancer Inst.* 2011;103(7):527–529.
75. Iqbal N, Iqbal N. Imatinib: a breakthrough of targeted therapy in cancer. *Chemother Res Pr.* 2014;2014:357027.
76. Annesley CE, Brown P. Novel agents for the treatment of childhood acute leukemia. *Ther. Adv. Hematol.* 2015;6(2):61–79.
77. Schultz KR, Bowman WP, Aledo A, et al. Improved early event-free survival with imatinib in Philadelphia chromosome - Positive acute lymphoblastic leukemia: A Children's Oncology Group Study. *J. Clin. Oncol.* 2009;27(31):5175–5181.
78. Tallman MS, Kim HT, Paietta E, et al. Acute monocytic leukemia (French-American-British classification M5) does not have a worse prognosis than other subtypes of acute myeloid leukemia: A report from the Eastern Cooperative Oncology Group. *J. Clin. Oncol.* 2004;22(7):1276–1286.
79. Schultz KR, Carroll A, Heerema NA, et al. Long-term follow-up of imatinib in pediatric Philadelphia chromosome-positive acute lymphoblastic leukemia:

Children's Oncology Group study AALL0031. *Leukemia*. 2014;28(7):1467–71.

80. Soverini S, De Benedittis C, Papayannidis C, et al. Drug resistance and BCR-ABL kinase domain mutations in Philadelphia chromosome-positive acute lymphoblastic leukemia from the imatinib to the second-generation tyrosine kinase inhibitor era: The main changes are in the type of mutations, but not in the fr. *Cancer*. 2014;120(7):1002–1009.
81. Porkka K, Koskenvesa P, Lund??n T, et al. Dasatinib crosses the blood-brain barrier and is an efficient therapy for central nervous system philadelphia chromosome positive leukemia. *Blood*. 2008;112(4):1005–1012.
82. Gordon MS. M. S. Gordon, MD Dasatinib in Imatinib-Resistant Philadelphia Chromosome–Positive Leu- kemias. 2006;144–145.
83. Cortes JE, Kim D-W, Pinilla-Ibarz J, et al. A Phase 2 Trial of Ponatinib in Philadelphia Chromosome–Positive Leukemias. *N. Engl. J. Med.* 2013;369(19):1783–1796.
84. Mullighan CG, Zhang J, Harvey RC, et al. JAK mutations in high-risk childhood acute lymphoblastic leukemia. *Proc. Natl. Acad. Sci. U. S. A.* 2009;106(23):9414–9418.
85. Daver N, Cortes J. Molecular targeted therapy in acute myeloid leukemia. *Hematology*. 2012;17 Suppl 1:S59–62.
86. Maude SL, Tasian SK, Vincent T, et al. Targeting mTOR and JAK2 in xenograft models of CRLF2-overexpressing Acute Lymphoblastic Leukemia (ALL). *Blood*. 2011;118.:
87. Weigert O, Lane AA, Bird L, et al. Genetic resistance to JAK2 enzymatic inhibitors is overcome by HSP90 inhibition. *J. Exp. Med.* 2012;209(2):259–73.
88. Waibel M, Solomon VS, Knight DA, et al. Combined Targeting of JAK2 and Bcl-2/Bcl-xL to Cure Mutant JAK2-Driven Malignancies and Overcome Acquired Resistance to JAK2 Inhibitors. *Cell Rep.* 2013;5(4):1047–1059.
89. Andraos R, Qian Z, Bonenfant D, et al. Modulation of activation-loop phosphorylation by JAK inhibitors is binding mode dependent. *Cancer Discov.* 2012;2(6):512–523.
90. Park S, Chapuis N, Tamburini J, et al. Role of the PI3K/AKT and mTOR signaling pathways in acute myeloid leukemia. *Haematologica*. 2010;95(5):819–828.
91. Recher C, Beyne-Rauzy O, Demur C, et al. Antileukemic activity of rapamycin in acute myeloid leukemia. *Blood*. 2005;105(6):2527–2534.
92. Teachey DT, Sheen C, Hall J, et al. mTOR inhibitors are synergistic with methotrexate: An effective combination to treat acute lymphoblastic leukemia. *Blood*. 2008;112(5):2020–2023.

93. Maira S-M, Stauffer F, Brueggen J, et al. Identification and characterization of NVP-BEZ235, a new orally available dual phosphatidylinositol 3-kinase/mammalian target of rapamycin inhibitor with potent in vivo antitumor activity. *Mol. Cancer Ther.* 2008;7(7):1851–1863.
94. Baumann P, Mandl-Weber S, Oduncu F, Schmidmaier R. The novel orally bioavailable inhibitor of phosphoinositol-3-kinase and mammalian target of rapamycin, NVP-BEZ235, inhibits growth and proliferation in multiple myeloma. *Exp. Cell Res.* 2009;315(3):485–497.
95. Chiarini F, Grimaldi C, Ricci F, Tazzari PL, Evangelisti C. Activity of the Novel Dual Phosphatidylinositol 3-Kinase / Mammalian Target of Rapamycin Inhibitor NVP-BEZ235 against T-Cell Acute Lymphoblastic Leukemia Activity of the Novel Dual Phosphatidylinositol 3-Kinase / Mammalian Target of Rapamycin Inhibitor NV. *Cancer Res.* 2010;70(20):8097–107.
96. Schult C, Dahlhaus M, Glass A, et al. The dual kinase inhibitor NVP-BEZ235 in combination with cytotoxic drugs exerts anti-proliferative activity towards acute lymphoblastic leukemia cells. *Anticancer Res.* 2012;32(2):463–474.
97. Scott AM, Wolchok JD, Old LJ. Antibody therapy of cancer. *Nat. Rev.* 2012;12(4):278–287.
98. Rettig WJ OL. Immunogenetics of human cell surface differentiation. *Ann. Rev. Immunol*. 1989;7:481–511.
99. TJ C. Cancer Immunotherapy. 2013.
100. Golay J, Lazzari M, Facchinetti V, et al. CD20 levels determine the in vitro susceptibility to rituximab and complement of B-cell chronic lymphocytic leukemia: Further regulation by CD55 and CD59. *Blood*. 2001;98(12):3383–3389.
101. Davis TA, Grillo-López AJ, White C a, et al. Rituximab anti-CD20 monoclonal antibody therapy in non-Hodgkin's lymphoma: safety and efficacy of re-treatment. 2000.
102. McLaughlin P, Grillo-L??pez AJ, Link BK, et al. Rituximab chimeric anti-CD20 monoclonal antibody therapy for relapsed indolent lymphoma: Half of patients respond to a four-dose treatment program. *J. Clin. Oncol.* 1998;16(8):2825–2833.
103. Coiffier B, Lepage E, Briere J, et al. CHOP chemotherapy plus rituximab compared with CHOP alone in elderly patients with diffuse large-B-cell lymphoma. *N. Engl. J. Med.* 2002;346(4):235–42.
104. Narlikar GJ, Fan HY, Kingston RE. Cooperation between complexes that regulate chromatin structure and transcription. *Cell*. 2002;108(4):475–487.

105. Johnstone RW. Histone-deacetylase inhibitors: novel drugs for the treatment of cancer. *Nat. Rev. Drug Discov.* 2002;1(4):287–299.
106. Kelly WK, O'Connor OA, Krug LM, et al. Phase I study of an oral histone deacetylase inhibitor, suberoylanilide hydroxamic acid, in patients with advanced cancer. *J. Clin. Oncol.* 2005;23(17):3923–31.
107. Della Ragione F, Criniti V, Della Pietra V, et al. Genes modulated by histone acetylation as new effectors of butyrate activity. *FEBS Lett.* 2001;499(3):199–204.
108. Dinarello C a, Donath MY, Mandrup-Poulsen T. Role of IL-1beta in type 2 diabetes. *Curr. Opin. Endocrinol. Diabetes. Obes.* 2010;17(4):314–321.
109. Vojinovic J, Damjanov N, D'Urzo C, et al. Safety and efficacy of an oral histone deacetylase inhibitor in systemic-onset juvenile idiopathic arthritis. *Arthritis Rheum.* 2011;63(5):1452–1458.
110. Leoni F, Fossati G, Lewis EC, et al. The histone deacetylase inhibitor ITF2357 reduces production of pro-inflammatory cytokines in vitro and systemic inflammation in vivo. *Mol. Med.* 2005;11(1-12):1–15.
111. Finazzi G, Vannucchi AM, Martinelli V, et al. A phase II study of Givinostat in combination with hydroxycarbamide in patients with polycythaemia vera unresponsive to hydroxycarbamide monotherapy. *Br. J. Haematol.* 2013;161(5):688–694.
112. Pinazza M, Borga C, Agnusdei V, et al. An immediate transcriptional signature associated with response to the histone deacetylase inhibitor Givinostat in T acute lymphoblastic leukemia xenografts. *Cell Death Dis.* 2016;6(1):e2047–12.
113. Fienberg H, Nolan GP. High-Dimensional Single Cell Analysis Mass Cytometry, Multi-parametric Flow Cytometry and Bioinformatic Techniques. 2014.
114. Irish JM, Czerwinski DK, Nolan GP, Levy R. Kinetics of B cell receptor signaling in human B cell subsets mapped by phosphospecific flow cytometry. *J. Immunol.* 2006;177(3):1581–1589.
115. Bandura DR, Baranov VI, Ornatsky OI, et al. Mass cytometry: Technique for real time single cell multitarget immunoassay based on inductively coupled plasma time-of-flight mass spectrometry. *Anal. Chem.* 2009;81(16):6813–6822.
116. Bendall SC, Simonds EF, Qiu P, et al. Single-cell mass cytometry of differential immune and drug responses across a human hematopoietic continuum. *Science*. 2011;332(6030):687–96.
117. Bendall SC, Nolan GP, Roederer M, Chattopadhyay PK. A deep profiler's guide to cytometry. *Trends Immunol.* 2012;33(7):323–332.
118. Bendall SC, Nolan GP. From single cells to deep phenotypes in cancer. *Nat.*

Biotechnol. 2012;30(7):639–647.

119. Qiu P, Simonds EF, Bendall SC, et al. Extracting a cellular hierarchy from high-dimensional cytometry data with SPADE. *Nat. Biotechnol.* 2011;29(10):886–891.
120. Van Der Maaten LJP, Hinton GE. Visualizing high-dimensional data using t-sne. *J. Mach. Learn. Res.* 2008;9:2579–2605.
121. Amir ED, Davis KL, Tadmor MD, et al. viSNE enables visualization of high dimensional single-cell data and reveals phenotypic heterogeneity of leukemia. *Nat. Biotechnol.* 2013;31(6):545–52.
122. Mullighan CG, Goorha S, Radtke I, et al. Genome-wide analysis of genetic alterations in acute lymphoblastic leukaemia. *Nature*. 2007;446(7137):758–64.

Chapter 2

Haematologica. 2015; 100 (6): e229-e232
doi:10.3324/haematol.2014.114447

Fine tuning of Surface CRLF2 Expression and Its Associated Signaling Profile in Childhood B-Cell Precursor Acute Lymphoblastic Leukemia

Cristina Bugarin[1], **Jolanda Sarno**[1], Chiara Palmi[1], Angela Maria Savino[1], Geertruy te Kronnie[2], Michael Dworzak[3], Angela Shumich[3], Barbara Buldini[2], Oscar Maglia[1], Simona Sala[1], Ilaria Bronzini[2], Jean-Pierre Bourquin[4], Ester Mejstrikova[5], Ondrej Hrusak[5], Drorit Luria[6], Giuseppe Basso[2], Shai Izraeli[6], Andrea Biondi[1,7], Giovanni Cazzaniga[1] and Giuseppe Gaipa[1]. On behalf of the I-BFM study group

[1] Pediatric Clinic, University of Milano Bicocca, M. Tettamanti Research Center, Monza, Italy; [2] Lab. Hemato-Oncology, University of Padua, Padua, Italy; [3] Children's Cancer Research Institute and St. Anna Children's Hospital, Dept. of Pediatrics, Medical University of Vienna, Vienna, Austria. [4] University of Zurich, CH-8006 Zurich, Switzerland; [5] Childhood Leukaemia Investigation Prague, Department of Paediatric Haematology and Oncology, Charles University Prague, 2nd Medical School, Czech Republic; [6] Pediatric Hematology Oncology, Schneider Children's Medical Center of Israel, Israel; [7] Dept. Department of Pediatrics, Hospital San Gerardo/Fondazione MBBM

Genomic rearrangements of the cytokine receptor-like factor 2 (*CRLF2*) gene[1,2], which is part of the thymic stromal lymphopoietin receptor (TSLPR), result in overexpression of *CRLF2* itself leading to JAK2-mediated activation of STAT5, which regulates cell proliferation, survival, and apoptosis[3,4,11-13]. In this regard, childhood B-cell precursor acute lymphoblastic leukemias (BCP-ALLs), bearing a rearranged *CRLF2*, display a high rate of relapse[5-10]. Furthermore, *CRLF2* genomic rearrangements are strictly associated with its surface overexpression, rendering this marker suitable for detection by flow cytometry (FCM) [14].

To determine *CRLF2* expression in childhood BCP-ALLs, we first assessed TSLPR surface expression. For this purpose, we carried out, at diagnosis, standard multiparametric FCM (Dworzak *et al.*, manuscript in preparation) on 421 consecutive diagnostic bone marrow (BM) samples from BCP-ALL children (256 males and 165 females), enrolled in six centers of the AIEOP-BFM-ALL-2009 trial between December 2010 and June 2013. Our gating strategy used to measure TSLPR surface expression (Supplemental Figure 1) allowed us to distinguish three blast subpopulations according to the intensity of TSLPR staining: the first one was defined as negative (i.e. positivity <10%), the second one was weakly positive (i.e. positivity ≥ 10% to <50%), and the third one was strongly positive (i.e. positivity ≥ 50%). We found 383 (91.2%) negative samples, 8 (1.9%) weakly positive, and 29 (6.9%) strongly positive.

Representative examples are reported in Figure 1 panels A, B, and C.

Inter-center distribution of patient's subgroups is shown in Table 1.

Table 1. TSLPR reactivity in BCP-ALL blasts at diagnosis analyzed in 6 different centers

TSLPR profile	Centers #						Overall
	1 n=86	2 n=28	3 n=128	4 n=79	5 n=54	6 n=46	n=421
Negative	79 (91.8%)	25 (89.3%)	115 (89.9%)	76 (96.2%)	48 (88.8%)	41(89.1%)	384 (91.2%)
Weakly positive	1 (1.2%)	1 (3.6%)	4 (3.1%)	0 (0.0%)	1 (1.9%)	1 (2.2%)	8 (1.9%)
Strongly Positive	6 (7.0%)	2 (7.1%)	9 (7.0%)	3 (3.8%)	5 (9.3%)	4 (8.7%)	29 (6.9%)

Centers:

1) M. Tettamanti Research Center, Monza, Italy.
2) Lab. Hemato-Oncology, Padua, Italy.
3) Children's Cancer Research Institute and St. Anna Children's Hospital, Vienna, Austria.
4) University of Zurich, Zurich, Switzerland.
5) Pediatric Hematology Oncology, Schneider Children's Medical Center of Israel, Israel.
6) Childhood Leukaemia Investigation Prague, Department of Paediatric Haematology and Oncology, Czech Republic.

We then studied the immunophenotypic profile of TSLPR among the 86 patients enrolled in Center 1 during initial screening. Fine tuning of fluorescence distribution of 79/86 patients that had been previously found negative for TSLPR (i.e. positivity <10%, Table 1) allowed us to further distinguish three different expression patterns: 1) TSLPR-stained blasts overlapping with control fluorescence (n 72, mean positivity 0.52% ± 0.52%, range 0.0% – 2.2%); 2) a second lump of TSLPR-stained blasts clearly shifted to the right (n 5, mean % positivity 2.72% ± 0.16%, range 2.5% – 2.9%), which was identical to the TSLPR weak pattern we

observed previously in the diagnostic screening apart from TSLPR positivity being less than 10%; 3) a third pattern showing two clearly distinct blast populations: a larger one, TSLPR-negative, and a smaller one, shifted to the right (n 2, positivity was 1% and 3.5%, respectively). Hereinafter, we will refer to these three patterns as fully negative, weakly positive (<10%), and partially positive, respectively. Representative examples are shown in Figure 1 panels D, E and F. Interestingly, one TSLPR weakly positive (<10%), and two TSLPR partially positive patients (UPNs 016, 013, and 039, respectively) showed low levels of P2RY8-CRLF2 expression (F.C. < 0.50), suggesting the presence of a minor CRLF2 sub clone (Supplemental Table 2).

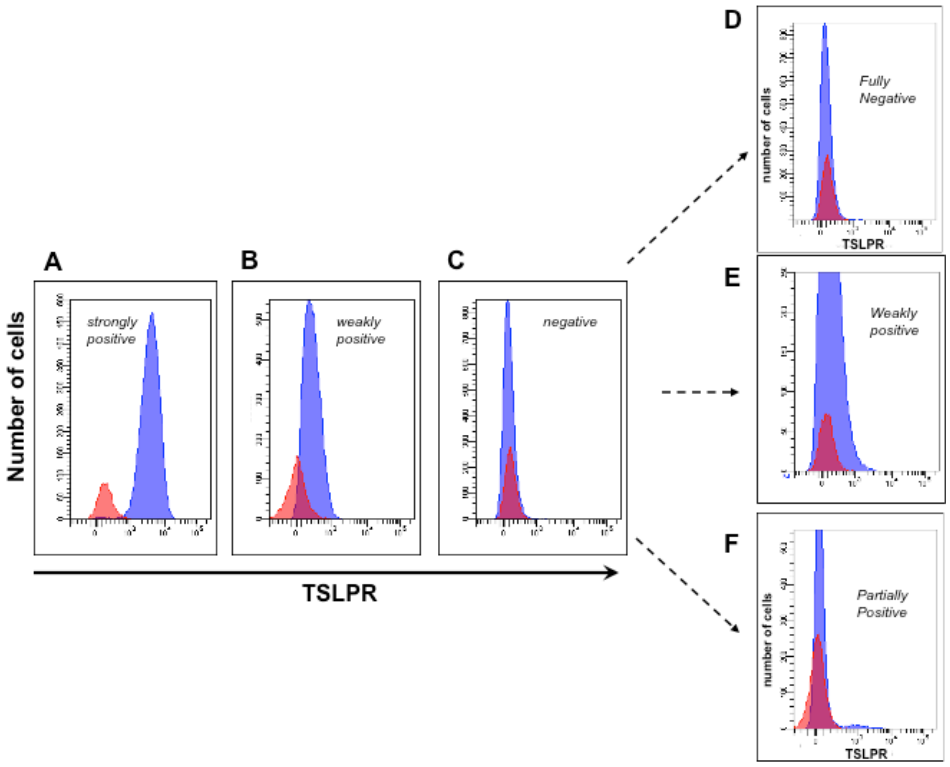

Figure 1. **Different patterns of TSLPR expression in representative BCP-ALL cases**. Strongly positive (positivity ≥50%, panel A), weakly positive (positivity ≥10% - <50%, panel B), and negative (positivity <10%, panel C). Fine tuning of TSLPR negative cases revealed three possible patterns of TSLPR positivity below the threshold of 10%: TSLPR fully negative (Panel D); weakly positive (Panel E); and partially positive (Panel F). The blue histograms represent the blast cells, the red ones represent the normal residual lymphocytes. Mean fluorescence intensity (MFI) of lymphocytes *vs* blasts were measured in each representative case: Panel A: 174.0 *vs* 3.899; Panel B: 149.0 *vs* 333; Panel C and panel D (same representative patient): 93.0 *vs* 97.0; Panel E: 88.0 *vs* 175.0; Panel F: 48.0 *vs* 1001.0

Next, *CRLF2* transcripts levels, *CRLF2* aberrations (*P2RY8-CRLF2*, *IGH@CRLF2*, F232C), and *JAK2* and *IL-7R* mutations were analyzed in 86 of our BCP-ALL samples collected in Center 1 as described previously (9). We detected *CRLF2* overexpression in 9.3% of BCP-ALL patients. Seventy-nine of these patients (91.8%) were negative for surface TSLPR expression as assessed by both FCM (<10%) and RQ-PCR (<20 FC), while only seven (8.1%) were concordantly positive. Intriguingly, one patient (UPN 084) showed overexpression of *CRLF2*, whereas TSLPR expression levels were undetectable (FC 33.2). However, this patient did not display *P2RY8-CRLF2* gene fusion. Two of the 7 patients with CRLF2 overexpression (UPN 30 and UPN 62), as assessed by both techniques, were negative for P2RY8-CRLF2 fusion and *IGH@-CRLF2* translocation. Conversely, 5 non-overexpressed cases showed barely detectable levels of *P2RY8-CRLF2* gene fusion. Thus, while our results seem to indicate a lack of correlation between genomic rearrangement and *CRLF2* overexpression, as assessed by PCR, they clearly show that *CRLF2*-overexpressing BCP-ALLs are characterized by a strong positivity for TSLPR when analyzed by FCM.

To determine a functional read out CRLF2 genomic rearrangements, MUTZ5 cells (*IGH@-CRLF2; JAK2 R683G*), MHH-CALL4 cells (*IGH@-CRLF2*; *JAK2 I682F*), or primary thawed cells were subject to phospho flow cytometric assay (see supplemental materials). Likewise, a total of 41 cryopreserved BCP-ALL samples obtained according to their availability

in cell banks – 28 were obtained from the consecutive series of Center 1 (total of 86) and 15 from a local cell bank – and viability after thawing (cut off ≥80%) were subject to phospho flow assay. Twenty-four BCP-ALL samples were TSLPR fully negative, 5 weakly positive (all of them <10%), and 12 strongly positive.

Next, we sought to determine basal and TSLP-induced pSTAT5 expression in CD45 intermediate/ CD10+/ CD7- blasts. The mean level of basal pSTAT5 detected in the three subgroups fully negative, weakly positive, and strongly positive for TSLPR was 0.71% ± 1.03% (range 0.0% – 4.0%), 2.64% ± 3.64% (range 0.2% – 9.0%), and 11.30% ± 18.31% (range 0.0% – 65.6%), respectively (p=0.0086). As expected, we observed much higher phosphorylation of STAT5 in the TSLPR strongly positive samples than the fully negative ones, with a mean of pSTAT5+ cells of 60.79% ± 12.79% (range 37.0% – 83.6%) and 2.95% ± 3.26% (range 0.2 %– 11.0%), respectively (p<0.0001) (Figure 2, Panel A). Furthermore, CRLF2 rearranged MUTZ5 and MHH-CALL4 cells showed aberrant TSLP-induced pSTAT5 compared with CRLF2 wt REH cells (data not shown). Interestingly, the group of 5 patients that were TSLPR weakly positive (<10%) showed enhanced pSTAT5 response with a mean of 22.36% ± 7.63% (range 16.0%- 34.3%), significantly higher than TSLPR fully negative patients (Figure 2, panel A, p< 0.0001). We also studied TSLP-induced signaling through the PI3K/AKT/mTOR pathway (S6, 4EBP1 and AKT) in 36 out of 41 BCP-ALL patients [9 TSLPR strongly positive, 5 weakly

positive (i.e. <10%), and 22 fully negative]. TSLP stimulation led to a significant increase in phosphorylation levels of S6, 4EBP1, and AKT in TSLPR strongly positive samples as compared to both the fully negative ($p < 0.0001$, $p = 0.0045$, and $p = 0.0040$, respectively) and weakly positive cases ($p = 0.0285$, $p =$ n.s., and $p =$ n.s., respectively), in good agreement with Tasian *et al* (14). Interestingly, as with pSTAT5, pS6 expression in TSLPR weakly positive patients was significantly higher than that observed in fully negative cases ($p= 0.0052$). In contrast, TSLP-induced phosphorylation of 4EBP1 and AKT473 in TSLPR weakly positive cases did not differ significantly from that observed in fully negative cases (Figure 2, panels, B, C and D). Contrary to what reported by Tasian *et al*, in our samples, we observed no significant difference in basal phosphorylation of S6, 4EBP1, and AKT that could be ascribed to differences in TSLPR expression levels.

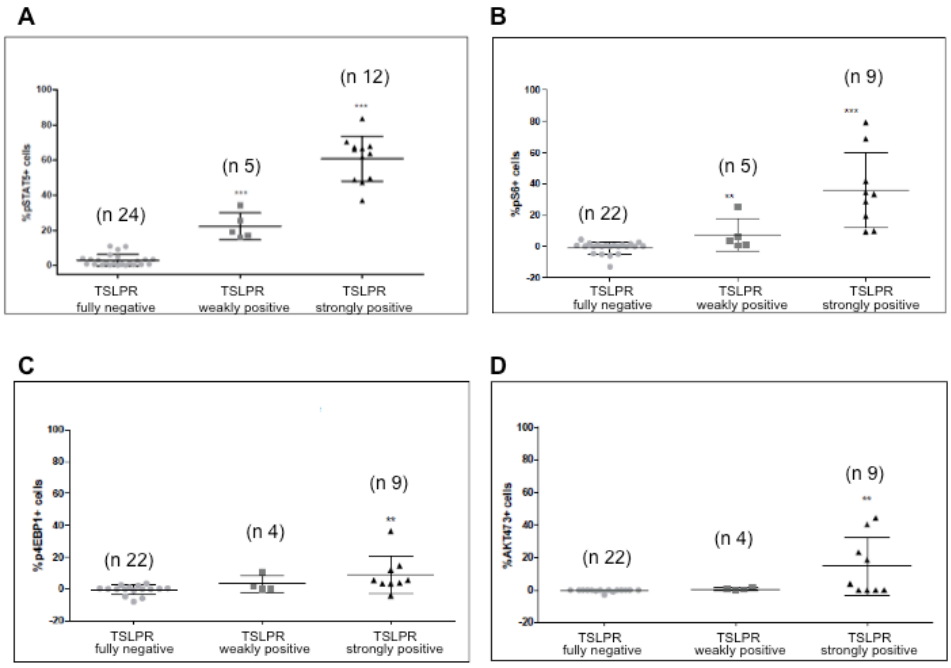

Figure 2. TSLP-induced phosphoprotein responses in BCP-ALL patients according to TSLPR expression (fully negative, weakly positive, or strongly positive). Distribution of positive cells is represented as scatter plot of 5th and 95th percentile with means and ranges. *** means p= 0.0001**.** Panel A shows pSTAT5 response (n 41); panels B, C, and D show TSLP-induced pS6, p4EBP1 and pAKT expression (n 36, 35, and 35 respectively). Data were normalized to the basal phosphorylation level of each phosphoprotein.

Strikingly, neither TSLPR fully negative nor TSLPR weakly positive cases showed mutations in *JAK2, CRLF2,* or *IL7Rα*. However, the observation of enhanced level of basal pSTAT5 in TSLPR weakly positive as compared to the fully negative patients may indicate the presence of a *CRLF2* rearranged sub clone below the level of detection in this latter subgroup of patients. In favor of this hypothesis, TSLPR strongly positive

patients displayed an heterogeneous mutational profile: 10/12 carried *P2RY8-CRLF2* rearrangement - one of these also carrying a mutation in *JAK* insertion L681-I682 insGL and another one carrying the *IL7Rα* mutation S185C; 1/12 displayed *IGH@-CRLF2* translocation and *JAK* point mutation R683G; 1/12 was wild type also for *P2RY8-CRLF2* and *IGH@CRLF2* rearrangements. SNP at codon 244 (rs151218732) of *CRLF2* as well as SNP at codon 244 (rs6897932) of *IL7Ralpha* were randomly distributed independent of TSLPR overexpression. A summary of phenotypic, molecular and signaling features of the analyzed patients is described in Supplemental Table 2.

To the best of our knowledge, this is the first report showing BCP-ALL patients weakly positive for TSLPR characterized by aberrant pSTAT5 and pS6 expression. We are currently investigating whether this signature refers to the presence of minor clones or is due to additional mechanisms driving aberrant JAK/STAT and PI3K/mTOR signal transduction.

In this regard, Tasian *et al.*, has pointed to a potential diagnostic value of TSLP-mediated phosphosignaling in patients weakly positive for TSLPR staining (i.e. TSLPR-dim) as it would be a *bona fide* functional read out of the CRLF2 *status*. However, he did not provide any evidence of TSLPR-dim patients. In our study, we demonstrate the existence of CRLF2 weakly positive patients characterized by an activated phosphosignaling cascade. Thus, it is possible that Tasian *et al.* failed to identify TSLPR

weakly positive patients because TSLPR expression was assessed after fixation and permeabilization, a procedure that is known to mask the presence of several surface antigens.

In summary, screening of TSLPR expression in BCP-ALL patients can be successfully achieved using standardized FCM protocols. FCM and PCR are highly concordant in detecting both *CRLF2* overexpressed and non-overexpressed patients. However, patients characterized by a weak or partially positive TSLPR expression associated with aberrant pSTAT5 and pS6 expression could only be detected by FCM analysis. Thus, our findings might prove useful in refining future diagnostic screening of ALL patients and help develop novel CRLF2 inhibitors-based therapies. In this regard, it is important to point out that approximately 50% of ALL patients with a Ph-like gene expression profile, which is associated with a poor outcome, have CRLF2 rearrangements[15].

SUPPLEMENTARY FIGURES

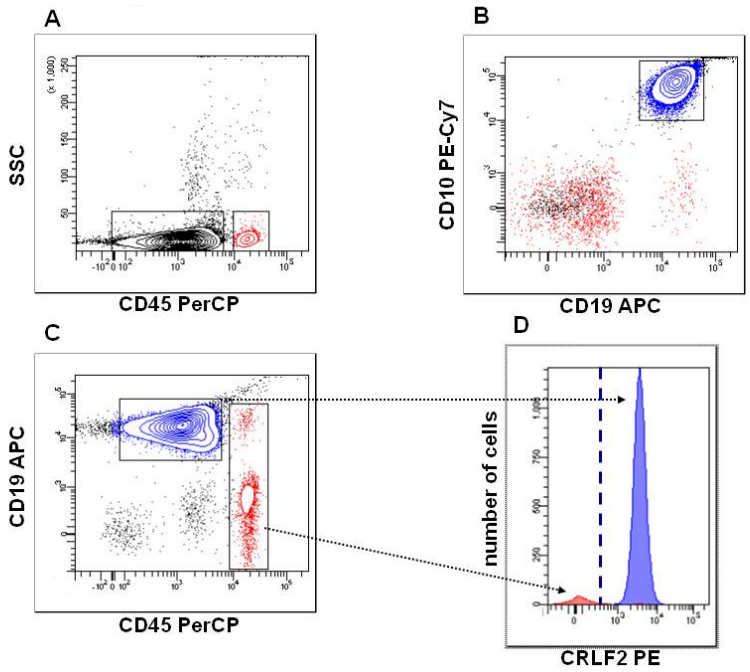

Supplemental Figure 1. Gating strategy employed to measure TSLPR surface expression in blast cells. Immature cells (black) were distinguished from mature lymphocytes (red) in SCC/CD45 dual dot plot (panel A). Within immature cells leukemic blasts (blue) are distinguished by CD19+/CD10+/CD45 intermediate immunophenotype (panel B). Based on CD19/CD45 expression (panel C), TSLPR expression is assessed as % of positive cells by setting the histogram marker exactly at the right end of mature lymphocytes peak (panel D). In all samples prevalence of mature lymphocytes was always ≥ 1.5%. Staining to measure TSLPR surface expression was performed using the combination: CRLF2PE/CD45PerCP/CD19APC/CD10PE-cy7/CD7ECD

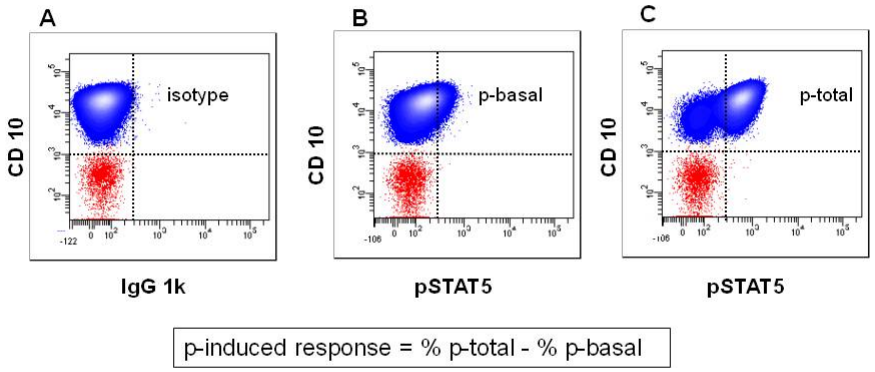

Supplemental Figure 2. Representative phosphoflow analysis in leukemic blast population (blue) gated on CD45-intermediate/SSC-low/CD10+ cells to measure signalling response after cytokine stimulation. Positivity threshold was established by an isotype IgG phospho-specific antibody (panel A). Basal and total levels of p-proteins were calculated as % of positive cells in unstimulated (panel B) and stimulated (panel C) conditions, respectively. p-induced response was then calculated by the indicated formula

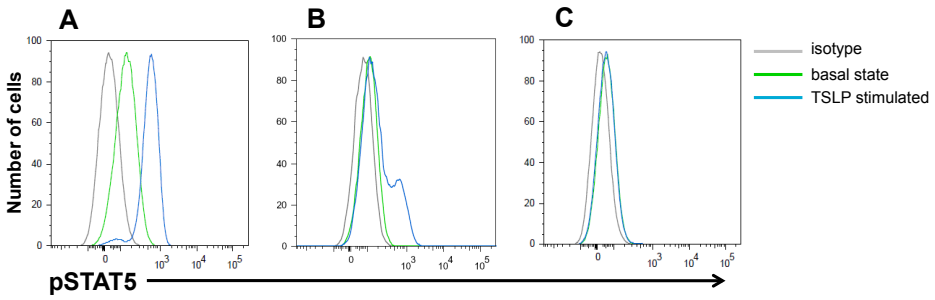

Supplemental Figure 3. TSLP-induced pSTAT5 response in three representative BCP-ALL patients. TSLP-induced pSTAT5 response (blue line) is compared to basal state (green line) and isotype control (grey line) by overlaying histograms. Hyperactive responses induced in a TSLPR strongly positive and in a TSLPR weakly positive patient are shown in Panel A and B respectively; Panel C shows a TSLPR fully negative patient with no pSTAT5

response. Of note pSTAT5 fluorescence intensity is shifted in TSLPR weakly positive blasts in a manner similar to that observed in TSLPR strongly positive blasts (MFI 731 vs 612), even though the proportion of shifted cells is minor (25.5% vs 67.8%).

SUPPLEMENTARY TABLES

Supplemental Table 1. Characteristics of selected antibodies and staining combinations for TSLPR immunophenotypic screening and phosphoflow cytometry assay.

Selected Antibodies					
Reactivity	**Clone**	**Fluorochrome**	**Source**	**Ig class**	**Use**
TSLPR	1D3	PE	Biolegend	mouse IgG2aλ	10µl/1x10^{6}cells
TSLPR	1B4	PE	Biolegend	Mouse IgG1K	10µl/1x10^{6}cells
CD19	SJ25C1	APC	BD	mouse IgG1 k	3µl/1x10^{6}cells
CD10	HI10a	PE	Biolegend	mouse IgG1 k	2µl/1x10^{6}cells
CD10	HI10a	PE-CY7	BD	mouse IgG1 k	2µl/1x10^{6}cells
CD45	2D1	PerCP	BD	mouse IgG1 k	2µl/1x10^{6}cells
CD7	8H8	ECD	Beckman Coulter	mouse IgG2a	1µl/1x10^{6}cells
IgG1 k Isotype control	MOPC-21	Alexa Fluor 488	BD	mouse IgG1 k	10µl/1x10^{6}cells
IgG1 k Isotype control	MOPC-21	Alexa Fluor 647	BD	mouse IgG1 k	10µl/1x10^{6}cells
p-Stat5 (Y694)	47	Alexa Fluor 488	BD	mouse IgG1	10µl/1x10^{6}cells
p-S6 (pS235/pS236)	N7-548	Alexa Fluor 647	BD	mouse IgG1 k	10µl/1x10^{6}cells
IgG Isotype control	236B4	Alexa Fluor 488	Cell Signaling	rabbit IgG	2µl/1x10^{6}cells
IgG Isotype control	DA1E	Alexa Fluor 647	Cell Signaling	rabbit IgG	2µl/1x10^{6}cells
p-4E-BP1 (Thr37/46)	236B4	Alexa Fluor 488	Cell Signaling	rabbit IgG	2µl/1x10^{6}cells
anti p-AKT (S473)	D9E	Alexa Fluor 647	Cell Signaling	rabbit IgG	8µl/1x10^{6}cells

Staining Panels					
Immunophenotype					
Tube 1	TSLPR PE	CD45 PerCP	CD10 PE-CY7	CD19 APC	CD7 ECD
Phosphoflow					
Tube 1	IgG1 k Isotype control Alexa 488	IgG1 k Isotype control Alexa 647	CD10 PE	CD45 PerCP	CD7
Tube 2	p-Stat5 Alexa 488	p-S6 Alexa 647	CD10 PE	CD45 PerCP	CD7
Tube 3	p-4E-BP1 Alexa 488	p-AKT Alexa 647	CD10 PE	CD45 PerCP	CD7

Supplemental Table 2: Phenotypic, molecular, and signaling features in 101 patients according to surface TSLPR expression

UPN	TSLPR pattern	TSLPR surface expression (%)*	CRLF2 RQ-PCR overexpression**	CRLF2 rearrangement	CRLF2 mutation	JAK2 mutation	IL7Rα mutation	pSTAT5 response	pS6 response	p4EBP1 response	pAKT response
034	Strongly positive	99.9	Yes (132.9)	P2RY8-CRLF2	wt	neg	wt	83.6%	33.3%	36.2%	23.2%
059		99.9	Yes (108.8)	P2RY8-CRLF2	wt[c]	neg	wt	67.8%	68,8%	14,7%	18,7%
099		99.1	Yes (127.2)	P2RY8-CRLF2	wt	neg	wt	47.1%	34,4%	5,5%	0,0%
096		98.7	Yes (1032.7)	IGH@CRLF2	wt	R683G	wt	37.0%	41,6%	3,9%	40,4%
090		95.7	Yes (44.0)	P2RY8-CRLF2	wt	neg	wt	70.4%	n.t.	n.t.	n.t.
091		96.0	Yes (300.0)	P2RY8-CRLF2	wt	neg	wt	61.8%	n.t.	n.t.	n.t.
031		96.3	Yes (102.8)	P2RY8-CRLF2	wt	neg	S185C, T244I	66.0%	79,3%	3,5%	44,3%
032		95.2	Yes (397.6)	P2RY8-CRLF2	wt	L681-I682 insEA	wt[#]	67.3%	28,6%	3,4%	0,0%
097		95.1	Yes (102.2)	P2RY8-CRLF2	wt	neg	wt	49.6%	19,4%	-4,2%	0,0%
062		85.0	Yes (22.1)	wt	wt	neg	wt[#]	66.5%	9,7%	5,4%	0,0%
095		81.8	Yes (201.3)	P2RY8-CRLF2	wt	neg	wt	63.7%	9,4%	11.9%	3,8%
087		78.2	Yes (30.0)	P2RY8-CRLF2	wt	neg	wt	48.7%	n.t.	n.t.	n.t.
030		71.2	Yes (207.9)	wt	wt	neg	wt	n.t.	n.t.	n.t.	n.t.
013	Partially positive	3.5	No (2.49)	P2RY8-CRLF2 low[§]	wt	neg	wt	n.t.	n.t.	n.t.	n.t.
039		1.0	No (3.3)	P2RY8-CRLF2 low[§]	wt	neg	wt	n.t.	n.t.	n.t.	n.t.
073	Weakly positive (≥ 10%)	11.3	Yes (27.7)	wt (IGH@CRLF2 n.t.)	wt	neg	wt[#]	n.a.	n.a.	n.a.	n.a.
047	Weakly positive (<10%)	2.9	No (6.2)	wt	wt	neg	wt[#]	34.3%	25.4%	0.4%	1.9%
016		2.8	No (1.4)	P2RY8-CRLF2 low[§]	wt	neg	wt[#]	25.5%	1.0%	n.t.	n.t.
078		2.8	No (4.1)	wt	wt	neg	wt	16.0%	3.5%	10.7%	0.5%
067		2.6	No (12.0)	wt	wt	neg	wt[#]	19.0%	6.1%	1.7%	0.4%
037		2.5	No (2.4)	wt	wt	neg	wt[#]	17.0%	0.5%	0.0%	0.0%
004	Fully negative	2.2	No (1.8)	wt	wt	neg	wt	3.5%	0.0%	n.t.	n.t.
072		2.2	No (4.0)	wt	wt	neg	wt	1.2%	1.5%	0.3%	-0.5%
035		1.6	No (2.0)	wt	wt[a]	neg	wt	n.t.	n.t.	n.t.	n.t.
008		1.6	No (3.5)	wt	wt	neg	wt	n.t.	n.t.	n.t.	n.t.
028		1.5	No (2.3)	wt	wt	neg	wt[#]	n.t.	n.t.	n.t.	n.t.
055		1.5	No (0.6)	wt	wt[a]	neg	wt	0.7%	1.0%	n.t.	n.t.
049		1.5	No (9.3)	wt	wt	neg	wt	n.t.	n.t.	n.t.	n.t.
080		1.5	No (0.4)	wt	wt	neg	wt[#]	n.t.	n.t.	n.t.	n.t.
069		1.4	No (1.2)	wt	n.t.	n.t.	n.t.	n.t.	n.t.	n.t.	n.t.
094		1.2	No (4.0)	wt	wt	neg	wt	1.5%	-4.7%	0.2%	0.0%
061		1.1	No (0.1)	wt	wt	neg	wt[#]	0.4%	1.8%	3.5%	0.0%
079		1.0	No (0.7)	wt	wt	neg	wt	n.t.	n.t.	n.t.	n.t.
045		0.9	No (1.2)	wt	wt[a]	neg	wt[#]	3.0%	0.6%	n.t.	n.t.
086		0.9	No (0.1)	wt	wt	neg	wt[#]	n.t.	n.t.	n.t.	n.t.
082		0.9	No (3.6)	wt	n.t.	n.t.	n.t.	n.t.	n.t.	n.t.	n.t.
071	Fully negative	0.8	No (6.1)	wt	wt	neg	wt	n.t.	n.t.	n.t.	n.t.
052		0.8	No (0.7)	wt	wt	neg	wt	n.t.	n.t.	n.t.	n.t.
041		0.7	No (2.6)	P2RY8-CRLF2 low[§]	wt	neg	wt	n.t.	n.t.	n.t.	n.t.
036		0.7	No (0.3)	wt	wt	neg	wt	n.t.	n.t.	n.t.	n.t.
048		0.7	No (18.8)	wt	wt	neg	wt	n.t.	n.t.	n.t.	n.t.
019		0.6	No (4.1)	wt	wt	neg	wt[#]	n.t.	n.t.	n.t.	n.t.
101		0.6	No (0.2)	wt	wt	neg	wt[#]	0.2%	-5.9%	0.5%	-1.0%
066		0.6	No (3.2)	wt	wt	neg	wt	11.0%	0.1%	-7.9%	0.0%
046		0.6	No (2.3)	P2RY8-CRLF2 low[§]	wt	neg	wt	4.0%	n.t.	n.t.	n.t.
042		0.6	No (0.3)	wt	wt	neg	wt[#]	0.3%	0.0%	n.t.	n.t.
077		0.6	No (5.1)	wt	wt	neg	wt	n.t.	n.t.	n.t.	n.t.
002		0.6	No (0.5)	wt	wt	neg	wt	n.t.	n.t.	n.t.	n.t.
010		0.6	No (0.9)	wt	wt	neg	wt	n.t.	n.t.	n.t.	n.t.
001		0.5	No (0.2)	wt	wt	neg	wt	n.t.	n.t.	n.t.	n.t.
076		0.5	No (3.7)	wt	wt	neg	wt[#]	n.t.	n.t.	n.t.	n.t.
060		0.5	No (0.2)	wt	wt	neg	wt	0.2%	-5.1%	0.8%	0.0%
081		0.5	No (0.2)	wt	wt	neg	wt[#]	0.4%	2.5%	1.9%	0.0%
098		0.5	No (1.1)	wt	wt	neg	wt[#]	0.6%	0.0%	-4.7%	0.0%
038		0.5	No (0.6)	wt	wt	neg	wt	4.7%	0.7%	0.0%	0.0%
050		0.5	No (0.0)	wt	wt	neg	wt[#]	n.t.	n.t.	n.t.	n.t.
025		0.5	No (0.7)	wt	wt	neg	wt	n.t.	n.t.	n.t.	n.t.
100		0.4	No (0.1)	wt	wt[a]	neg	wt[#]	2.5%	0.0%	-0.9%	-2.8%
068		0.4	No (2.6)	wt	wt[a]	neg	wt[#]	n.t.	n.t.	n.t.	n.t.
093		0.4	No (5.4)	wt	wt	n.a.	wt	0.8%	-13.1%	2.3%	0.0%
092		0.4	No (5.9)	wt	wt	neg	wt[#]	3.3%	4.4%	-5.9%	0.0%
088		0.4	No (0.5)	wt	wt	n.a.	wt	6.1%	-5.0%	0.0%	0.0%
051		0.4	No (0.0)	wt	wt[a]	neg	wt	n.t.	n.t.	n.t.	n.t.
089		0.3	No (3.3)	wt	wt	neg	wt	1.0%	n.t.	n.t.	n.t.
075		0.3	No (2.1)	wt	wt	neg	wt	n.t.	n.t.	n.t.	n.t.
070		0.3	No (1.6)	wt	wt	neg	wt[#]	n.t.	n.t.	n.t.	n.t.
063		0.3	No (0.0)	wt	wt	neg	wt[#]	n.t.	n.t.	n.t.	n.t.
058		0.3	No (0.9)	wt	wt	neg	wt	n.t.	n.t.	n.t.	n.t.
018		0.3	No (0.2)	wt	wt	neg	wt[#]	n.t.	n.t.	n.t.	n.t.
003		0.3	No (0.1)	wt	wt[a]	neg	wt	n.t.	n.t.	n.t.	n.t.
023		0.2	No (2.8)	wt	wt	neg	wt	9.1%	0.9%	0.0%	0.0%
022		0.2	No (1.2)	wt	wt[a]	neg	wt[#]	10.8%	0.0%	0.0%	0.0%
084		0.2	Yes (33.2)	wt	wt	neg	wt	1.4%	0.0%	n.t.	n.t.
026		0.2	No (0.1)	wt	wt	neg	wt[#]	n.t.	n.t.	n.t.	n.t.
065		0.2	No (4.1)	wt	wt[a]	neg	wt	n.t.	n.t.	n.t.	n.t.
064		0.2	No (0.2)	wt	wt	neg	wt[#]	n.t.	n.t.	n.t.	n.t.
005		0.2	No (6.5)	wt	wt	neg	wt[#]	n.t.	n.t.	n.t.	n.t.
054		0.2	No (0.7)	wt	wt	neg	wt	n.t.	n.t.	n.t.	n.t.

040		0.2	No (0.1)	wt	wt	neg	wt[#]	n.t.	n.t.	n.t.	n.t.
033		0.2	No (0.2)	wt	wt	neg	wt[#]	n.t.	n.t.	n.t.	n.t.
085		0.1	No (0.1)	wt	wt	neg	wt	3.4%	0.7%	0.6%	n.t.
044		0.1	No (0.5)	wt	wt	neg	wt[#]	0.9%	0.2%	n.t.	n.t.
083		0.1	No (0.1)	wt	wt	neg	wt	n.t.	n.t.	n.t.	n.t.
074		0.1	No (0.4)	wt	wt	neg	wt	n.t.	n.t.	n.t.	n.t.
057		0.1	No (0.1)	wt	wt	neg	wt	n.t.	n.t.	n.t.	n.t.
056		0.1	No (0.1)	wt	wt[°]	neg	wt	n.t.	n.t.	n.t.	n.t.
053		0.1	No (0.0)	wt	wt	neg	wt[#]	n.t.	n.t.	n.t.	n.t.
043		0.1	No (0.2)	wt	wt	neg	wt[#]	n.t.	n.t.	n.t.	n.t.
029	Fully negative	0.1	No (0.1)	wt	wt	neg	wt	n.t.	n.t.	n.t.	n.t.
027		0.1	No (0.7)	wt	wt	neg	wt	n.t.	n.t.	n.t.	n.t.
021		0.1	No (0.1)	wt	wt[°]	neg	wt	n.t.	n.t.	n.t.	n.t.
020		0.1	No (1.5)	wt	wt[°]	neg	wt[#]	n.t.	n.t.	n.t.	n.t.
011		0.1	No (0.8)	wt	n.t.	n.t.	n.t.	n.t.	n.t.	n.t.	n.t.
024		0.1	No (0.5)	wt	n.t.	n.t.	n.t.	n.t.	n.t.	n.t.	n.t.
017		0.1	No (0.3)	wt	wt	neg	wt	n.t.	n.t.	n.t.	n.t.
014		0.1	No (0.3)	wt	wt[°]	neg	wt[#]	n.t.	n.t.	n.t.	n.t.
009		0.1	No (15.4)	wt	wt	neg	wt[#]	n.t.	n.t.	n.t.	n.t.
007		0.1	No (0.0)	wt	wt[°]	neg	wt	n.t.	n.t.	n.t.	n.t.
015		0.0	No (1.7)	wt	wt[°]	neg	wt	n.t.	n.t.	n.t.	n.t.
012		0.0	No (0.2)	wt	wt	neg	wt	n.t.	n.t.	n.t.	n.t.
006		0.0	No (0.2)	wt	wt	neg	wt[#]	n.t.	n.t.	n.t.	n.t.

n.t.= not tested; wt = wild type; n.a. = not available

* patients are listed by descendent order of values

** CRLF2 was considered over expressed in patients with levels of gene expression 20 times higher than the median of the considered cohort as described in Palmi *et al* (see ref.9)].

[§] P2RY8-CRLF2 Fold Change < 0.50

[#]These patients showed a T244I polymorphism

[°]These patients showed a V244M polymorphism

note: Among patients tested for p-STAT5, UPNs from 1 to 86 are patients from the prospective series of 421, UPNs from 87 to 101 are patients selected retrospectively from the cell bank

SUPPLEMENTARY METHODS

Phospho flow cytometry

MUTZ5 cells harboring IGH@-CRLF2 translocation and JAK2 R683G mutation, MHH-CALL4 displaying IGH@-CRLF2 translocation and JAK2 I682F mutation, or primary thawed cells were subject to phospho flow cytometric assay. For this purpose, cells were starved in X-vivo medium and rested at 37°C for 16 hours or 1 hour. Then, cells were stimulated with rh-TSLP (10 ng/mL) for 30 minutes at 37°C to allow signal

transduction, and treated according to an established internal protocol. Starved cells were fixed with paraformaldehyde (1.5%) and permeabilized with 90% ice-cold methanol and then incubated with anti-phospho-protein-directed MoAbs (or isotype matched IgG) and surface antigen-directed MoAbs. Characteristics of MoAbs and staining combinations are described in Supplemental Table 1. Cells were acquired on a FACSaria™ flow cytometer (BD) equipped with 488-nm, 633-nm and 405-nm lasers. Data were collected (at least 100000 events per tube) and analyzed using DIVA™ software (BD). Positivity threshold for phosphoprotein expression was established by the use of isotype IgG-negative control (Supplemental Figure 2 panel A). Basal levels of each phosphoprotein were then calculated as percentage (%) of phosphoprotein positive (p-positive) cells in unstimulated conditions (Supplemental Figure 2 panel B). Response to each cytokine (rhTSLP) was calculated by subtracting the % of p-positive cells in the basal state from that obtained upon exposure to cytokine (Supplemental Figure 2 panel C).

Quantitative expression of CRLF2

CRLF2 transcript levels on diagnostic samples were analyzed using TaqMan Gene Expression Assay Hs00913509_s1 (Applied Biosystems, Foster City,CA,USA) following the manufacturer's instructions. The presence and level of the fusion transcript P2RY8-CRLF2 was analyzed by Universal Probe Library System (UPL) (Roche Diagnostic, Basel,

Switzerland) as well as the housekeeping GUS gene transcript, tested as internal control. Optimal primers and probe for P2RY8-CRLF2 and GUS amplification were selected using the Roche ProbeFinder software (https://www.roche-appliedscience.com/sis/rtpcr/upl). In particular, for P2RY8-CRLF2 amplification we used primers designed in the first exon of P2RY8 (5'-gctacttctgccgctgctt-3') and in the first exon of CRLF2 (5'-gcagaaagacggcagctc-3') with the UPL probe n. 28 (Roche UPL cat. n. 04687604001). Each cDNA sample (20 ng RNA equivalent) was tested in duplicate (Ct range between replicates <1.5). The amplification reaction was performed on the 7900HT FAST Real Time PCR System instrument (Applied Biosystems) for CRLF2 expression and on the Light Cycler 480 (Roche) for P2RY8-CRLF2 with the following protocol: initial step at 95°C for 10 min, then 50 cycles at 95°C for 15s and at 60°C for 1 min. Relative gene expression (indicated as fold change) was quantified by the 2-DDCt method (22). The DDCts for CRLF2 expression were calculated by subtracting the median of the DCt of a published cohort of 464 BCP-ALL patients enrolled in Italy in the AIEOP-BFM ALL2000 study from February 2003 to July 2005 (22) to the DCt of each sample. The DDCts for P2RY8-CRLF2 expression were calculated by subtracting the DCt of a selected positive patient external to this cohort to the DCt of each sample.

Mutational screening of JAK2, CRLF2 and IL7Rα

Mutational screening of *JAK2, CRLF2* and *IL7Rα* was performed in 82/86 consecutive patients and in 15/15 patients (13/15 for JAK2) selected retrospectively from Monza's cell bank for phospho flow analysis. High Resolution Melting (HRM) analysis was applied to identify JAK2 mutations in exon 16 using HRM Master (Roche Diagnostics) as previously described (21). Sequencing of CRLF2 exon 6 and IL7R exons 5 and 6 was performed by Sanger sequencing of PCR products from patients DNA after whole genome amplification using GenomePhi V2 DNA Amplification Kit (GE Healthcare Life Science); we designed the following primers for CRLF2-F (5'-AGGGAGACTGGTTAGGGATGA-3'), CRLF2-R (5'-TGGGCATTGTATGGAAACTG -3') and for IL7R exon 5 IL7R-F (5'-GCAACACCTCTTTTCCATC-3') and IL7R-R (5'-GGGAACAAAAACTCTACCACCA-3') and exon 6 IL7R-F(5'-TGCATGGCTACTGAATGCTC-3') and IL7R-R (5'-CCCACACAATCACCCTCTTT- 3').

Statistical analysis

The parametric Student's T-test was used to determine the significance of the differences among subgroups of patients with different expression of TSLPR. p values less than 0.05 were considered statistically significant.

ACKNOWLEDGEMENTS

This work was supported by Fondazione Tettamanti, Fondazione Benedetta è la Vita ONLUS, Comitato M.L. Verga, Fondazione Città della Speranza and Grant Ric. Corrente OBG 2006/02/R/001822, Associazione Italiana per la Ricerca sul Cancro (AIRC; to ABi and FL), Fondazione Cariplo (ABi), Ministero dell'Istruzione, Università e Ricerca (MIUR; ABi). We also thank the AIEOP centers for their support. We would like to thank Dr. Chiara Buracchi for her technical support in preparing the manuscript.

CORRESPONDENCE TO:
Prof. Andrea Biondi, MD
M. Tettamanti Research Center, University of Milano Bicocca
Via Pergolesi, 33 20900 Monza (MB)
tel. +39 039 2333661 fax +39 039 2332167
e-mail abiondi.unimib@gmail.com; andrea.biondi@unimib.it

REFERENCES

1. Mullighan CG, Collins-Underwood JR, Phillips LA, Loudin MG, Liu W, Zhang J, et al. Rearrangement of CRLF2 in B-progenitor- and Down syndrome-associated acute lymphoblastic leukemia. Nat Genet. 2009 Nov;41(11):1243-6.
2. Russell LJ, Capasso M, Vater I, Akasaka T, Bernard OA, Calasanz MJ, et al. Deregulated expression of cytokine receptor gene, CRLF2, is involved in lymphoid transformation in B-cell precursor acute lymphoblastic leukemia. Blood. 2009 Sep 24;114(13):2688-98.
3. Harvey RC, Mullighan CG, Chen IM, Wharton W, Mikhail FM, Carroll AJ, et al. Rearrangement of CRLF2 is associated with mutation of JAK kinases, alteration of IKZF1, Hispanic/Latino ethnicity, and a poor outcome in pediatric B-progenitor acute lymphoblastic leukemia. Blood. 2010 Jul 1;115(26):5312-21.
4. Roll JD, Reuther GW. CRLF2 and JAK2 in B-progenitor acute lymphoblastic leukemia: a novel association in oncogenesis. Cancer Res. 2010 Oct 1;70(19):7347-52.
5. Attarbaschi A, Morak M, Cario G, Cazzaniga G, Ensor HM, te Kronnie T, et al. Treatment outcome of CRLF2-rearranged childhood acute lymphoblastic leukaemia: a comparative analysis of the AIEOP-BFM and UK NCRI-CCLG study groups. Br J Haematol. 2012 Sep;158(6):772-7.
6. Cario G, Zimmermann M, Romey R, Gesk S, Vater I, Harbott J, et al. Presence of the P2RY8-CRLF2 rearrangement is associated with a poor prognosis in non-high-risk precursor B-cell acute lymphoblastic leukemia in children treated according to the ALL-BFM 2000 protocol. Blood. 2010 Jul 1;115(26):5393-7.
7. Chen IM, Harvey RC, Mullighan CG, Gastier-Foster J, Wharton W, Kang H, et al. Outcome modeling with CRLF2, IKZF1, JAK, and minimal residual disease in pediatric acute lymphoblastic leukemia: a Children's Oncology Group study. Blood. 2012 Apr 12;119(15):3512-22.
8. Ensor HM, Schwab C, Russell LJ, Richards SM, Morrison H, Masic D, et al. Demographic, clinical, and outcome features of children with acute lymphoblastic leukemia and CRLF2 deregulation: results from the MRC ALL97 clinical trial. Blood. 2011 Feb 17;117(7):2129-36.
9. Palmi C, Vendramini E, Silvestri D, Longinotti G, Frison D, Cario G, et al. Poor prognosis for P2RY8-CRLF2 fusion but not for CRLF2 over-expression in children with intermediate risk B-cell precursor acute lymphoblastic leukemia. Leukemia. 2012 Oct;26(10):2245-53.

10. van der Veer A, Waanders E, Pieters R, Willemse ME, Van Reijmersdal SV, Russell LJ, et al. Independent prognostic value of BCR-ABL1-like signature and IKZF1 deletion, but not high CRLF2 expression, in children with B-cell precursor ALL. Blood. 2013 Oct 10;122(15):2622-9.
11. Isaksen DE, Baumann H, Trobridge PA, Farr AG, Levin SD, Ziegler SF. Requirement for stat5 in thymic stromal lymphopoietin-mediated signal transduction. J Immunol. 1999 Dec 1;163(11):5971-7.
12. Levin SD, Koelling RM, Friend SL, Isaksen DE, Ziegler SF, Perlmutter RM, et al. Thymic stromal lymphopoietin: a cytokine that promotes the development of IgM+ B cells in vitro and signals via a novel mechanism. J Immunol. 1999 Jan 15;162(2):677-83.
13. Rochman Y, Kashyap M, Robinson GW, Sakamoto K, Gomez-Rodriguez J, Wagner KU, et al. Thymic stromal lymphopoietin-mediated STAT5 phosphorylation via kinases JAK1 and JAK2 reveals a key difference from IL-7-induced signaling. Proc Natl Acad Sci U S A. 2010 Nov 9;107(45):19455-60.
14. Tasian SK, Doral MY, Borowitz MJ, Wood BL, Chen IM, Harvey RC, et al. Aberrant STAT5 and PI3K/mTOR pathway signaling occurs in human CRLF2-rearranged B-precursor acute lymphoblastic leukemia. Blood. 2012 Jul 26;120(4):833-42.
15. Roberts KG, Morin RD, Zhang J, Hirst M, Zhao Y, Su X, et al. Genetic alterations activating kinase and cytokine receptor signaling in high-risk acute lymphoblastic leukemia. Cancer Cell. 2012 Aug 14;22(2):153-66.

Chapter 3

Manuscript in preparation

Single-cell analysis uncovers functional targetable subpopulations in CRLF2 rearranged B-cell precursor acute lymphoblastic leukemia

Jolanda Sarno[1], Angela M Savino[1,5], Stefania Pinto[1], Cristina Bugarin[1], Chiara Buracchi[1], Astraea Jager[2], Chiara Palmi[1], Ruth C Barber[3], Daniela Silvestri[4], Shai Israeli[5], Martin JS Dyer[6], Giovanni Cazzaniga[1], Garry P Nolan[2], Andrea Biondi[1], Kara L Davis[2,7]* and Giuseppe Gaipa[1]*

* Co-senior authors

[1] Pediatric Clinic, University of Milano Bicocca, M. Tettamanti Research Center, Monza, Italy
[2] Baxter Laboratory in Stem Cell Biology, Department of Microbiology and Immunology, Stanford University, Stanford, CA, USA
[3] Leicester Drug Discovery & Diagnostic Centre, University of Leicester, United Kingdom
[4] Biostatistics and Clinic Epidemiology Center, University of Milano Bicocca, Monza, Italy
[5] Cancer Research Center, Sheba Medical Center, Ramat Gan, Israel
[6] Ernest and Helen Scott Haematological Research Institute, University of Leicester, Leicester, United Kingdom
[7] Hematology and Oncology, Department of Pediatrics, Stanford University, Stanford, CA, USA

ABSTRACT

Rearrangements of the *CRLF2* gene are present in 7-15% of childhood B-cell Precursor Acute Lymphoblastic Leukemia (BCP-ALL), and are correlated with poor response to the current chemotherapy and high rates of relapse. Thus, there is an urgent need to understand the biochemical mechanisms underlying CRLF2-associated treatment failure and to investigate alternative therapies. Taking advantage of the high dimensional single cell mass cytometry (CyTOF) we aim to dissect, with previously unattainable resolution, the CRLF2-driven signaling in primary BCP-ALL samples and to test different treatment agents. Twelve BCP-ALL primary samples, 6 *CRLF2* rearranged *(CRLF2r)* and 6 *CRLF2* wild type (*CRLF2wt*), were investigated and the expression of 24 phenotypic and 18 functional proteins were measured at single cell level using CyTOF.

We observed at diagnosis aberrant TSLP-induced activation of pSTAT5, prpS6, pERK and pCREB in *CRLF2r* as compared to *CRLF2wt* patients that were inhibited, although at different levels, by Dasatinib, Ruxolitinib and by the an anti-TSLPR monoclonal antibody (A10 mAb). Dissecting the TSLP-related signaling we identified a TSLPR-positive cell subset with heterogeneous capability to respond to the TSLP since they were responsive in term of prpS6 activation even thought they did not activate pSTAT5. Interestingly the treatment with Dasatinib or with A10 mAb was able to abrogate the prpS6 activation. In 3 additional *CRLF2r* primary samples, we investigated signaling profile of residual blasts

(MRD) collected at Day 8 and Day 15 of remission induction therapy demonstrating the maintenance of TSLPR expression in the MRD cells.
Residual blasts were still able to respond to TSLP, and the STAT5 activation was effectively inhibited by A10 mAb and Ruxolitinib.
We then tested, in BaF3 CRLF2/IL7Rα expressing cells, the *in vitro* efficacy of different kinase inhibitor (KI) treatments as well as the A10 anti-TSLPR mAb alone and in combinations. Combinatorial treatment showed synergic effect of JAK/STAT inhibitors (Ruxolitinib or A10 mAb) with either Dasatinib or NVP-BEZ235 (CI<1) in the induction of apoptosis.
Overall, our data suggest an heterogeneity of TSLPR-related signaling network in *CRLF2r* cells, both at diagnosis and at early time-point of induction therapy, that can be optimally inhibited by KIs or anti-TSLPR mAb treatments. Yet, the concomitant blockade of JAK/STAT pathway either with BCR or PI3K pathways is able to induce apoptosis suggesting a rationale for testing combinatorial inhibitory regimen rather then single agent in *CRLF2r* BCP-ALLs.

INTRODUCTION

B-cell precursor acute lymphoblastic leukemia (BCP-ALL) is a heterogeneous disease resulting from the accumulation of genetic alterations in B lymphoid precursor cells and represents the most common malignant disease in childhood[1,2]. Five-year survival rates now exceed 85% in children, however the survival following relapse is still

poor[3,4]. In BCP-ALL one subgroup of patients with poor clinical prognosis are those patients harboring alterations in *CRLF2* gene[5,6]. These alterations result in overexpression of one of the component of the heterodimeric cytokine receptor for the Thymic Stromal Lymphopoietin (TSLPR). *CRLF2* overexpression is the result of chromosomal rearrangements giving rise to a *IGH@-CRLF2* fusion gene or a focal deletion upstream of *CRLF2* resulting in the expression of the *P2RY8-CRLF2* fusion gene[7]. Overexpression of *CRLF2* is present in up to 7% of standard risk and 14% of high-risk BCP-ALL patients[8], up to 50% of Down Syndrome–associated BCP-ALL patients and up to 50% of Ph-like BCP-ALL[9–11]. These patients have poor response to standard chemotherapy regimens thus there is an urgent need to better understand the biology of this subtype of BCP-ALL to uncover new approaches to treatment. Moreover, subsets of *CRLF2*-overexpressing cells also have a gain-of-function *CRLF2 F232C* mutation or activating mutations in *JAK* and *IKZF1* genes[12,13], also conferring poor clinical prognosis[14].

As recently demonstrated by our group and others, alterations in *CRLF2* and/or *JAK2* are responsible for increased basal phosphorylation/activation of JAK2, STAT5 and rpS6 proteins and these signals may be further activated in response to TSLP[15,16]. An *in vivo* study of Ph+ *CRLF2r JAK2*-mutated BCP-ALL demonstrated that addressing the over-activation of JAK/STAT and PI3K pathways with molecularly targeted therapy decreases both basal and induced (TSLP) activation of

STAT5, rpS6 and 4EBP1 proteins, representing a promising clinical approach for this specific subgroup of patients currently being tested in clinical trials[17].

To better understand the complexity of signaling nodes involved in the leukemic process, we herein report the dissection of the TSLPR-related signaling pathways in primary diagnostic *CRLF2r* BCP-ALL bone marrow by single-cell mass cytometry (CyTOF)[18]. Using the high dimensional single-cell capability of the CyTOF we were able to examine simultaneously in single cells the activation of multiple pathways. Moreover, we investigated the response of leukemic cells to two different monoclonal antibodies (mAbs) directed against the TSLP receptor and three relevant kinase inhibitors (KIs): *Ruxolitinib* (a JAK1/2 inhibitor[17,19]); *Dasatinib* (dual BCR-ABL and Src family inhibitor[20,21]); and *NVP-BEZ235* (a dual PI3K/mTOR inhibitor)[22,23], alone or in combination. This approach uncovered subpopulations, present in all primary samples, with different signaling architecture. Further, we demonstrate the feasibility to use CyTOF to identify and characterize leukemic cells resistant to the treatment *in vivo*, known as minimal residual disease (MRD) cells, in *CRLF2r* samples. MRD detection has been widely demonstrated to be an independent prognostic marker of individual response to therapy and MRD levels are now used for risk-assignment in several protocols for childhood ALL[24,25]. Notably, we demonstrated that the MRD cells of *CRLF2r* patients maintain the TSLPR overexpression

showing activated signaling patterns as well as responsiveness to signal transduction inhibitors.

MATERIALS AND METHODS

Patients and samples

We analyzed a total of 15 diagnostic bone marrow BCP-ALL samples, 9 out of 15 were *CRLF2* rearranged (r), and 6 were *CRLF2* wild type (wt) (Table 1). Patient samples were selected based on overexpression of *CRLF2* calculated by RQ-PCR and on the overexpression of TSLPR protein assessed by Flow Cytometry (FCM) as previously described[5,16]. Three of 9 *CRLF2r* patients were also studied during early phases of remission induction therapy (2 samples per patient collected at Day 8 and Day 15). Diagnostic leukemia samples were obtained, under informed consent, from I-BFM trials (AIEOP-ALL 2000 and AIEOP-ALL 2009 protocols) at Pediatric Clinic of University Milano-Bicocca (Monza, Italy) and cryopreserved at M. Tettamanti Research Center (Monza, Italy). Investigation has been conducted in accordance with the ethical standards, with the declaration of Helsinki and has been approved by the authors' institutional review boards.

Table 1: Features of studied patients

Primary samples	Age at diagnosis (years)	Sex	Immunophenotype EGIL classification	TSLPR overexpression	CRLF2 rearrangements	JAK2 alterations	MRD risk	Prednisone response	Final risk
#1	15	Male	B-II	positive	P2RY8-CRLF2	L681 I682 ins GL	HR-SER	PGR	HR
#2	12	Male	B-II	positive	IGH@CRLF2	R683G	IR	PGR	IR
#3	4	Female	B-III	positive	P2RY8-CRLF2	wild type	IR	PGR	HR
#4	17	Female	B-III	positive	P2RY8-CRLF2	wild type	SR	PGR	SR
#5	2	Male	B-II	positive	P2RY8-CRLF2	wild type	SR	PGR	SR
#6	12	Female	B-II	positive	P2RY8-CRLF2	wild type	IR	PGR	HR
#7	6	Female	B-II	negative	wild type	wild type	IR	PGR	SR
#8	4	Male	B-II	negative	wild type	wild type	HR-SER	PGR	HR
#9	4	Female	B-II	negative	wild type	wild type	HR-SER	PGR	HR
#10	4	Female	B-II	negative	wild type	wild type	IR	PGR	IR
#11	2	Female	B-II	negative	wild type	wild type	IR	PGR	IR
#12	16	Female	B-II	negative	wild type	wild type	IR	PGR	IR
#13	17	Male	B-II	positive	IGH@CRLF2	wild type	HR-SER	PPR	HR
#14	4	Female	B-II	positive	P2RY8-CRLF2	wild type	IR	PGR	IR
#15	4	Male	B-II	positive	P2RY8-CRLF2	wild type	IR	PGR	HR

HR= high risk; IR= intermediate risk; SR=standard risk; SER= slow early responder
Prednisone response: PGR=prednisone good responder; PPR=prednisone poor responder

Sample preparation and acquisition

Samples were processed as previously described[18]. Briefly, viably preserved bone marrow cells were thawed and re-suspended in RPMI with 10% FCS, 1% L-glutamine, 1% penicillin/streptomycin, 20 U/mL sodium heparin (Sigma) and 0.025 U/mL benzonase (Sigma). Cells were stained for viability with cisplatin as described[26], rested for 30 minutes at 37° C and then perturbed as shown in Figure 1 (panel B). Following perturbations with TSLP (10 ng/mL for 30 minutes) or agents treatments (as reported in Supplemental Table 1), cells were fixed with formaldehyde (PFA; Electron Microscopy Sciences, Hatfield, PA) to a final concentration of 1.6% for 10 minutes at room temperature. Cells were barcoded using palladium-based labeling reagents as recently described[27]. Cells were pelleted, washed twice with cell staining media (CSM; PBS with 0.5% BSA, 0.02% sodium azide) to remove residual PFA, combined into a single FACS tube and then blocked with Purified Human Fc Receptor Binding Inhibitor (eBioscience Inc., San Diego, CA) following manufacturer's instructions. Surface marker antibodies were added yielding 50 or 100 uL final reaction volumes and stained at room temperature for 30 min. Following staining, cells were again pelleted and washed with CSM before being permeabilized with 4° C methanol for at 10 min at 4° C, then optionally stored at -80° C for later use. Cells were then washed twice in CSM to remove remaining methanol and stained with intracellular antibodies cocktail in 50 µL for 30 min at room

temperature. Cells were washed once in CSM, then stained with 1 mL of 1:5000 191/193Ir DNA intercalator (2) (DVS Sciences, Richmond Hill, Ontario, Canada) diluted in PBS with 1.6% PFA for 20 mins at room temperature. Cells were then washed once with CSM and then finally with water alone before running on the CyTOF mass cytometer (Fluidigm, Inc.).

Normalization of signal intensity loss during the CyTOF run was performed as described before utilizing metal standard beads mixed with the sample during the data acquisition[28]. A workflow of the experiments is shown in Figure 1.

Supplementary Table 1: Treatment conditions

Conditions	Concentration	Time of treatment (minutes)
basal		
PVO_4	125 µM	15’
TSLP	10 ng/mL	30’
Dasatinib + TSLP	500 nM + 10 ng/mL	30’ + 30’
Ruxolitinib + TSLP	250 nM + 10 ng/mL	30’ + 30’
NVP-BEZ235 + TSLP	1 µM + 10 ng/mL	30’ + 30’
A10 mAb + TSLP	20 ug/mL + 10 ng/mL	30’ + 30’
H3 mAb + TSLP	20 ug/mL + 10 ng/mL	30’ + 30’

All the treatments were performed after 30 minutes of starvation. The pervanadate ($PV0_4$) was used as positive control since is able to induce the maximum phosphorylation of phospho-epitopes.

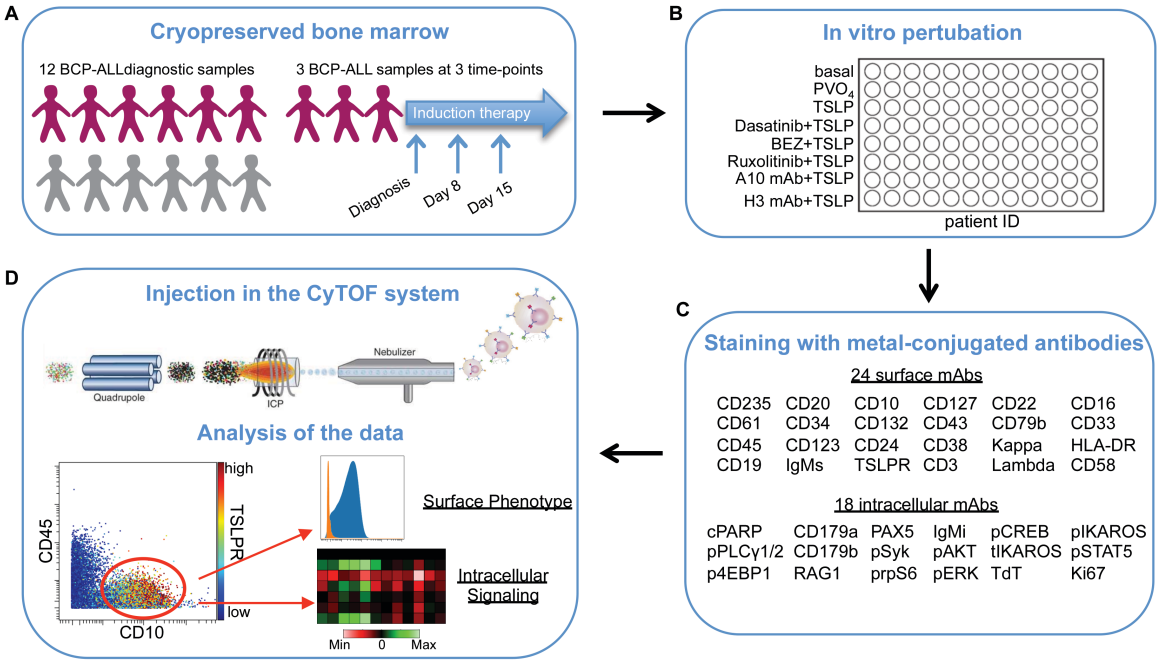
A
Cryopreserved bone marrow
12 BCP-ALLdiagnostic samples
3 BCP-ALL samples at 3 time-points
Induction therapy
Diagnosis
Day 8
Day 15
B
In vitro pertubation
basal
PVO4
TSLP
Dasatinib+TSLP
BEZ+TSLP
Ruxolitinib+TSLP
A10 mAb+TSLP
H3 mAb+TSLP
patient ID
C
Staining with metal-conjugated antibodies
24 surface mAbs
CD235 CD20 CD10 CD127 CD22 CD16
CD61 CD34 CD132 CD43 CD79b CD33
CD45 CD123 CD24 CD38 Kappa HLA-DR
CD19 IgMs TSLPR CD3 Lambda CD58
18 intracellular mAbs
cPARP CD179a PAX5 IgMi pCREB pIKAROS
pPLCγ1/2 CD179b pSyk pAKT tIKAROS pSTAT5
p4EBP1 RAG1 prpS6 pERK TdT Ki67
D
Injection in the CyTOF system
Nebulizer
Quadrupole
ICP
Analysis of the data
high
TSLPR
low
CD45
CD10
Surface Phenotype
Intracellular Signaling
Min
0
Max

Figure 1: Workflow of mass cytometry analysis.

(A) Cohorts of pediatric BCP-ALL patients analyzed: 9 CRLF2 rearranged (purple men) and 6 CRLF2 wild-type (grey men).

(B) Summary of *in vitro* perturbations performed on 12 BCP-ALL primary samples. All the concentrations and time of stimulation/treatment are described in Supplementary Table 2.

(C) Panel of 42 metal-conjugated antibodies used to stain primary cells.

(D) Method of CyTOF operation: stained cells were injected into a nebulizer and passed through an ICP TOF mass spectrometer and the individual ions are counted. The fcs files generated were uploaded in Cytobank (Cytobank Inc. Mountain View, CA) and analyzed by using 2D plots to gate cells, histograms to study the surface phenotype and heatmap to represent signaling responses to cytokines and or drugs treatments. Figure adapted from Bendall SC and Nolan GP review[47]

Mass cytometry data and statistical analysis

Single-cell de-convolution algorithm was used as previously described[27,29], giving a FCS file for each barcode population. All FCS files were analyzed and graphs generated using Cytobank (Cytobank.org; Cytobank Inc. Mountain View, CA). Data were transformed with the inverse hyperbolic sine (arcsinh) equation and the ratio of the treated conditions (TSLP and/or drugs) with the basal state was calculated. The heatmaps are colored with a scale from red to green, considering black as levels of proteins at the basal state and green/red increased *versus* decreased levels of the phosphoproteins in the treated conditions respectively.

ViSNE analysis

Live cells (DNA+, cPARP-) were visualized using VISNE based on the expression of 11 antigens typical of T, B and Red Blood Cells (RBC) lineages: CD45, CD19, CD10, CD20, CD3, CD235-CD61, IgMi, IgMs, CD34, CD38 by using viSNE[30] powered by Cytobank software.

Flow cytometry screening of TSLPR over-expressed patients and MRD detection

The overexpression of the TSLPR proteins was investigated at diagnosis by using standard multiparametric FCM on fresh samples processed within 24 hours from collection. Patients cells were stained by using the following combination of MoAbs: CRLF2PE/CD45PerCP/CD19APC/CD10PE-cy7/CD7ECD and 30,000 total events were acquired on a FACScanto™ flow cytometer and analyzed with Diva™ software (Becton Dickinson). Measurement of TSLPR expression was calculated as % of positive cells on blast population by setting the histograms marker exactly at the right end of normal residual lymphocytes peak and the threshold for antigen positivity was established as ≥10%.

The MRD detection by Flow Cytometry (FCM) was performed based on a standardized protocol evolved from a previously described method[31]. Briefly, the following monoclonal antibodies were used in six-eight color combinations: CD45, CD34, CD19, CD20, CD38, CD10, CD123, Syto16,

CD58, CLL1, CD11a. All combinations included six back bones markers useful for tracking leukemia-associated phenotypes in different tubes. For FCM-MRD measurements, at least 3×10^5 ungated events were acquired on a FACSCanto II™ flow cytometer and analyzed with Diva™ software (Becton Dickinson).

Molecular screening of CRLF2 expression and JAK2 alterations

CRLF2 overexpression and *P2RY8-CRLF2* fusion were analyzed as previously described[5]. Briefly, relative gene expression (indicated as fold change) was quantified by the $2^{-\Delta\Delta Ct}$ method. For *CRLF2* expression, the $\Delta\Delta$Cts were calculated by subtracting to the ΔCt of each sample, the median of the ΔCt of a published cohort of 464 BCP-ALL patients enrolled in Italy in the AIEOP-BFM ALL2000 study from February 2003 to July 2005[5]. Patients were considered *CRLF2* overexpressed when the relative gene expression was 20 fold-above the median. Patients were further characterized for JAK2 alterations by HRM technique and for other BCP-ALL associated aberrations by Multiplex Ligation-dependent Probe Amplification (MLPA; SALSA MLPA P335-A3 ALL-IKZF1 probemix, MRC-Holland, Amsterdam, The Netherlands) according to the manufacturer's instruction. Patients were further characterized for *JAK2* alterations by HRM technique and for other BCP-ALL associated aberrations by Multiplex Ligation-dependent Probe Amplification (MLPA;

SALSA MLPA P335-A3 ALL-IKZF1 probemix, MRC-Holland, Amsterdam, The Netherlands) according to the manufacturer's instruction.

Detection of IGH@CRLF2 translocation

IGH@-CRLF2 translocation was searched in *CRLF2* over-expressed AIEOP patients, for which fixed cells from BM at diagnosis were available, by Fluorescence in situ hybridization (FISH) on interphase nuclei using CRLF2 Breakapart Probe (Cytocell Ltd, Cambridge, UK). Analyses were carried out using Zeiss Axio Imager Z2 fluorescent microscope (Carl Zeiss AG Corporate, Oberkochen, Germany) and ISIS software (MetaSystems GmbH, Altlussheim, Germany). For each case 150/200 interphase nuclei were scored.

Cell culture

The murine pro B cell line BaF3-hTSLPR, kindly provided by Shai Izraeli, is derived from BaF3 cells transduced with retrovirus containing human *CRLF2* and *IL-7Rα* genes, thus a functional human TSLP complex. Transduced cells were sorted by flow cytometer 2-4 days later by using PE anti-human CRLF2 (322806; BioLegend) and Alexa Fluor 647 anti-human CD127 (IL-7Rα, 317606; BioLegend) antibodies[32]. BaF3-hTSLPR cell line was maintained in RPMI medium supplemented with 10% of fetal bovine serum (FBS), 1% penicillin-streptomycin, 1% L-glutamine and 2% of interleukin-3 (IL-3) at 37° C incubator with 5% CO_2.

Cell proliferation and drug combinations assays

BaF3-hTSLPR cells were seed at concentration of $4*10^5$ cell/mL in 24-well plates and treated with increasing doses of TSLP in the absence of IL-3. Proliferation assays were performed by quantitative counts of live cells by FACS and experiments were performed in triplicate. In the context of inhibition assay cells were first exposed to TSLP (10 ng/mL) cytokine for 1h and then treated with different concentration of anti-TSLPR mAbs and/or KIs alone and in combination. Cytotoxicity assay were performed after 72 hours of treatment by using GFP CERTIFIED® Apoptosis/Necrosis detection kit (Enzo Life Science, Inc., Lausen, Switzerland) following the manufacturer instructions. The doses used for the combination assays were the IC50 value for each agent, calculated with CompuSyn Software (Compusyn; Biosoft, Cambridge, UK) and the ratio used were: Dasatinib (Das) to Ruxolitinib (Ruxo) 1:1, Das to NVP-BEZ235 (BEZ) 1:0.25, Ruxo to BEZ was 1:0.25, Das to A10 mAb 1:40 and BEZ to A10 mAb 1:100. The addictive or synergic activity of the drugs was determined by using Combination Index (CI) model based on Chou-Talalay theorem[33] calculated by using CompuSyn Software. The combination index calculated at 50% of the fraction affected or IC50 (meaning 50% of death cells compared to the not treated cells) for each agent combination at 4 different concentrations indicates whether the agents act in a synergic ($CI<0.9$), additive ($0.9 < CI < 1.1$) or antagonist ($CI>1.1$) manner.[34]

Hybridoma cell lines growth conditions

The hybridoma cell lines were first grown in RPMI 'recovery medium' (GIBCO 31870-025) supplemented with 1 x Glutamax (GIBCO 35050-038), 100 Units/mL Penicillin and 100 ug/mL of Streptomycin (1:100 of PenStrep solution from GIBCO 15140-122), 1 M of HEPES (GIBCO 15630-056), 3.8 mM of Oxaloacetic Acid (Sigma O7753), 0.45 mM of Sodium Pyruvate (Sigma 58636) and 0.2 Units/mL of Insulin (Sigma 19278). Cultures were established from cryo-perserved hybridoma lines (A10 and H3) using 1 x 10^7 cells and maintained, as standard for suspension cell lines, until a doubling time of 2-4 days was obtained. The media was then gradually replaced at a 50:50 ratio for at least 4 weeks by Chemically Defined Hybridoma Media (GIBCO 11279-023) supplemented with 3.8 mM of Oxaloacetic Acid (Sigma O7753)**,** 0.45 mM of Sodium Pyruvate (Sigma 58636) and 0.2 Units/mL of Insulin (Sigma 19278), as before, and 1 x Cholesterol (GIBCO 12531018). The cultures were expanded until at least 1L of cells was obtained. Cells were then left for 4-6 weeks to 'over-grow' and to accumulate secreted monoclonal antibody. The media was then harvested, by removal of cells via centrifugation at 230 G for 5 mins at 4° C, followed by filtration using with a 0.22 µm, polyethersulfone stericup-GP vacuum filter system (Millipore SCGPU11RE). The resulting supernatant was then stored at 4°C until purified.

Purification of monoclonal antibodies

Monoclonal antibodies were purified at Immunopharmacology Lab at Humanitas Research Center by using Fast Protein Liquid Chromatography (FPLC).

Drugs

Dasatinib (BMS-354825, Sprycel), Ruxolitinib (INCB018424, Jakafi) and NVP-BEZ235 (Dactolisib) were purchased from LC Laboratories ® (www.LCLabs.com).

Statistical Analysis

Statistical analysis regarding the levels of the phosphoproteins after treatments were performed with ANOVA test followed by Dunn's test for multiple comparison and graphs data are reported as mean ± SEM. Unpaired two-sided student's t test was used to analyze the statistical significance of differences in the expression of the phosphoproteins between the *CRLF2r* and *CRLF2wt* patients. A p values ≤ 0.05 was considered statistically significant. The statistical analyses were performed by using GraphPad Prism v 6.0 software (GraphPad, La Jolla, CA) * $p<0.5$, ** $p<0.01$, *** $p<0.001$.

RESULTS

Mass Cytometry Identifies TSLPR overexpression

Single cells from twelve BCP-ALL primary diagnostic bone marrow samples (6 *CRLF2r* and 6 *CRLF2wt*) were analyzed with a 42-antibody panel (see Figure 1 C) by CyTOF. Cells were gated as shown in Figure 2 A-E and the mass cytometry platform faithfully identified TSLPR over-expressing cells. As expected, samples identified to carry rearrangements of *CRLF2* had higher expression of the TSLPR than controls (mean level of TSLPR expression was 16.15 vs 0.91 in CRLF2wt, p=0.0450). The mass cytometry plots demonstrating TSLPR expression in two representative cases are shown, Figure 2 F (TSLPR positive) and Figure 2 G (TSLPR negative).

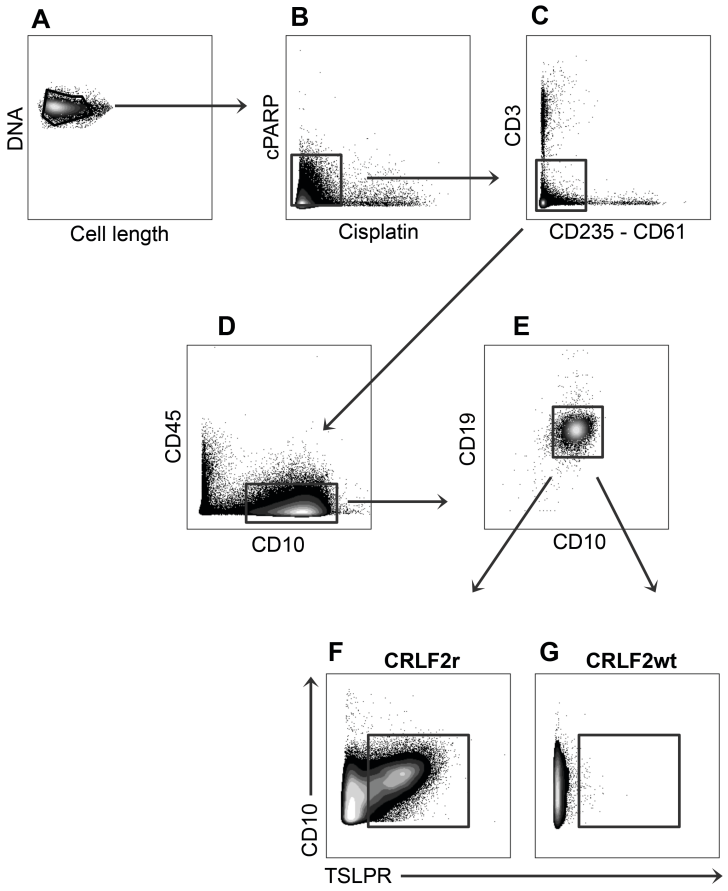

Figure 2: Hierarchical gating strategy employed to measure TSLPR expression.

(A) Cells (DNA positive) were distinguished from debris.

(B) Cells were gated to be live (cPARP negative/cisplatin negative).

(C) T-cells (CD3 positive), red blood cells (CD235) and platelets (CD61 positive) were excluded from the analysis.

(D-E) B-cell blasts were selected to be CD45 negative/CD10 positive and CD19 positive.

(F-G) TSLPR expression was assessed in blast cells of a *CRLF2r* patient (panel F) and a *CRLF2wt* patient (panel G).

TSLP stimulation induces activation of multiple signaling pathways in CRLF2r BCP-ALL

Since mass cytometry allows the simultaneous measurement of many intracellular proteins in single cells, we examined multiple pathways concurrently. In the basal state there were no statistically significant differences between *CRLF2r* and *CRLF2wt* samples in the activation of functional proteins. However, we observed higher levels of pSTAT5 (mean 0.27 vs 0.07, p=0.0842) in *CRLF2r* compared to the *CRLF2wt* samples. In this regard, this tendency could be explained by the presence of one *CRLF2r* patient (Pt #2) bearing also the R683G JAK2 mutation and one patient (Pt #1) harboring a not previously described JAK2 insertion (L681-I682 ins GL) in exon 16.

Yet, *in vitro* stimulation with TSLP clearly demonstrated different signaling potentials between *CRLF2r* and *CRLF2wt* samples. *CRLF2r* patients had increased levels of pSTAT5 (arcsinh ratio CRLF2r 0.21 *vs* CRLF2wt 0.02, p=0.0054) and prpS6 (arcsinh ratio 1.48 *vs* -0.15, p=0.0006) after TSLP stimulation compared to the *CRLF2wt* samples, which showed no significant response to TSLP (Figure 3 A). In addition to activation of STAT5 and rpS6, we also observed activation of ERK and CREB following TSLP stimulation (pERK arcsinh ratio 0.09 *vs* -0.01, p=0.0313; pCREB arcsinh ratio 0.15 *vs* -0.04, p=0.0260). There was no significant TSLP-induced activation of p4EBP1, pPLCγ1/2, pAKT and pSyk in either cohort of patients.

To understand whether the TSLP-induced activation of STAT5, rpS6, CREB and ERK occurred in the same cells or in different subpopulations we analyzed the data at the single cell level. We observed that within the TSLPR+/IL7Rα+ cells there was a consistent subset able to co-activate all these four phospho-

proteins simultaneously (Figure 3 B first and second rows). These cells also express the highest levels of Ki67, an antigen associated with cellular proliferation, suggesting the co-activation of these pathways occurs in dividing cells (Figure 3 B third row). The single cell analysis of the remaining patients is shown in Supplementary Figure 1.

Thus, applying this high-dimensional single-cell analysis to TSLPR over-expressing cells, we observed co-activation of JAK/STAT, PI3K, RAS/MAF/ERK, and CREB pathways in response to TSLP exposure. To further dissect the structure of these activated networks we subjected cells to pharmacologic inhibition.

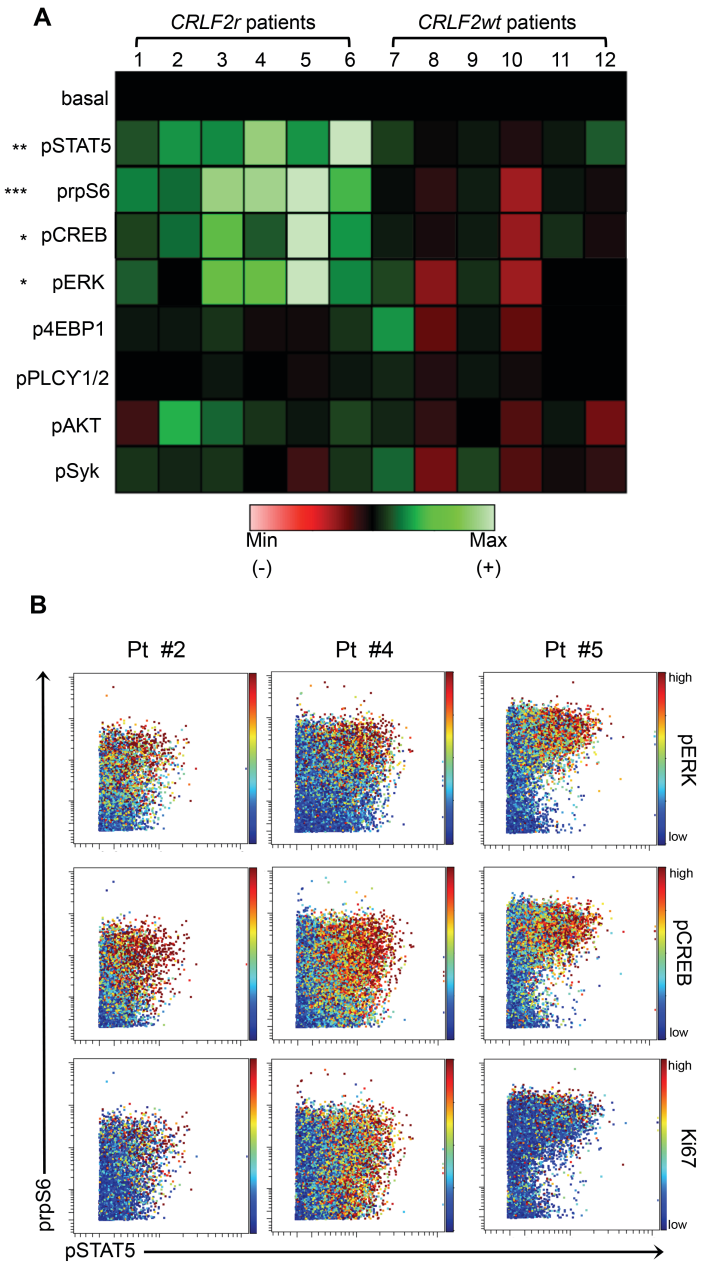
A
CRLF2r patients
CRLF2wt patients
1 2 3 4 5 6 7 8 9 10 11 12
basal
** pSTAT5
*** prpS6
* pCREB
* pERK
p4EBP1
pPLCY1/2
pAKT
pSyk
Min
(-)
Max
(+)
B
Pt #2
Pt #4
Pt #5
high
low
pERK
pCREB
Ki67
prpS6
pSTAT5

Figure 3: TSLP-induced signaling in BCP-ALL leukemia.

(A) Heatmap overview of the TSLP-induced signaling: in the columns are represented 12 BCP-ALL primary samples, from 1 to 6 are *CRLF2r* and from 7 to 12 *CRLF2wt*; in the rows are shown all the tested phosphoproteins and each phosphoprotein is showed as arcsinh ratio of the TSLP stimulated condition compared with its basal. The p-value is indicated by asterisks (* p<0.5, ** p<0.01, *** p<0.001)

(B) Representative plots of a TSLP-activated signaling in 3 *CRLF2r* patients (Pt2, Pt4 and Pt5). The single cells plots represent the levels of pSTAT5 (x axis), prpS6 (y axis) and are colored by the expression of pERK (first row), pCREB (second row) and Ki67 (third row) based on a colorimetric scale from blue (low expression) to red (high expression).

Treatment with KIs and anti-TSLPR mAb inhibit TSLPR-related signaling in *CRLF2r* primary samples

Having observed coordinated activation of multiple signaling pathways within primary TSLPR-overexpressing cells, we attempted to inhibit these pathways through two mechanisms: monoclonal antibodies directed at the TSLP receptor and kinase inhibitors (KIs). Taking advantage of the high TSLPR expression in the *CRLF2r* patients, we tested two monoclonal antibodies directed against the TSLPR, referred to as A10 and H3. We compared their activity to 3 KIs (Ruxolitinib, NVP-BEZ235 and Dasatinib) acting on different pathways (JAK1/2, PI3K/mTOR and ABL/SRC, respectively; Figure 4 A).

As expected, the JAK inhibitor, Ruxolitinib, decrease STAT5 activation after treatment with TSLP (mean arcsinh ratio not treated 0.24 vs treated 0.12). However, pSTAT5 could be better inhibited by Dasatinib

(arcsinh ratio not treated 0.24 *vs* treated 0.04, p=0.0045) or the A10 mAb (mean arcsinh ratio not treated 0.24 *vs* treated 0.04, p=0.0078) in the *CRLF2r* treated samples. This effect was not seen in the *CRLF2wt* samples (Figure 4 B). The TSLP-dependent activation of prpS6 in *CRLF2r* patients (Figure 4C) was also strongly inhibited by Dasatinib (mean arcsinh ratio not treated 1.40 *vs* treated -1.09, p<0.0001), which abrogated both basally activated prpS6 as well as TSLP induced activation. This effect was not limited to the *CRLF2r* samples alone, as the *CRLF2wt* controls also showed inhibition of prpS6 after treatment with Dasatinib. Again, the A10 mAb inhibited the TSLP-driven activation of prpS6 in all *CRLF2r* patients compared to controls (mean arcsinh ratio not treated 1.40 *vs* treated -0.20, p=0.0169). Ruxolitinib blunted the TSLP-mediated prpS6 activation in the *CRLF2r* treated cells compared to the untreated condition (mean arcsinh ratio not treated 1.40 *vs* treated 0.08, p=0.0436), however this response was more patient-specific as patients #1, #2 (both *JAK2* alterated), and patient #6 showed the best response. Finally, treatment with the PI3K/mTOR specific inhibitor, NVP-BEZ235 also appeared effective in inhibiting prpS6 activation but did not reach statistical significance (mean arcsinh ratio not treated 1.40 *vs* treated 0.21, p=0.0678), likely due to our small cohort.

Regarding ERK and CREB activation (Figure 4D and 4E respectively) Dasatinib was the only agent able to inhibit their TSLP-mediated activation (mean arcsinh ratio not treated 0.09 *vs* -0.04, p=0.0006 and

0.12 *vs* -0.15, p=0.0060 respectively) in *CRLF2r* samples as well as the basal activation of ERK and CREB also in *CRLF2wt* patients. Ruxolitinib, NVP-BEZ235, and A10 mAb also inhibited ERK activation, yet not as well as Dasatinib. The A10 mAb overall, showed promising inhibition of multiple downstream pathways, as compared to the H3 clone which did not show inhibitory activity and for this reason was not further tested *in vitro.* Scatter plots summarizing the data of all the 4 phosphoproteins in the *CRLF2r* patients are shown in Supplementary Figure 2.

Furthermore, we observed that the KIs and the A10 mAb were both effective specifically on the cells with co-activatation of pSTAT5, prpS6, pERK, pCREB and Ki67. Dasatinib displays the best ability to inhibit the activation of all the proteins, in particular Ki67 and pCREB (Supplementary Figure 3).

In order to investigate whether the observed heterogeneity response to treatment, in particular with Ruxolitinib and NVP-BEZ235, could be dependent by the presence of a specific resistant cell subset, we further dissected the TSLPR-driven signaling network.

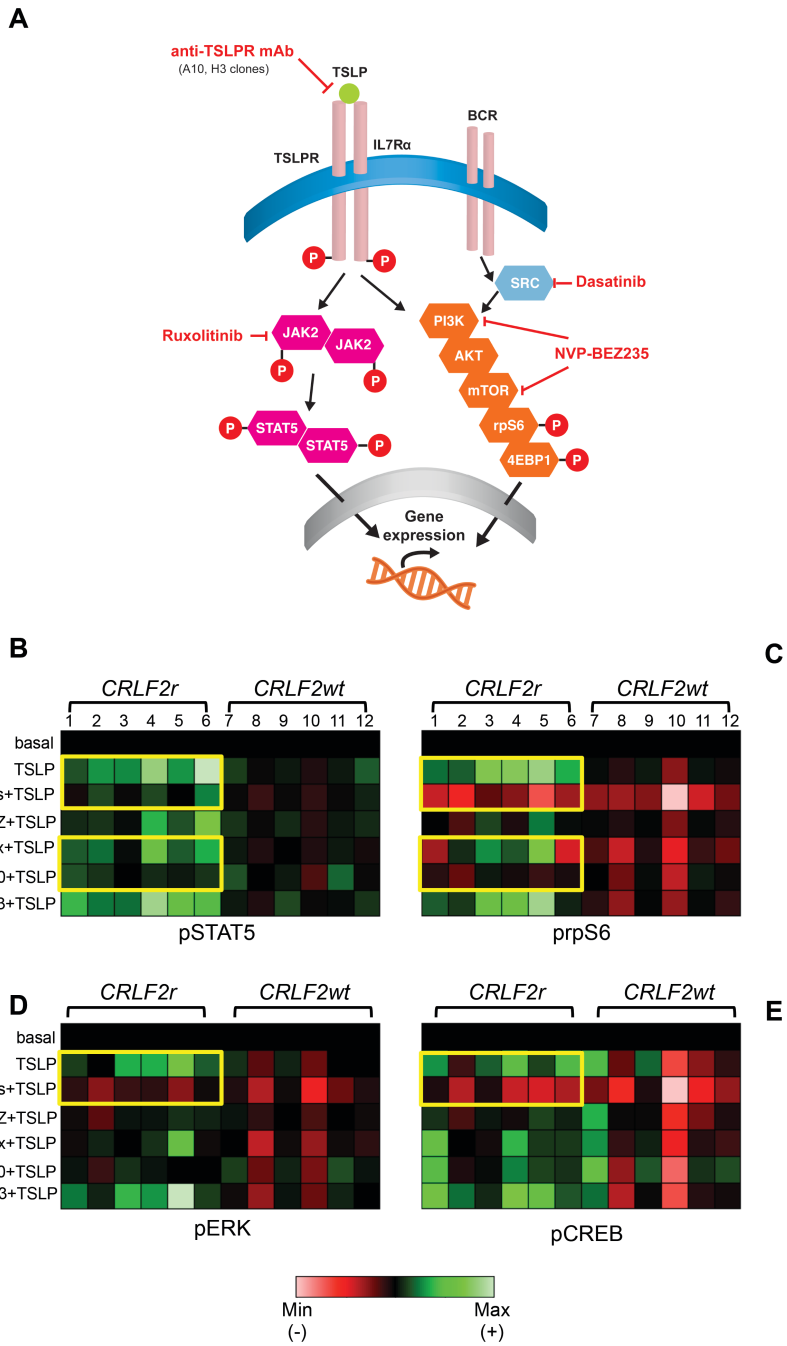
A
anti-TSLPR mAb
(A10, H3 clones)
TSLP
BCR
TSLPR
IL7Rα
P
SRC
Dasatinib
PI3K
Ruxolitinib
JAK2
JAK2
NVP-BEZ235
AKT
mTOR
rpS6
STAT5
STAT5
4EBP1
Gene
expression
B
C
CRLF2r
CRLF2wt
1 2 3 4 5 6 7 8 9 10 11 12
basal
TSLP
Das+TSLP
BEZ+TSLP
Rux+TSLP
A10+TSLP
H3+TSLP
pSTAT5
prpS6
D
E
pERK
pCREB
Min
(-)
Max
(+)

Figure 4: Effects of KIs and anti-TSLPR mAbs on TSLP-related signaling.

(A) Schematic representation of TSLPR heterodimer signaling transduction in childhood *CRLF2r* BCP-ALL and therapeutic strategies used in this study to target activated signaling nodes.

(B-E) Heatmaps overviews of the agents effects on TSLP-activated phosphoproteins in *CRLF2r* and *CRLF2wt* BCP-ALL primary samples. In the rows are shown all the different treatment conditions and each phosphoprotein is showed as arcsinh ratio of the treated condition compared with its basal. The yellow box highlights effective treatments

Das=Dasatinib, Ruxo=Ruxolitinib, BEZ=NVP-BEZ235, A10=A10 anti-TSLPR mAb, H3=H3 anti-TSLPR mAb.

Dissection of TSLP related signaling revealed cell subset with signaling heterogeneity

Taking advantage of the multi-parametric potential of mass cytometry, we identified a subpopulation of TSLPR+/IL7Rα+ cells that did not activate pSTAT5 upon TSLP stimulation. This cell subset was found in all of the *CRLF2r* primary samples analyzed (Figure 5 A, red rectangle), at variable frequency (mean ± SD: 51.36% ± 12.77%).

Compared to pSTAT5 responsive cells this non-responsive subset expressed lower levels of TSLPR (p=0.0319) suggesting that there is a minimal threshold of TSLPR expression necessary to activate the JAK/STAT signaling.

As we had expected, the STAT5 responsive subset displayed TSLP-induced activation of rpS6 that was inhibited by Dasatinib, A10 mAb,

Ruxolitinib and NVP-BEZ235 ($p<0.0001$, $p=0.0100$, $p=0.0437$, $p=0.0437$ respectively) (Figure 5 B).

Interestingly, we noticed that the STAT5 non-responsive cells maintained the ability to activate prpS6 (mean arcsinh ratio pSTAT5+ 1.31 *vs* pSTAT5- 1.13, $p=0.2215$), meaning that both pSTAT5 responsive and non-responsive cells were similarly able to activate prpS6 in the presence of TSLP. (Figure 5 C and D). To investigate the potential of our panel of inhibitors, we asked if the STAT5 non-responsive population could be inhibited by the KIs or mAb treatments. Treatment with Dasatinib or A10 mAb completely blunted the TSLP-mediated prpS6 activation in all patients (mean arcsinh ratio 1.14 *vs* -0.99, $p<0.0001$ and mean arcsinh ratio 1.14 *vs* -0.08, $p=0.0101$ respectively; Figure 5 C and D). Ruxolitinib and NVP-BEZ235 were less effective across the cohort (mean arcsinh ratio 1.14 *vs* 0.16, $p=0.0678$ and mean arcsinh ratio 1.14 *vs* 0.14, $p=0.0678$ respectively) with inhibition observed in a patient-specific manner. Ruxolitinib was effective on patients #1, #2, #3 and #4 whereas NVP-BEZ235 was efficient in patients #1, #2, #4 and #6. These latter results can be explained also by the presence of patients (Pt #1 and #2) bearing alterations in the *JAK2* gene.

From the single cell analysis we showed that the pSTAT5 not responsive cells were less proliferative having lower Ki67 expression as compared to the STAT5 responsive subset ($p=0.0006$). These cells were

also less responsive to TSLP-mediated activation of ERK and CREB ($p=0.0239$ and $p=0.00275$ respectively; Figure 5 E).

Overall, these data showed that *CRLF2r* BCP-ALL cells display a complex TSLP-driven signaling network as well as a functional heterogeneity associated to different cell subsets.

In view of developing effective targeted therapeutic approach for *CRLF2r* BCP-ALL patients, we next asked if these complex functional signatures were persistent in chemo-resistant MRD cells.

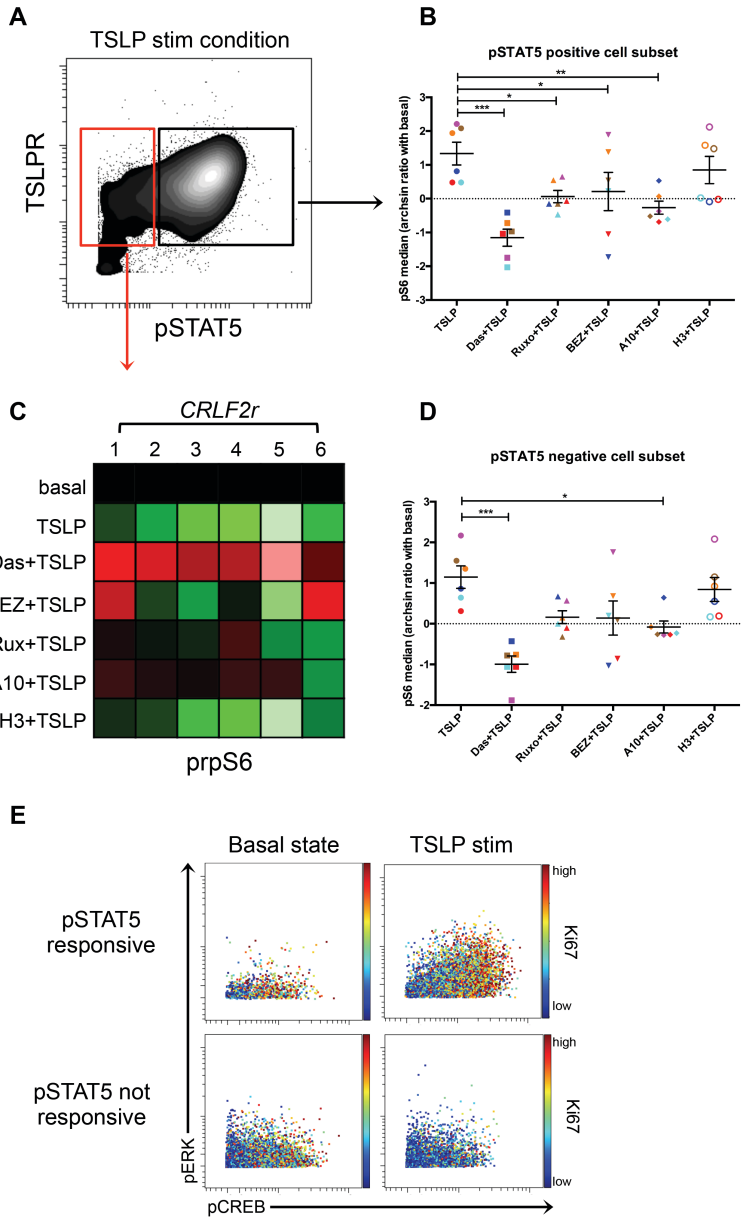
A
TSLP stim condition
TSLPR
pSTAT5
B
pSTAT5 positive cell subset
pS6 median (arcsin ratio with basal)
TSLP
Das+TSLP
Ruxo+TSLP
BEZ+TSLP
A10+TSLP
H3+TSLP
C
CRLF2r
1 2 3 4 5 6
basal
TSLP
Das+TSLP
BEZ+TSLP
Rux+TSLP
A10+TSLP
H3+TSLP
prpS6
D
pSTAT5 negative cell subset
pS6 median (arcsin ratio with basal)
E
Basal state
TSLP stim
pSTAT5 responsive
pSTAT5 not responsive
high
low
Ki67
pERK
pCREB

Figure 5: TSLPR signaling heterogeneity in *CRLF2r* BCP-ALL primary samples

(A) Contour plot of pSTAT5 activation after TSLP stimulation in a representative *CRLF2r* case. The red rectangle highlights the pSTAT5 negative cell subset and the black rectangle underlines the pSTAT5 positive cell subset.

(B) Levels of prpS6 median in TSLP-induced pSTAT5 positive population, calculated as arcsinh ratio of the TSLP or treated+TSLP conditions compared to the basal state.

(C) Heatmap of the prpS6 levels in TSLP-not induced pSTAT5 negative cell subset. The data are showed in 6 CRLF2r patients (columns) and in all the different conditions (rows) calculated as arcsinh ratio of the basal state of prpS6.

(D) Graph representing the prpS6 median in pSTAT5 negative cell subset, calculated as arcsinh ratio of the TSLP or treated+TSLP conditions compared to the basal state.

(E) Representative plots of the basal and TSLP-activated signaling the pSTAT5 responsive cells (first row) and the pSTAT5 not-responsive population (second row) in one CRLF2r patient (Pt #4). The plots show the levels of pCREB (x axis) and pERK (y axis) colored by the expression of Ki67 based on a colorimetric scale from blue (low expression) to red (high expression).

Das=Dasatinib, Ruxo=Ruxolitinib, BEZ=NVP-BEZ235, A10=A10 anti-TSLPR mAb, H3=H3 anti-TSLPR mAb. * $p<0.5$, ** $p<0.01$, *** $p<0.001$.

In the graphs (panel B and D) each patient is associated to a different color: Pt #1 red; Pt #2 cyan; Pt #3 orange; Pt #4 brown; Pt #5 magenta; Pt #6 blue

Minimal Residual Disease (MRD) detection in *CRLF2r* primary samples reveals a TSLPR expression persistence and in vitro responsiveness

CRLF2r BCP-ALL is associated with poor clinical outcomes but the role of TSLPR overexpression in promoting the persistence of a resistant clone is still unclear. Thus, to determine if TSLPR expressing clones persist at early on-therapy time points, we investigated the phenotypic and signaling profiles of cells from MRD samples in 3 additional *CRLF2r* patients (Pt #13, #14, #15) at two time points of early treatment (Day 8 and Day 15 post induction initiation). MRD cells were quantitatively detectable by mass cytometry equivalent to MRD detection by FCM, which is considered together with the RQ-PCR the clinical gold standard[31] (Table 2 and Supplementary Figure 4).

Table 2: Comparison of FCM and CyTOF in the detection of MRD

Patient	Diagnosis		Day 8		Day 15	
	FCM	CyTOF	FCM	CyTOF	FCM	CyTOF
#13	94.0%	88.2%	66.0%	58.5 %	9.1%	10.3 %
#14	85%	95.3	0.03%	0.07%	0.02%	0.08%
#15	86%	85.7%	5.6%	4.4%	12%	13.4%

As shown by using viSNE visualization, TSLPR expression was maintained at Day 8 and Day 15 in all *CRLF2r* samples (purple cells in Figure 6 A). In 2 of 3 samples (#13 and #15), both classified high risk based on MRD (Table 1), the basal levels of rpS6 and CREB expression in MRD cells at Day 8 and Day 15 were increased as compared to the diagnostic untreated blasts. By contrast, patient #14, classified as

intermediate risk (Table 1), demonstrated decreasing levels of basal pCREB and increasing level of prpS6 in the MRD cells (Figure 6 B). Of note, STAT5 was not basally activated in patients #13 and #15 at any time-point; by contrast patient #14 did have activated STAT5 at diagnosis but not at MRD time points.

In one case (pt #13), there was sufficient cellular material to examine induced responses to TSLP alone or in combination with Ruxolitinib or mAb A10 at Day 8 and Day 15 post-induction therapy. At all time points STAT5 was responsive to TSLP treatment but activation of rpS6, CREB, or ERK was only seen at diagnosis or Day 8. At Day 8 the activation of pSTAT5 was only weakly inhibited by Ruxolitinib or A10 mAb, however both agents could inhibit prpS6 and pERK.

Yet, at Day 15, Ruxolitinib and the A10 mAb efficiently inhibited the activation of STAT5. Regarding prpS6, pCREB and pERK although were not activated by the TSLP, probably due to already really high basal levels, both Ruxolitinib and A10 mAb were able to decrease their levels confirming their efficacy not only on JAK/STAT pathway but also on PI3K/AKT and RAS/MEK pathways. Raw heatmaps are shown in Supplementary Figure 4 C.

Collectively, we observed an effective activity of different signal transduction inhibitors in *CRLF2r* cells and demonstrated that such investigation can also be extended to MRD cells.

However, is still not clear if these signaling targeting may impact on cell apoptosis and survival.

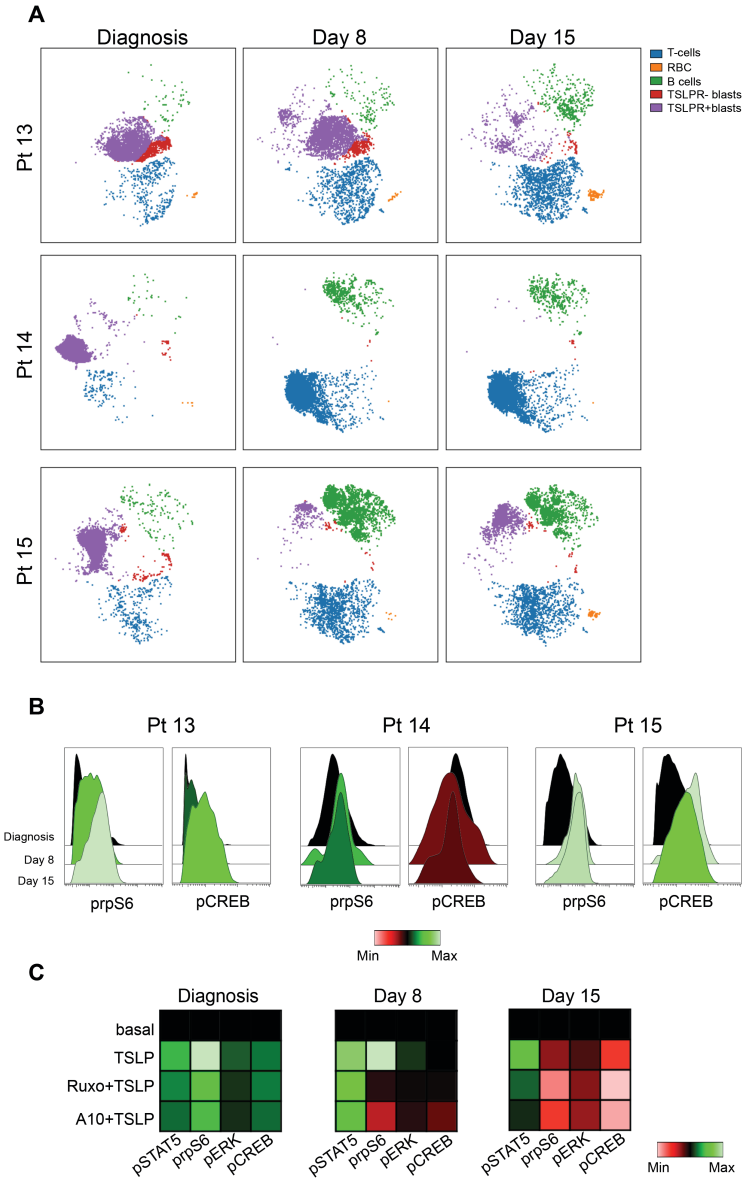

Figure 6: MRD detection in *CRLF2r* BCP-ALL primary samples.

(A) MRD cells visualization by viSNE of 3 *CRLF2r* BCP-ALL primary samples (rows) at the 3 different time-points of treatment disease (columns): cells were clustered based on 11 markers (CD45, CD19, CD10, CD20, CD3, CD235, CD61, IgMi, IgMs, CD34, CD38) and then gated to discriminate T cells (blue dots), RBC cells (orange dots), normal B cells (green), TSLPR negative blasts (red dots) and TSLPR positive blasts (purple dots).

(B) Histogram overlays of prpS6 and pCREB in 3 *CRLF2r* BCP-ALL primary samples at diagnosis, day 8 and day 15 post induction initiation. Histograms are colored with a scale from red (low expression) to green (high expression) by arcsinh ratio of prpS6 and pCREB mean at day 8 and day 15 compared to their levels at diagnosis.

(C) Heatmaps of pSTAT5, prpS6, pERK and pCREB levels (columns of the heatmaps) in 4 different conditions (rows) at diagnosis, day 8 and day 15 in one *CRLF2r* patient (Pt #13). Heatmaps are colored with a scale from red to green based on phosphoproteins levels calculated as arcsinh ratio of their levels in the treated conditions (TSLP, Ruxolitinib and A10 mAb) compared to the basal state.

In vitro agents combinations treatment revealed a synergic effect of JAK/STAT inhibitors with Dasatinib or NVP-BEZ235.

We investigated the effect of combination inhibitor treatments to induce apoptosis in *CRLF2r* blasts by targeting several pathways simultaneously. To this end, we tested combinations of A10 mAb and KIs in BaF3 CRLF2/IL7Rα expressing cells[32] (Figure 7 A). BaF3 CRLF2/IL7Rα cells grow in a TSLP dose-dependent fashion (Figure 7 B).

Dasatinib was the most effective single agent treatment able to induce apoptosis over 72 hours (Figure 7 C, claret open circle). However, Dasatinib in combination with either the A10 mAb or Ruxolitinib was

more effective at lower concentrations in inducing cell death (Figure 7 C). The remaining combinations (NVP-BEZ235 plus Ruxolitinib and NVP-BEZ235 plus A10 mAb) were also more effective than the single agent alone yet not as potent as the Dasatinib combinations (Figure 7 C). In order to evaluate if the combination effects on apoptosis are synergistic or additive, we calculated the Combination Index (CI) values by applying the Chou-Talalay method.

Dasatinib in combination with Ruxolitinib or A10 mAb was synergistic (Combination Index at IC_{50}= 0.65 and 0.63 respectively; (Figure 7 D black circles and green triangles). NVP-BEZ235 synergized with Ruxolitinib or A10 mAb (Combination Index at IC_{50}= 0.50 and 0.49 respectively; (Figure 7 D blue diamonds and purple triangles). The combination of Dasatinib with NVP-BEZ235 resulted in an additive effect only (Combination Index at IC_{50}=1.04) (Figure 7 D red squares).

This data strongly suggests that inhibition of the JAK/STAT pathway (with either Ruxolitinib or A10 mAb) alone is not sufficient to induce cell death. Nevertheless, this pathway has a significant signaling role and its targeting should be combined with further agents acting on additional activated pathways (Dasatinib or NVP-BEZ235).

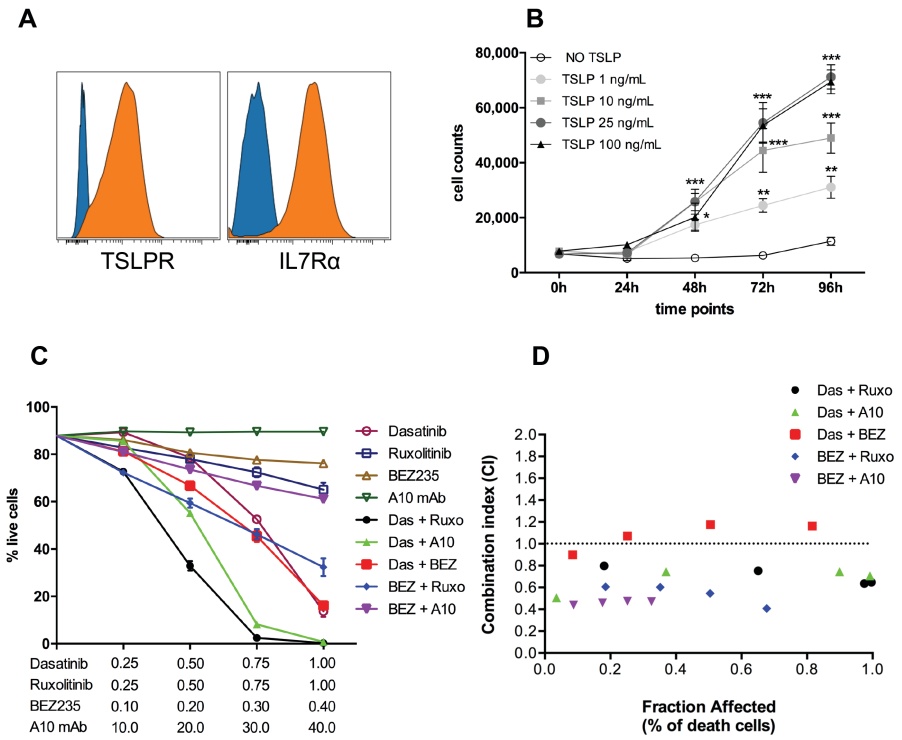

Figure 7: BaF3 CRLF2/IL7Rα cells characterization and in vitro agents combinations treatment.

(A) Phenotypic characterization of BaF3 CRLF2/IL7Rα cells. Overlays shows the TSLPR and IL7Rα positivity of the cells by FACS analysis. Blue histograms indicates the FMO condition and orange histograms the stained condition.

(B) Proliferation assay of TSLP dose dependent growth of BaF3 CRLF2/IL7Rα cells. Cells where treated with increasing doses of TSLP and the viable cells where quantitative counted by FACS at 5 time-points and in 5 different conditions: without TSLP (black curve), with TSLP 1 ng/mL (red curve), TSLP 10 ng/mL (green curve), TSLP 25 ng/mL (purple curve) and TSLP 100 ng/mL (blue curve) and the p-value is indicated by using asterisks (* $p<0.5$, ** $p<0.01$, *** $p<0.001$). Experiments were performed in triplicates.

(C) Graph representing the in vitro drug combinations effects: BaF3 CRLF2/IL7Rα expressing cells were treated with increasing doses of

Dasatinib (from 0.25 μM to 0.75 μM), Ruxolitinib (from 0.25 μM to 0.75 μM), NVP-BEZ235 (from 0.10 μM to 0.3 μM) and A10 mAb (from 10 μg/mL to 40 ug/mL) alone and in combination and the ratio of the percentage of treated and not treated cells was calculated after 72 hours of treatment. The experiments were performed in 4 replicates and the SEM at each point are represented.

Das=Dasatinib, Ruxo=Ruxolitinib, BEZ=NVP-BEZ235, A10=A10 anti-TSLPR mAb, H3=H3 anti-TSLPR mAb

(D) Combination Index (CI) values[33,34] calculated by CompuSyn Software in 4 different concentrations maintaining the same drug ratios. Black circles indicated the fraction affected in Dasatinib + Ruxolitinib combination, red squares indicates the Dasatinib + NVP-BEZ235 combination, green triangle the Dasatinib + A10 mAb combination, purple triangle NVP-BEZ235 + A10 mAb combination and blue diamond Ruxolitinib + NVP-BEZ235 combination. Dotted lines indicated CI=1 threshold: CI <1 indicates synergy, 0.9 <CI <1.1 indicates additivity and CI>1 indicates antagonism.

DISCUSSION

CRLF2 rearranged BCP-ALL comprises approximately 7-10% of pediatric BCP- ALL[7,11,12] and about 50% of Ph-like ALL, a new genetic subgroup characterized by a gene expression profile similar to that of BCR-ABL positive ALL and a poor outcome[10]. Importantly, *CRLF2* rearrangements and other Ph-like-related kinase alterations are associated with a greater risk of relapse and inferior outcomes in high-risk ALL patients[35]. Although the role of *CRLF2* aberrations (as well as the TSLP driven signaling) in the leukemic transformation are not clearly understood, in the last few years several groups hypothesized TSLPR targeting as a treatment strategy by using different approaches, such as T cells engineered with a chimeric antigen receptor (CAR) directed against the TSLPR protein[36], monoclonal antibodies directed against the TSLPR receptor[37,38], and anti-CRLF2 antibody-armored biodegradable nanoparticles.[39] We herein further investigate the TSLPR-related signaling in *CRLF2r* primary samples in order to better understand the biological mechanism(s) underlying this receptor network, and to identify new achievable targetable molecules potentially helpful in the context of targeted therapeutic approaches for this subgroup of ALL patients.

To these aims we performed an extensive single cell profiling of activated phosphoproteins in BCP-ALL leukemic cells in two series of

CRLF2r primary samples by using mass cytometry, which allows the measurement of both surface and signaling features simultaneously in a large number of cells[18,40]. Furthermore, in the same series of patients, we tested the *in vitro* effects of two monoclonal antibodies directed against the TSLPR receptor, and three different kinase inhibitors (KIs) acting at different levels of the TSLPR-related signaling. We confirmed and further extended previous data[15,16] demonstrating a TSLP-dependent hyper-activation of JAK/STAT, PI3K/mTOR RAS/MEK pathways, as well as the transcription factor CREB. From a single cell analysis we demonstrated that the cell subset responsive to TSLP co-expressed pSTAT5, prpS6, pERK and pCREB. Since these cells were also positive for the Ki67 proliferation marker, we speculate that the co-activation of this complex network may arise in proliferating cells potentially responsible for the survival advantages of the *CRLF2r* blast cells.

Interestingly treatment with Dasatinib, despite it is not expected to be specific for the *CRLF2*-driven pathway, was the most effective treatment able to completely switch-off the TSLP-mediated activation of all phosphoproteins. Additionally we observed a significant inhibitory activity induced by the treatment with the A10 mAb, which was able to inhibit both the pSTAT5 and prpS6 TSLP-dependent activations in *CRLF2r* patients. Surprisingly, although the activity of Ruxolitinib on JAK/STAT pathway is well known[17,41,42], we observed such an effect on pSTAT5 in

only 4 out of 6 tested patients including one patient (Pt #2) bearing the R683G *JAK2* mutation and one patient (Pt #1) harboring a not previously described insertion in exon 16 of *JAK2* gene (L681-I682 ins GL). This insertion is located in the pseudokinase domain of JAK2 in the same location of other already described insertions known to confer activating phenotype [12,43].

Moreover, Ruxolitinib showed a significant decrease of prpS6 in all the tested patients. Finally, regarding the NVP-BEZ235 treatment, as expected, it was effective only in prpS6 signaling although its activity was observed in 5 out of 6 tested patients.

Taking advantage of the multi-parametric single cell analysis suitable by using mass cytometry, we finely dissect the TSLP-mediated signaling and we identified a minor TSLPR/IL7Rα double positive cell subset, present at different levels in all the *CRLF2r* patients, which did not phosphorylate STAT5 upon TSLP stimulation; however, these cells were responsive to TSLP by prpS6 activation, which was completely abrogated by either Dasatinib or A10 anti-TSLPR mAb treatments suggesting a promising therapeutic approach thanks to their broad spectrum activity.

We next asked if the *CRLF2r* MRD chemo-resistant cells where still TSLPR positive and how the complex signaling network present at diagnosis impact on the *in vivo* persistence of these cells.

To this end, by CyTOF we analyzed MRD ALL cells collected at early time points of remission induction regimen. Phenotype and prevalence of

these cells were similar to those assessed by traditional FCM approach on fresh cells, demonstrating the feasibility and accuracy of CyTOF approach also in the analysis of such rare cell subset. By using viSNE software[30] we were able to easily detect the MRD cells demonstrating their maintenance of the TSLPR expression. Interestingly, these cells also showed a basal activation of prpS6 and pCREB (particularly evident in the two out of the three tested patients who were classified as high risk for MRD level) as well as a TSLP-induced pSTAT5 and prpS6 activation, both blunted by the treatment with either Ruxolitinib or A10 mAb. Although performed in a very limited series of samples these experiments represent an important proof of principle for future applications of the CyTOF technology in the study of the functional profile of MRD cells.

In view of the signaling heterogeneity here reported at both diagnosis and MRD time points, and considering the hypothesis that *CRLF2* aberrations may not be directly driving the leukemogenesis [44], we hypothesized that the TSLP-induced activation of JAK/STAT pathway may not be the only event responsible for the survival advantage of the *CRLF2r* blasts, suggesting that a combined rather than a single agent therapeutic approach should be considered.

Therefore, we decided to test *in vitro* both the KIs and A10 anti-TSLPR mAb in order to assess a functional read out of their signaling inhibition activity. For this purpose we took advantage of a widely used cellular model represented by the murine pro-B BaF3 cells transfected with

genes of interest.[45] In our experiments we used a IL3-independent/TSLP-dependent BaF3 CRLF2/IL7Rα expressing cells[32] and we demonstrated a strong synergic activity of Dasatinib either with Ruxolitinib or A10 mAb in inducing a pro-apoptotic effect in *CRLF2r* leukemic cells. PI3K/mTOR inhibitor, NVP-BEZ235 also showed a significant synergic activity in combination with either Ruxolitinib or A10 mAb, although this activity was less cytotoxic as compared to the combination of Dasatinib plus Ruxolitinib or Dasatinib plus A10 mAb. This latter result can be explained by considering that NVP-BEZ235 activity has been demonstrated to act more on the induction of cell cycle arrest in G_0-G_1 phase than cellular death[23,46].

In conclusion we finely dissected the TSLPR related signaling in BCP-ALL patients bearing *CRLF2* alterations and we successfully tested different *in vitro* treatments able to significantly inhibit the TSLP pathway and to induce apoptosis in pro-B BaF3 CRLF2/IL7Rα expressing cells.

Although a further series of experiments would be necessary to fully validate these data, the demonstration of functional active TSLPR-positive resistant cells suggests a role of *CRLF2r* in the persistence of the leukemic cells and its targeting to treat late and refractory stages of the disease.

ACKNOWLEDGEMENTS

This project was supported by grants from the Associazione Italiana per la Ricerca sul Cancro (AIRC), from the parents' association "Benedetta è la vita ONLUS".

AUTHORSHIP CONTRIBUTIONS

J.S., A.M.S., S.P., C.B., K.D., performed the experiments; J.S, A.M.S., K.D., C.B., C.P., analyzed the data; J.S., R.B., K.D., G.G. wrote the manuscript; G.G., K.D., M.D., A.B., G.P.N., supervised the research; K.D., G.G. designed the study.

AUTHORS' DISCLOSURES OF POTENTIAL CONFLICTS OF INTEREST

G. P. N. and K.D. are employees of Fluidigm, Inc: Honoraria and Equity Owner respectively.
All other authors declare nothing to disclose.

CORRESPONDENCE TO:

Prof. Andrea Biondi, MD
M. Tettamanti Research Center, University of Milano Bicocca
Via Pergolesi, 33 20900 Monza (MB)
tel. +39 039 2333661 fax +39 039 2332167
e-mail abiondi.unimib@gmail.com; andrea.biondi@unimib.it

REFERENCES

1. Mullighan CG, Goorha S, Radtke I, et al. Genome-wide analysis of genetic alterations in acute lymphoblastic leukaemia. *Nature*. 2007;446(7137):758–64.
2. Inaba H, Greaves M, Mullighan CG. Acute lymphoblastic leukaemia. *Lancet*. 381(9881):1943–55.
3. Pui C-H, Robison LL, Look AT. Acute lymphoblastic leukaemia. *Lancet*. 2008;371(9617):1030–43.
4. Bhojwani D, Pui C-H. Relapsed childhood acute lymphoblastic leukaemia. *Lancet Oncol.* 2013;14(6):e205–17.
5. Palmi C, Vendramini E, Silvestri D, et al. Poor prognosis for P2RY8-CRLF2 fusion but not for CRLF2 over-expression in children with intermediate risk B-cell precursor acute lymphoblastic leukemia. *Leukemia*. 2012;26(10):2245–53.
6. Cario G, Zimmermann M, Romey R, et al. Presence of the P2RY8-CRLF2 rearrangement is associated with a poor prognosis in non-high-risk precursor B-cell acute lymphoblastic leukemia in children treated according to the ALL-BFM 2000 protocol. *Blood*. 2010;115(26):5393–5397.
7. Mullighan CG, Collins-Underwood JR, Phillips L a a, et al. Rearrangement of CRLF2 in B-progenitor- and Down syndrome-associated acute lymphoblastic leukemia. *Nat. Genet.* 2009;41(11):1243–6.
8. Ghazavi F, Lammens T, Van Roy N, et al. Molecular basis and clinical significance of genetic aberrations in B-cell precursor acute lymphoblastic leukemia. *Exp. Hematol.* 2015;43(8):640–653.
9. Hertzberg L, Vendramini E, Ganmore I, et al. Down syndrome acute lymphoblastic leukemia, a highly heterogeneous disease in which aberrant expression of CRLF2 is associated with mutated JAK2: A report from the International BFM Study Group. *Blood*. 2010;115(5):1006–1017.
10. Roberts KG, Li Y, Payne-Turner D, et al. Targetable Kinase-Activating Lesions in Ph-like Acute Lymphoblastic Leukemia. *N. Engl. J. Med.* 2014;371(11):1005–1015.
11. Harvey RC, Mullighan CG, Chen IM, et al. Rearrangement of CRLF2 is associated with mutation of JAK kinases, alteration of IKZF1, Hispanic/Latino ethnicity, and a poor outcome in pediatric B-progenitor acute lymphoblastic leukemia. *Blood*.

2010;115(26):5312–5321.

12. Roll JD, Reuther GW. CRLF2 and JAK2 in B-progenitor acute lymphoblastic leukemia: A novel association in oncogenesis. *Cancer Res.* 2010;70(19):7347–7352.
13. Russell LJ, Capasso M, Vater I, et al. Deregulated expression of cytokine receptor gene, CRLF2, is involved in lymphoid transformation in B-cell precursor acute lymphoblastic leukemia. *Blood*. 2009;114(13):2688–2698.
14. Chen I-M, Harvey RC, Mullighan CG, et al. Outcome modeling with CRLF2, IKZF1, JAK, and minimal residual disease in pediatric acute lymphoblastic leukemia: a Children's Oncology Group study. *Blood*. 2012;119(15):3512–22.
15. Tasian SK, Doral MY, Borowitz MJ, et al. Aberrant STAT5 and PI3K/mTOR pathway signaling occurs in human CRLF2-rearranged B-precursor acute lymphoblastic leukemia. *Blood*. 2012;120(4):833–842.
16. Bugarin C, Sarno J, Palmi C, et al. Fine Tuning of Surface CRLF2 Expression and Its Associated Signaling Profile in Childhood B Cell Precursor Acute Lymphoblastic Leukemia. *Child. B Cell Precursor Acute Lymphoblastic Leuk. Haematol.* 2015;1003324.:
17. Maude SL, Tasian SK, Vincent T, et al. Targeting JAK1/2 and mTOR in murine xenograft models of Ph-like acute lymphoblastic leukemia. *Blood*. 2012;120(17):3510–3518.
18. Bendall SC, Simonds EF, Qiu P, et al. Single-cell mass cytometry of differential immune and drug responses across a human hematopoietic continuum. *Science*. 2011;332(6030):687–96.
19. Maude SL, Dolai S, Delgado-Martin C, et al. Efficacy of JAK/STAT pathway inhibition in murine xenograft models of early T-cell precursor (ETP) acute lymphoblastic leukemia. *Blood*. 2015;125(11):1759–67.
20. Dos Santos C, McDonald T, Ho YW, et al. The Src and c-Kit kinase inhibitor dasatinib enhances p53-mediated targeting of human acute myeloid leukemia stem cells by chemotherapeutic agents. *Blood*. 2013;122(11):1900–1913.
21. Shah NP, Tran C, Lee FY, et al. Overriding imatinib resistance with a novel ABL kinase inhibitor. *Science (80-.).* 2004;305(5682):399–401.
22. Sandhöfer N, Metzeler KH, Rothenberg M, et al. Dual PI3K/mTOR inhibition shows antileukemic activity in MLL-rearranged acute myeloid leukemia. *Leukemia*. 2014;(April):1–11.
23. Chapuis N, Tamburini J, Green AS, et al. Dual inhibition of PI3K and mTORC1/2 signaling by NVP-BEZ235 as a new therapeutic strategy for acute myeloid leukemia. *Clin. Cancer Res.* 2010;16(22):5424–5435.

24. van Dongen JJ, Seriu T, Panzer-Grumayer ER, et al. Prognostic value of minimal residual disease in acute lymphoblastic leukaemia in childhood. *Lancet*. 1998;352(9142):1731–1738.
25. Campana D. Minimal residual disease monitoring in childhood acute lymphoblastic leukemia. *Curr. Opin. Hematol.* 2012;19(4):313–318.
26. Fienberg HG, Simonds EF, Fantl WJ, Nolan GP. A Platinum-Based Covalent Viability Reagent for Single-Cell Mass Cytometry. 2012;(5):1–9.
27. Zunder ER, Finck R, Behbehani GK, et al. Palladium-based mass tag cell barcoding with a doublet-filtering scheme and single-cell deconvolution algorithm. *Nat. Protoc.* 2015;10(2):316–33.
28. Finck R, Simonds EF, Jager A, et al. Normalization of mass cytometry data with bead standards. *Cytom. Part A*. 2013;83 A(5):483–494.
29. Bodenmiller B, Zunder ER, Finck R, et al. Multiplexed mass cytometry profiling of cellular states perturbed by small-molecule regulators. *Nat. Biotechnol.* 2012;30(9):858–67.
30. Amir ED, Davis KL, Tadmor MD, et al. viSNE enables visualization of high dimensional single-cell data and reveals phenotypic heterogeneity of leukemia. *Nat. Biotechnol.* 2013;31(6):545–52.
31. Gaipa G, Cazzaniga G, Valsecchi MG, et al. Time point-dependent concordance of flow cytometry and real-time quantitative polymerase chain reaction for minimal residual disease detection in childhood acute lymphoblastic leukemia. *Haematologica*. 2012;97(10):1586–1593.
32. Shochat C, Tal N, Bandapalli OR, et al. Gain-of-function mutations in interleukin-7 receptor-α (IL7R) in childhood acute lymphoblastic leukemias. *J. Exp. Med.* 2011;208(5):901–908.
33. Chou TC. Drug combination studies and their synergy quantification using the chou-talalay method. *Cancer Res.* 2010;70(2):440–446.
34. Chou TC, Talalay P. Quantitative analysis of dose-effect relationships: the combined effects of multiple drugs or enzyme inhibitors. *Adv. Enzyme Regul.* 1984;22(C):27–55.
35. Loh ML, Zhang J, Harvey RC, et al. Tyrosine kinome sequencing of pediatric acute lymphoblastic leukemia : a report from the Children ' s Oncology Group TARGET Project. 2015;121(3):485–489.
36. Qin H, Cho M, Haso W, et al. Eradication of B-ALL using chimeric antigen receptor-expressing T cells targeting the TSLPR oncoprotein. *Blood*. 2015;126(5):629–639.
37. Vetter T, Borowski A, Wohlmann A, et al. Blockade of thymic stromal

lymphopoietin (TSLP) receptor inhibits TSLP-driven proliferation and signalling in lymphoblasts from a subset of B-precursor ALL patients. *Leuk. Res.* 2016;40:38–43.

38. Borowski A, Vetter T, Kuepper M, et al. Expression analysis and specific blockade of the receptor for human thymic stromal lymphopoietin (TSLP) by novel antibodies to the human TSLPRα receptor chain. *Cytokine*. 2013;61(2):546–555.
39. Raghunathan R, Mahesula S, Kancharla K, et al. Anti-CRLF2 antibody-armored biodegradable nanoparticles for childhood B-ALL. *Part. Part. Syst. Charact.* 2013;30(4):355–364.
40. Levine JH, Simonds EF, Bendall SC, et al. Data-Driven Phenotypic Dissection of AML Reveals Progenitor-like Cells that Correlate with Prognosis. *Cell*. 2015;162(1):184–197.
41. Furqan M, Mukhi N, Lee B, Liu D. Dysregulation of JAK-STAT pathway in hematological malignancies and JAK inhibitors for clinical application. *Biomark. Res.* 2013;1(1):5.
42. Quint??s-Cardama A, Verstovsek S. Molecular pathways: JAK/STAT pathway: Mutations, inhibitors, and resistance. *Clin. Cancer Res.* 2013;19(8):1933–1940.
43. Bercovich D, Ganmore I, Scott LM, et al. Mutations of JAK2 in acute lymphoblastic leukaemias associated with Down ' s syndrome. *Lancet*. 2008;372(9648):1484–1492.
44. Izraeli S, Shochat C, Tal N, Geron I. Towards precision medicine in childhood leukemia - Insights from mutationally activated cytokine receptor pathways in acute lymphoblastic leukemia. *Cancer Lett.* 2014;352(1):15–20.
45. Warmuth M, Kim S, Gu X. Ba/F3 cells and their use in kinase drug discovery. *Curr. Opin. …*. 2007;19(1):55–60.
46. Schult C, Dahlhaus M, Glass A, et al. The dual kinase inhibitor NVP-BEZ235 in combination with cytotoxic drugs exerts anti-proliferative activity towards acute lymphoblastic leukemia cells. *Anticancer Res.* 2012;32(2):463–474.
47. Bendall SC, Nolan GP. From single cells to deep phenotypes in cancer. *Nat. Biotechnol.* 2012;30(7):639–647.
48. Basso G, Veltroni M, Valsecchi MG, et al. Risk of relapse of childhood acute lymphoblastic leukemia is predicted by flow cytometric measurement of residual disease on day 15 bone marrow. *J. Clin. Oncol.* 2009;27(31):5168–5174.

SUPPLEMENTARY FIGURES

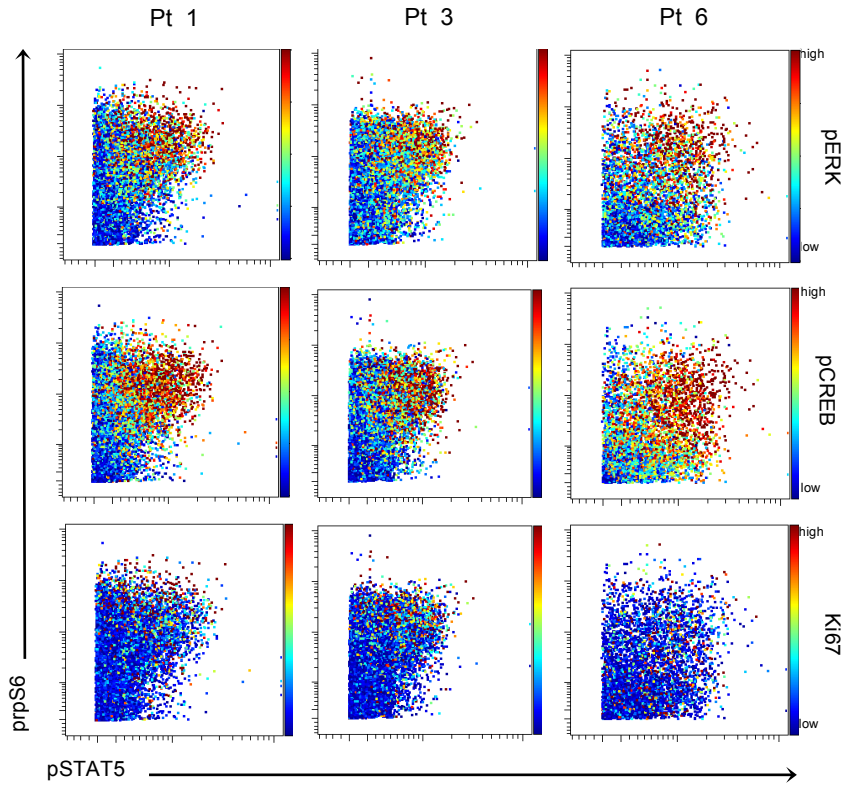

Supplementary Figure 1: Single cell analysis of TSLP-induced proteins
Plots indicating the TSLP-activated signaling in 3 *CRLF2r* patients not shown in Figure 3B (Pt #1, Pt #3 and Pt #6). The single cells plots represent the levels of pSTAT5 (x axis), prpS6 (y axis) and are colored by the expression of pERK (first row), pCREB (second row) and Ki67 (third row) based on a colorimetric scale from blue (low expression) to red (high expression).

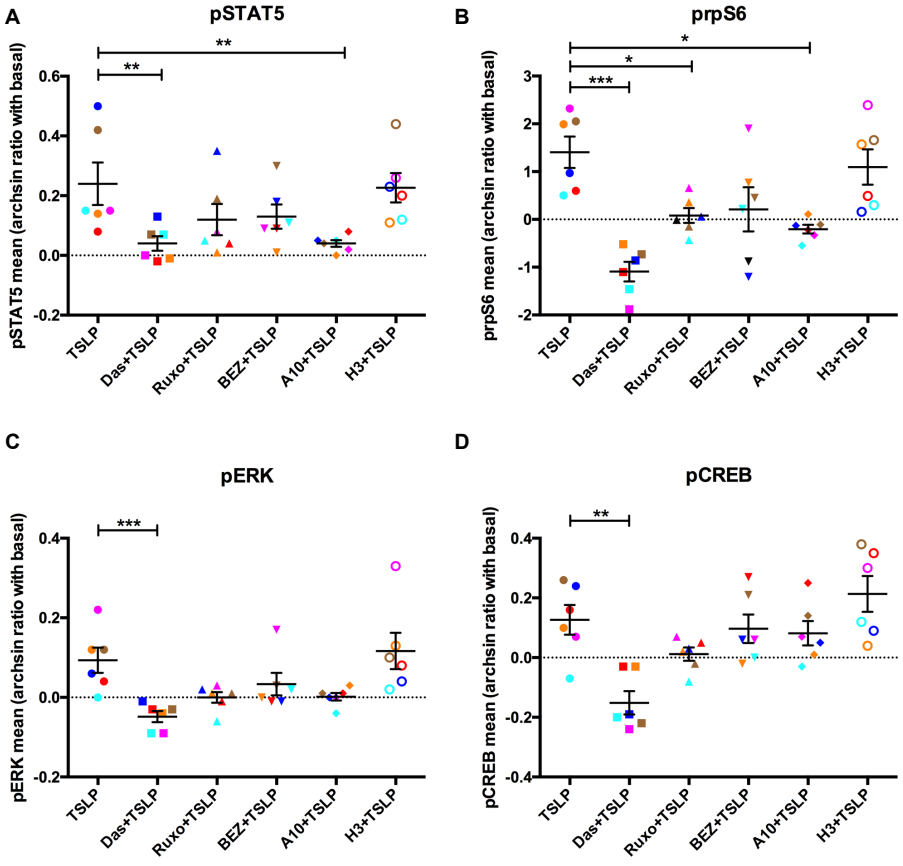

Supplementary Figure 2: Agents treatment effects on TSLP-related signaling

(A-D) Scatter plots indicating the levels of pSTAT5, prpS6, pERK and pCREB respectively in the TSLP alone and agents + TSLP treated conditions. In each condition the level of the phosphoprotein is calculated as arcsinh ratio of the treated condition compared to the basal state and the p-values are indicated by using asterisks (* p<0.5, ** p<0.01, *** p<0.001).

Each patient is associated to a different color: Pt #1 red; Pt #2 cyan; Pt #3 orange; Pt #4 brown; Pt #5 magenta; Pt #6 blue.

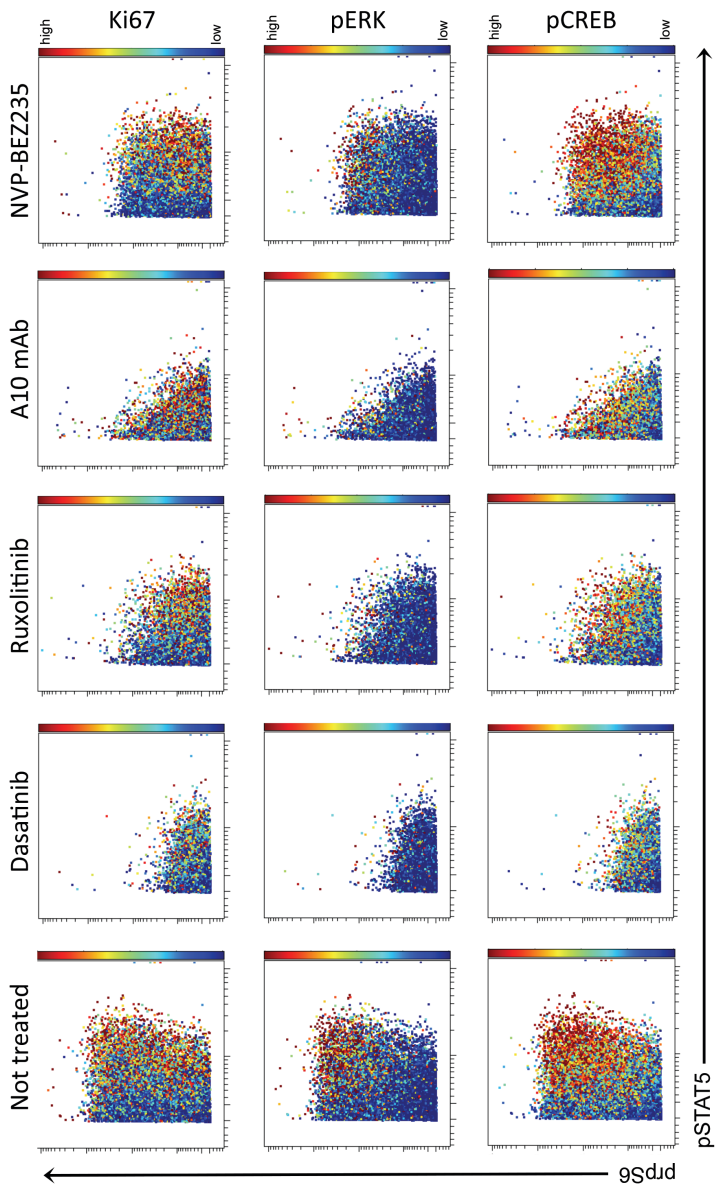

Supplementary Figure 3: Single cell analysis of treated cells
Plots indicating the levels of pSTAT5 (x axis), prpS6 (y axis) in one CRLF2r patient (Pt4) in not treated versus treated conditions. The dots are colored by the expression of Ki67 (first row), pERK (second row) and pCREB (third row) based on a colorimetric scale from blue (low expression) to red (high expression).

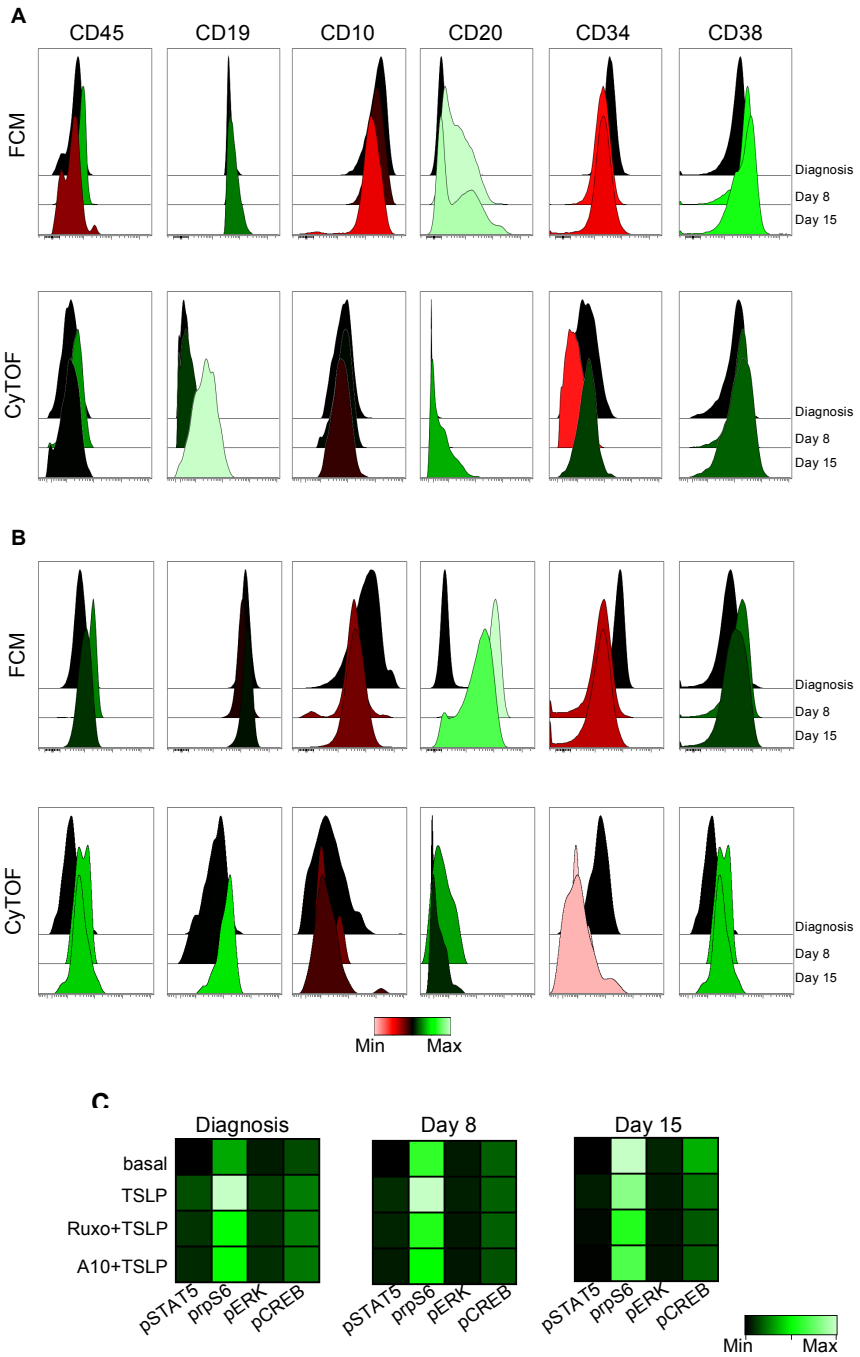
A
CD45
CD19
CD10
CD20
CD34
CD38
FCM
CyTOF
Diagnosis
Day 8
Day 15
B
Min
Max
C
Diagnosis
Day 8
Day 15
basal
TSLP
Ruxo+TSLP
A10+TSLP
pSTAT5
prpS6
pERK
pCREB
Min
Max

Supplementary Figure 4: MRD immunophenotypic comparison between Flow Cytometry and CyTOF

(A-B) Histogram overlay of the expression of the different markers at Diagnosis, Day 8 and Day 15 in 2 (panel A and B) out of 3 *CRLF2r* analyzed patients. The histograms are colored by statistics (arcsinh ratio of mean at day 8 and day 15 compared to the diagnosis). Although with different intensities, is possible to observe a similar trend expression of the immunophenotypic markers widely used for the MRD detection[48].

(C) Raw heatmaps representing the levels of pSTAT5, prpS6, pERK and pCREB in one *CRLF2r* patient (Pt #13) at diagnosis, day 8 and day 15 in 4 different conditions: basal state, TSLP stimulated, Ruxolitinib + TSLP and A10 mAb + TSLP treated cells.

Chapter 4

Paper submitted

The histone deacetylase inhibitor Givinostat (ITF2357) has a potent anti-tumor activity against *CRLF2* rearranged BCP-ALL

A.M. Savino [1], **J.Sarno** [1], L.Trentin [2], M. Vieri [1], G. Fazio [1], M. Bardini [1], C. Bugarin [1], G. Fossati [3], K. Davis [4], G. Gaipa [1], L.H. Meyer [5], G.P. Nolan [4], A. Biondi [1], G. Te Kronnie[2], C. Palmi [1]* and G. Cazzaniga [1]*.

*These authors share the senior authorship

1. Tettamanti Research Center, Department of Pediatrics, University of Milano Bicocca, Fondazione MBBM, Monza, Italy.
2. Department of Women's and Children's Health, University of Padova, Padova, Italy.
3. Preclinical R&D Department, Italfarmaco S.p.A., Cinisello Balsamo, Milan, Italy.
4. Baxter Laboratory in Stem Cell Biology, Department of Microbiology and Immunology, Stanford University, Stanford, CA 94305, USA; Hematology and Oncology, Department of Pediatrics, Stanford University, Stanford, CA 94305, USA.
5. Department of Pediatrics and Adolescent Medicine, Ulm University Medical Center, Ulm, Germany.

ABSTRACT

Inhibition of CRLF2/JAK2 signaling has potential as a therapeutic target for subgroups of poor prognostic patients with genomic alterations of *CRLF2* and *JAK2* genes deregulating JAK/STAT signaling. The HDAC inhibitor Givinostat/ITF2357 has been approved for the treatment of systemic juvenile idiopathic arthritis and polycythemia vera. In myeloproliferative neoplasms it showed a marked inhibition of JAK/STAT pathway, suggesting its translation to other contexts of deregulation of this signaling, i.e. CRLF2 rearranged BCP-ALL, currently lacking effective therapies. We demonstrated that Givinostat inhibited proliferation and induced apoptosis of BCP-ALL *CRLF2*-rearranged cell lines positive for exon 16 *JAK2* mutations and primary cells from patients carrying *CRLF2* rearrangements, sparing the normal hematopoietic counterpart. At low doses, Givinostat downregulated genes of the JAK/STAT pathway and inhibited the basal and ligand-induced signaling, reducing the phosphorylation of STAT5. *In vivo*, Givinostat significantly reduced engraftment of human blasts in xenograft models of CRLF2 positive BCP-ALL. Importantly, Givinostat intensified the effect of current chemotherapy in *in vitro* and *ex vivo* models. In conclusion, this drug may represent a novel and effective tool, in combination with current chemotherapy, to treat this difficult to handle subset of ALL, including CRLF2 rearranged and Down Syndrome BCP-ALL.

INTRODUCTION

B Cell Precursor Acute Lymphoblastic Leukemia (BCP-ALL) represents 35% of all cancer in pediatric age group. The cure rate for this disease approaches 90% with current treatment regimens[1]; however, with standard chemotherapy and/or hematopoietic stem cell transplantation, the probability of survival for patients who relapse is only 30%. Therefore, there is an urgent need to identify novel therapeutic approaches, in particular for the subgroups of patients with hallmarks of bad prognosis. Recently, alterations of *Cytokine Receptor-like Factor 2 (CRLF2)*, have been identified in up to 7% of pediatric BCP-ALL and associated to a poor outcome[2-3]. In particular, these patients represent half of Ph-like ALL[4] and half of Down Syndrome (DS)-associated BCP-ALL[5,6]. Rearrangements of *CRLF2* result in the overexpression of this component of the heterodimeric receptor for thymic stromal lymphopoietin (TSLP) and lead to deregulation of JAK/STAT and PI3K/mTOR pathways, causing hyperactive signaling[2,7,8]. Moreover, *CRLF2* overexpression is highly associated with point mutations in JAK family members[2,4,9,10] and experimental data showed that the introduction of *CRLF2* rearrangements and *JAK2* mutations together induced transformation of the murine BCP cell line BaF3[6].

The JAK/STAT pathway represents one of the main cascade mediating cytokine receptor signaling and plays an important role in hematopoietic cell growth, proliferation, differentiation and survival[11]. A variety of

hematologic malignancies are characterized by deregulated JAK/STAT signaling through several mechanisms, including JAK activating mutations, fusions and repression of negative regulators[12-13]. CRLF2 gene rearrangements are responsible for a relevant part of these deregulations. However, few data exist on effective treatment strategies against them. Some reports demonstrated the efficacy of heat shock protein 90 inhibition and minimal activity of JAK inhibitor BVB808 in *CRLF2* rearranged BCP-ALL[14]. Recently, Maude et al. reported *in vivo* efficacy of JAK1/2 inhibitor Ruxolitinib on xenografted ALL bearing JAK activating lesions[15] and early T precursors (ETP) ALL, a subset of T-ALL with hyperactivation of the JAK/STAT pathway[16]. Nevertheless, growing evidence of new resistance mechanisms to JAK inhibitors impairing their efficacy[17] underline the need for innovative therapeutic strategies. However, not all CRLF2 positive cases bear mutations in partner proteins such as JAK. Indeed, in *CRLF2* overexpressed cases without JAK mutations, Ruxolitinib showed only a modest effect in reducing tumor burden, indicating that a broader anti-tumoral effect is required for these cases[15].

Intriguingly, the pan histone deacetylase Givinostat (ITF 2357) showed efficacy in a Phase IIA clinical trial for myeloproliferative neoplasms (MPN) bearing *JAK2V617F* mutation, with hyperactivation of the JAK/STAT signaling pathway[18], as well as in a phase II trial for Polycythemia Vera, in which the *JAK2V617F* mutation comprises >95% of

patients[19,20]. This drug is also approved for pediatric autoimmune diseases[21], it is well tolerated, with manageable side effects.

Although JAK2 mutations are different in MPN and leukemia, nevertheless they produce a similar effect of the hyperactivation of JAK/STAT pathway. We therefore hypothesized that Givinostat could be efficacious as well against *CRLF2* rearranged leukemia, affecting the same JAK/STAT pathway as in MPN[20].

The rationale of using HDAC inhibitors to target the STAT5 hyperactivation in *CRLF2* rearranged leukemia, even in absence of JAK2 mutation, is also sustained by the discovery of STAT5 transcriptional regulation by acetylation mechanisms. Indeed, the deacetylase inhibitor trichostatin A (TSA) inhibits STAT5-mediated transcription by preventing recruitment of the transcriptional machinery downstream to STAT5 binding to DNA[22], through a rapid increase in global histone acetylation.

Moreover, Givinostat efficacy was recently demonstrated in T cell ALL[23], thus supporting our hypothesis on its effectiveness also in acute lymphoblastic disorders, and further showing that its potential to affect different pathways renders it very effective in different pathologies.

This study establishes the *in vitro* and *in vivo* efficacy of Givinostat in ALL cases with *CRLF2* rearrangements, alone or in combination with conventional chemotherapy. We showed that Givinostat causes transcriptional modulation of genes involved in JAK/STAT pathway, leading to the inactivation of this signaling network. Overall, this drug

may represent a novel and effective tool to treat this subset of ALL with poor outcome.

MATERIALS AND METHODS

Cell culture and patients samples

MHH-CALL4 and MUTZ5 are BCP-ALL cell lines overexpressing *CRLF2* via *IGH@-CRLF2* translocation and harboring *JAK2* mutations (*JAK2*I682F and R683G, respectively). The SET2 cell line bearing *JAK2*V617F mutation was chosen as a positive control for JAK/STAT pathway downregulation by Givinostat[24]. The *JAK2wt* K562cell line was included as a negative control with a high IC50 response to Givinostat[24] (obtained from DSMZ, Braunschweig, Germany). RS 4;11 (a BCP-ALL cell line bearing MLL-AF4 fusion) was used for its low basal pSTAT5 level. Cells were grown in RPMI medium supplemented with 10-20% fetal bovine serum, 1% L-glutammine and 1% penicillin/streptomycin at 37° C in humidified air with 5% CO_2.

Five patients were selected on the basis of their positivity for *CRLF2* alterations and availability of biological material (Table 1). Investigation has been conducted in accordance with the ethical standards, with the declaration of Helsinki and after institutional review board approval.

Primary leukemic cells from diagnostic bone marrows were used to establish xenograft mouse models.

Table 1. Main clinical and biological features of analyzed patients.

Sample no.	Protocol	age at diagnosis (years)	Sex	WBC x10^3/µl	Down Syndrome	Immunophenotype	Final risk	CRLF2r	JAK2	other genetic lesions
Pt # 1	ALL2000	5	F	16600	No	B-II	Standard Risk	P2RY8-CRLF2	wt	del CDKN2A/2B del BTG1 (exon 2)
Pt # 2	ALL2009	3	F	87210	No	B-II	Standard Risk	P2RY8-CRLF2	wt	del CDKN2A/2B del PAX5 (exon 1)
Pt # 3	ALL2009	2	M	23940	Yes	B-II	Standard Risk	P2RY8-CRLF2	wt	del CDKN2A/2B
Pt # 4	ALL2009	15	M	1870	Yes	B-II	High Risk	P2RY8-CRLF2	L681-I682 insGL	del IKZF1 (exons 2-7) del CDKN2A/2B (homo) del PAX5 (exon 5)
Pt # 5	ALL2009	4	F	-	Yes	B-III	High Risk	P2RY8-CRLF2	wt	del PAX5 (exon 2 and 5) del BTG1 (exon 2)

In vitro and *ex vivo* analysis of leukemia cells

Cells lines and xenograft leukemia blasts were incubated with Givinostat (ITF2357, Italfarmaco, Cinisello Balsamo, Italy) dissolved in DMSO, or only DMSO as vehicle, in 24-well plates. Freshly isolated blasts from xenograft models were plated in medium on a layer of confluent OP9 stroma. After 24 h up to one week (168h), non-adherent cells were collected. Citotoxicity assays were performed with Annexin V-FITC Apoptosis Detection Kit Plus (BioVision, San Francisco, California, USA) following the manufacturer instructions. Live cells (negative for both Annexin V and Sytox staining) were assessed by cytofluorymetric technique (FACS). Proliferation assays were performed only for cell lines by counting live cells by FACS. Experiments were performed in triplicate. STAT5 phosphorylation was measured by phosphoflow as previously described[25]. Cell lines and xenograft blasts were incubated for 24 h with Givinostat at 0.2 µM or DMSO at 37° C. After treatment, cells were

stimulated with rhTSLP (0.1-10 ng/mL) for 30 minutes at 37° C to allow signal transduction and pSTAT5 levels were evaluated by FACS.

Microarray analysis and qRT-PCR assay

Gene expression analysis was carried out on *ex-vivo* treated xenograft leukemia cells from primary or secondary transplantation (N=5) after 6 h of incubation with Givinostat or vehicle.

All microarray raw data (CEL files) and probe set signals are available at the National Center for Biotechnology Information Gene Expression Omnibus database (GEO, http://www.ncbi.nlm.nih.gov/geo/), series accession number GSE77270 (http://www.ncbi.nlm.nih.gov/geo/query/acc.cgi?token=mdwpqoeqhjuhzef&acc=GSE77270).

Validation of differentially expressed genes was performed by quantitative RT-PCR (qRT-PCR) using TaqMan Gene Expression Assays and the Universal Probe Library System (UPL) (Roche Diagnostic, Basel, Switzerland). Differences were considered statistically significant at p values <0.05, indicated in experiments with asterisks: *p<0.05; **p<0.01; ***p<0.001.

CyTOF analysis

Cytometry by Time Of Flight' (CyTOF) mass spectrometry analysis was performed using diagnostic samples for patient 2,3,5 and xenograft-

derived blasts for patient 4 (table 1), according to the availability of the cells. One million single cells per sample have been treated with Givinostat (0.2 µM) for 24 hours and then analyzed via CyTOF using previously described approach[26]. Cells were gated to exclude debris (DNA negative), dead cells (cPARP and cisplatinum positive)[27] and were proportionally clustered based on the expression of 17 up on 30 surface and intracellular markers using viSNE software powered by Cytobank (see supplementary table 1 for the complete list).

In vivo treatment

All in vivo experiments were conducted on protocols approved by Italian Health Ministry (64/2014 PR). For efficacy studies, once xenografts had engrafted (0.1-1% human blasts in the bone marrow), mice were randomized to treatment (30 mg/kg Givinostat) or vehicle (1% DMSO+PEG400-H2O 1:1) (3-5 mice per arm). Givinostat or vehicle was administered for 7 weeks (5 days/week) by intraperitoneal injection. At the end of treatment, mice were sacrificed and spleens and bone marrows were harvested. Disease burden was assessed at this end point, by measuring the absolute number of splenic and bone marrow blasts (total splenic or bone marrow count x %human CD10+/CD19+/CRLF2+ cells).

Drug combination assays

To mimic the effect of chemotherapy, Methyl-prednisolone (Sanofi, Italy) or a mix of Asparaginase (EUSA Pharma, UK), Vincristine (Pfizer, Italy) and Dexamethasone (Farmaceutici CABER, Italy) were used for combination assays. The doses employed for the combination were chosen under the IC50 value for each agent, calculated with Compusyn software (Compusyn; Biosoft, Cambridge, UK), after performing single dose/effect curves for each cell line or xenograft blasts (data not shown). Cells were incubated with vehicle, drugs alone or in combination for 72 hours and then inhibition of proliferation or cytotoxic effect was tested as previously described.

Drug additivity or synergy was determined by using the Bliss formula[28].

RESULTS

Givinostat inhibits growth, induces apoptosis and blocks STAT5 phosphorylation in *CRLF2* rearranged cell lines.

The treatment with Givinostat reduced the proliferation of MHH-CALL4 and MUTZ5 cells (both harboring *IGH@-CRLF2* rearrangement and *JAK2* mutation) within 72 hours, with IC50 values of 0.08±0.05μM and 0.17±0.07 μM, respectively (Fig 1A). Moreover, Givinostat induced a decrease in viable cells with IC50 of 0.17±0.03 μM for MHH-CALL4 and 0.25±0.03 μM for MUTZ5 cell line (Fig 1B). Of note, the IC50 values observed for MHH-CALL4 cells were lower than those of SET2 cells (bearing *JAK*2 V617F mutation), both for proliferation (0.08±0.05 μM *vs*. 0.14±0.03 μM) and apoptosis (0.17±0.03 μM *vs*.0.22±0.04 μM). The IC50 values were higher for the K562 cell line (JAK2wt).

To investigate if Givinostat had an effect on the CRLF2-mediated JAK/STAT signaling, we treated cells for 24 hours and then we examined the phosphorylation status of STAT5 in basal state or after TSLP stimulation. As expected, due to the activating *JAK2* point mutation, high basal levels of pSTAT5 were observed in MHH-CALL4 and MUTZ5 compared to other *JAK2wt* BCP-ALL cell lines such as RS4;11 (Supplementary Figure 1). However, low concentration of TSLP (1 ng/ml) significantly increased pSTAT5 (1.5 to 2.2 fold increase for MHH-CALL4 and MUTZ5, respectively). Givinostat (0.2 μM) inhibited basal pSTAT5 in both cell lines (3.9 and 4.5 fold decreases of pSTAT5 mean values for

MUTZ5 and MHH-CALL4, respectively) and reduced phosphorylation below basal levels after TSLP stimulation (2.8 and 2.1 fold decreases under basal levels for MUTZ5 and MHH-CALL4, respectively) (Fig 1C).

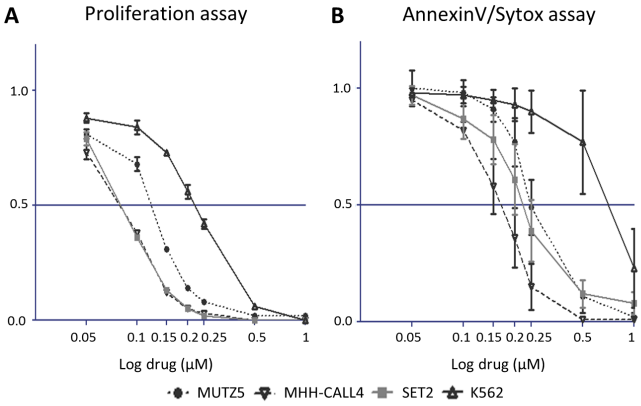

	IC_{50} (µM)
MHH-CALL4	0.08±0.05
SET2	0.14±0.03
MUTZ5	0.17±0.07
K562	0.29±0.07

	IC_{50} (µM)
MHH-CALL4	0.17±0.03
SET2	0.22±0.04
MUTZ5	0.25±0.03
K562	0.7±0.21

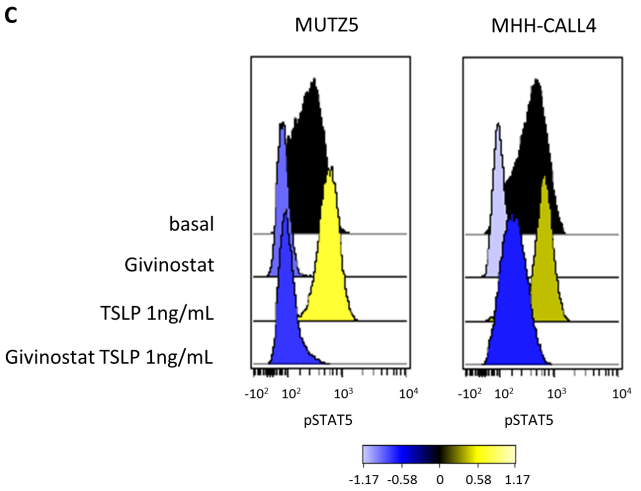

Figure 1. Anti-proliferative and pro-apoptotic effect of Givinostat on cell lines and effect on JAK/STAT signaling.

Analysis of the effect of Givinostat on proliferation (A) and apoptosis (B) for different cell lines. The proliferation assay was performed by flow cytometric count of live cells (Annex V/Sytox double negative) measured in a defined time interval (30''), while the pro-apoptotic assay was performed by measuring the percent of Annexin V/Sytox double negative cells. Y axis: percentage of Givinostat treated live cells (Annexin V/Sytox double negative) normalized on the percentage of vehicle treated cells; X axis: logarithmic increasing doses of Givinostat. The IC50 of the different tested cell lines are shown in reported tables both for proliferation and apoptosis. (C) Inhibition of basal and TSLP-induced STAT5 phosphorylation after treatment with Givinostat in *CRLF2* rearranged cell lines. Data were normalized on the basal pSTAT5 phosphorylation level for colorimetric depiction of signaling changes (blue indicates inhibition and yellow stimulation), and are expressed as arcsinh ratio with first row (isotype).

Givinostat induces apoptosis of *CRLF2* rearranged blasts.

We next investigated the effect of Givinostat on blasts from 5 *CRLF2* rearranged BCP-ALL primary patient samples harboring the *P2RY8-CRLF2* fusion (*CRLF2r*) leading to CRLF2 overexpression; 1 of them harbored a *JAK2* mutation (*JAKm*) consisting of a not previously described insertion (L681-I682 insGL) in exon 16 (Table 1 and Supplementary Figure 2). This insertion is located immediately upstream of R683 in the pseudokinase domain of JAK2 in the same location of other already described insertions[29] known to confer activating phenotype. We developed patient derived xenograft models (see supplementary results for details), and blasts isolated from xenografts were co-cultured on OP9 stroma to

perform *ex vivo* assays. Consistent with our findings in cell lines, Givinostat (0.2 μM) reduced the percentage of live cells in all primografts treated with the drug (Figure 2A). In particular, after 72 hours, Givinostat was able to kill from 70 up to >90% of blast cells in all 5 primografts, in contrast with the control samples which showed from 25 to 60% of blasts still alive.

The effect of Givinostat was also evaluated on primary samples from diagnosis and one primograft (Pt 4) using CyTOF. Although Givinostat was able to induce blast killing after 72 hours (as described in the co-colture experiments), by viSNE analysis, after only 24 hours of treatment with Givinostat, we noticed a decrease of total viable cells (22% to 36%) in treated samples compared to vehicle. Figure 2B indicates the effect of the drug on the downmodulation of the single markers analyzed for one representative case. While we observed a remarkable decrease of CRLF2 and CD10 positive blasts, on the other hand, the B normal counterpart (CD45 high positive cells, including normal T, red blood and myeloid cells) was not affected by the treatment (Fig 2B and Supplementary Figure 3A; details for each marker analyzed are reported in Supplementary Table 2). We further noticed a significant reduction in the number of CD10+ CRLF2 high cells in Givinostat treated sample compared with vehicle (Supplementary Figure 3B).

Givinostat inhibits signal transduction in xenograft *CRLF2* rearranged blasts.

We examined the effect of Givinostat on STAT5 phosphorylation in xenograft *CRLF2* rearranged blasts. Basal pSTAT5 level was lower in blasts than in cell lines due to the lack of mutation in most patients. Low concentration of TSLP (1 ng/ml) induced STAT5 activation in all xenograft blasts but one (Pt #1). At a higher dose of the cytokine (10ng/ml), Givinostat (0.2 μM) inhibited pSTAT5 in all tested xenograft blasts (average fold decrease of pSTAT5: 2.4±0.6) (Figure 2C). An exception was patient 4, who presented an insertion in *JAK2* gene sequence, suspected to be hyperactivating. The mean basal pSTAT5 value in this patient was 5.7 fold higher than the mean basal of the remaining patients, yet Givinostat reduced this pSTAT5 activation (pSTAT5 fold decrease: 6.6), suggesting that the drug is effective in patients with *JAK* mutations as well.

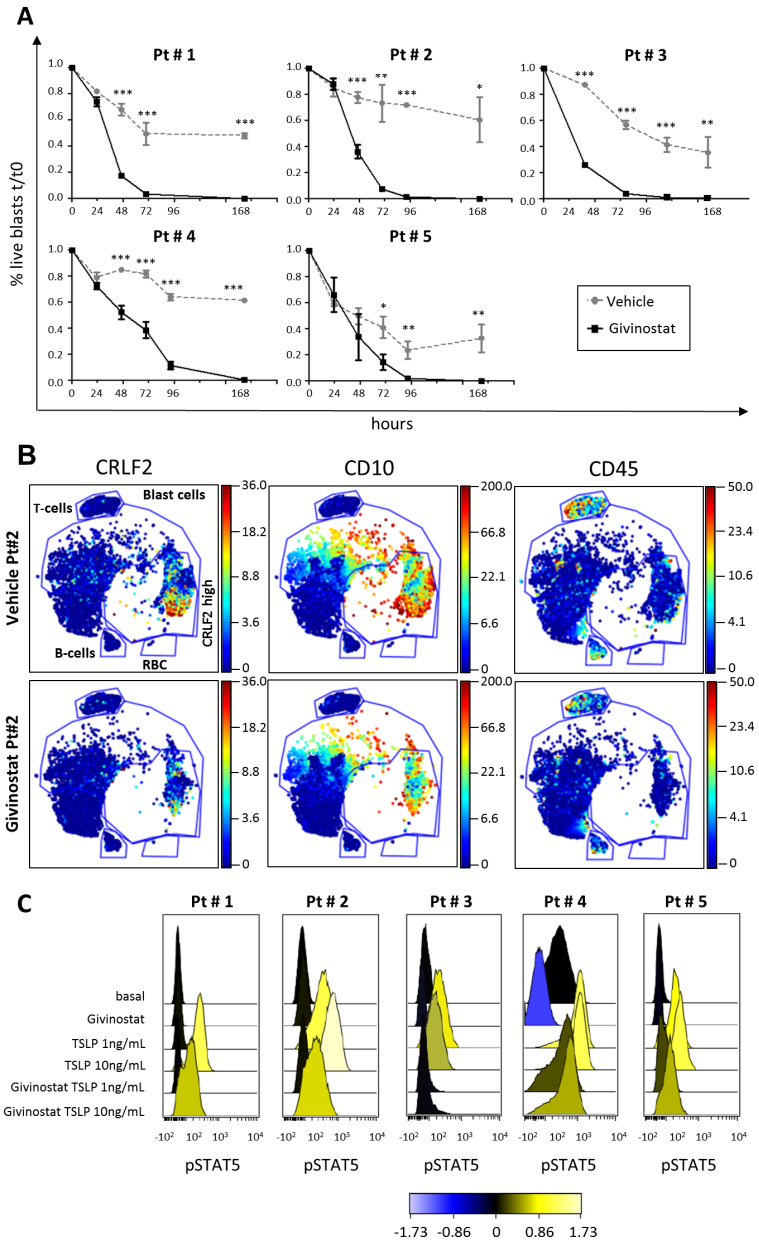
A
Pt # 1
Pt # 2
Pt # 3
Pt # 4
Pt # 5
% live blasts t/t0
hours
Vehicle
Givinostat
B
CRLF2
CD10
CD45
Vehicle Pt#2
Givinostat Pt#2
T-cells
Blast cells
B-cells
RBC
CRLF2 high
C
basal
Givinostat
TSLP 1ng/mL
TSLP 10ng/mL
Givinostat TSLP 1ng/mL
Givinostat TSLP 10ng/mL
pSTAT5
-1.73 -0.86 0 0.86 1.73

Figure 2. Induction of cell death and inhibition of JAK/STAT signaling in xenograft blasts by Givinostat.

Analysis of apoptosis of xenograft *CRLF2* rearranged blasts after exposure to Givinostat *ex-vivo*. The percentage of live (Annexin V/Sytox double negative) human CD10+/mouse CD45.1 negative cells, normalized on their T0, was shown in each panel. (B) Detailed panel of viSNE analyses with 3 representative markers for patient 2. Each point in the viSNE map represents an individual cell and colorimetric depiction for each plot indicates the different level of expression of the considered marker in the cell population analyzed. Blue dots represents blasts negative for that antigen while positivity is indicated by a colorimetric progressive range from yellow to red. Here we show only 3 selected markers from the original panel (CRLF2, CD10, CD45). After treatment with Givinostat the number of dots belonging to CD10+ CRLF2 high expressing group was drastically diminished whereas the high CD45 residue remains unaffected. Among the CD45 positive cells we distinguish T Cells (CD3+, top left), normal B cells (IgM surface/intracellular+, CD19+), Red blood cells-RBC (CD235+ CD61+). (C) Inhibition of STAT5 phosphorylation after treatment with Givinostat in xenograft blasts. Xenograft blasts were plated on OP9 stroma and exposed to 0.2uM Givinostat or vehicle for 24 hours. Stimulation with 1-10 ng/mL TSLP-induced phosphorylation of STAT5 in vehicle treated blasts and Givinostat was able to inhibit this effect. Data were normalized to the basal phosphorylation level of STAT5 protein for colorimetric depiction of signaling changes. Blue indicates inhibition and yellow stimulation

Givinostat modulates the JAK/STAT pathway in *CRLF2* rearranged leukemia cells.

To gain insights into molecular processes modulated by Givinostat in leukemia cells harboring the *CRLF2* rearrangement, we analyzed the gene expression profiles of primografts (N=5) incubated *ex vivo* with 0.2

μM Givinostat or vehicle for 6 hours. By unsupervised hierarchical clustering analysis, the samples clusterized according to treatment (Fig 3A). The global modifications of gene expression upon treatment with Givinostat are described in Supplemental Results and Supplementary Figure 4A.

By pathway analysis interrogating the KEGG database, the HDAC targets silenced by methylation (Supplementary Figure 4B, but also apoptosis, cell cycle, B cell receptor signaling, insulin signaling, p53 signaling and, as expected and hypothesized, JAK/STAT signaling, resulted within the top 20 ranked pathways modulated by the treatment (Supplementary Table 3 and Supplementary Figure 4C). In particular, the transcriptional modification induced by Givinostat in genes related to the JAK/STAT signaling pathway was also confirmed by the negative enrichment of the JAK/STAT gene signature according to GSEA in the treated samples (Fig 3B). Downmodulation of genes included in the JAK/STAT signaling pathway *STAT5A*, *JAK2*, *IL7Rα*, *CRLF2* was validated by qRT-PCR (Figure 3C). In addition, STAT5 target genes with oncogenic function, *BCL2L1* and *cMYC* were downregulated by the treatment. On the contrary, *PTPN1*, coding for a tyrosine phosphatase able to dephosphorylate JAK2, was upregulated in 3 out of 4 tested patients (Fig 3C).

Most importantly, the transcriptional downregulation of *CRLF2* resulted in the downmodulation of the protein as observed by flow cytometry (Fig 3D). The downmodulation of the CRLF2 protein on cell surface was

measured in all tested xenograft blasts after treatment with Givinostat at 0.2 µM for 24 hours. The median of the CRLF2 peak of Givinostat treated cells was 3.55±1.35 fold lower than control (paired t test, p=0.02) (Supplementary Table 4).

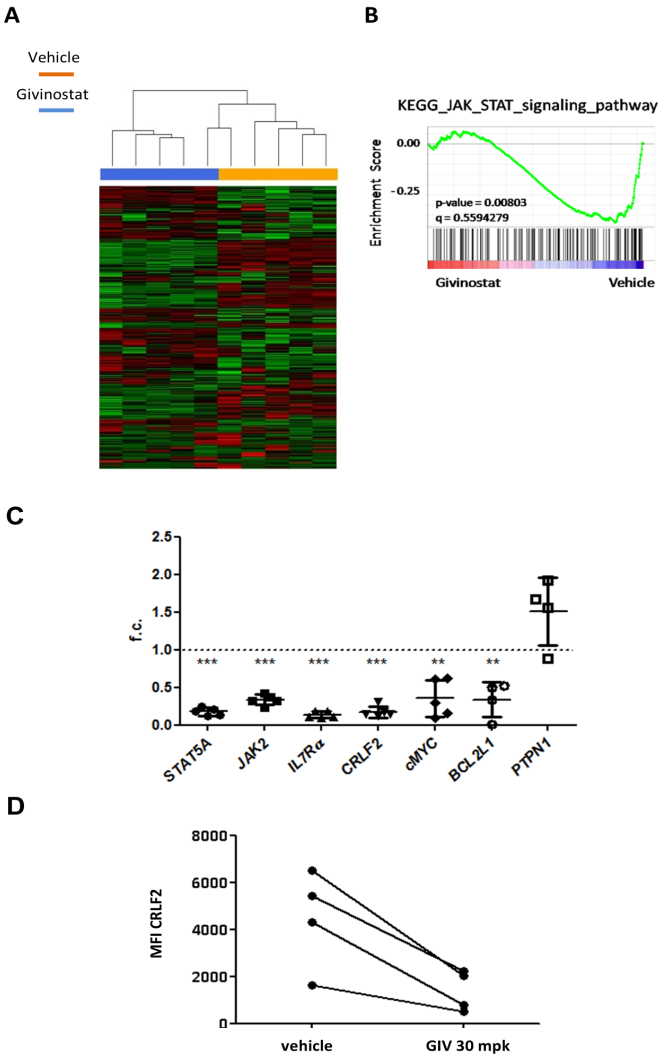

Figure 3. Effect of Givinostat on genes involved in JAK/STAT pathway.
(A) Unsupervised hierarchical clustering analysis using probe set values normalized with RMA and filtered by variance >90% between treated (in blue) and control samples (orange) to highlight associations between clusters of samples and clusters of genes. (B) GSEA analysis plot showing the negative enrichment of the "KEGG_JAK_STAT_signaling_pathway" gene set in Givinostat treated samples (negative Normalized Enrichment Score, NES=-1.4461855) and the corresponding positive enrichment in Vehicle treated samples. (C) Genes involved in JAK/STAT pathway were measured by RQ-PCR. The graphs report the relative gene expression of the indicated genes in drug-treated cells versus untreated cells whose gene expression was conventionally set at value 1. (D) Surface expression of CRLF2 after treatment with Givinostat. Mean Fluorescence Intensity (MFI) was plotted for 4 patients according to cells availability.

Givinostat inhibits blasts engraftment in xenograft models of *CRLF2* rearranged BCP-ALL.

We determined the efficacy and the therapeutic activity of Givinostat in an *in vivo* model of CRLF2+ BCP-ALL, by intravenously injecting blasts from patients 1, 2 and 3 in NOD/SCID mice. Seven days after transplantation, mice were randomized to receive Givinostat at 30 mg/kg or vehicle (5 days/week) via intraperitoneal injection. Disease burden was assessed after 7 weeks of treatment when mice were sacrificed and bone marrow and spleen were collected for analysis. All three *CRLF2* rearranged xenograft models exhibited decreased leukemia burden after Givinostat treatment compared to vehicle, evidenced by a

decreased total blast count in the bone marrow of treated mice (ranging from 1.9 to 34 fold decrease). Moreover, a decreased disease burden was observed in the spleen of xenograft derived from patient 1 (128 fold decrease). Unfortunately, the effect of Givinostat in the spleen was not evaluable for the other patients' derived xenografts, since in this organ very low level of blast engraftment was observed even in absence of the drug (Fig 4).

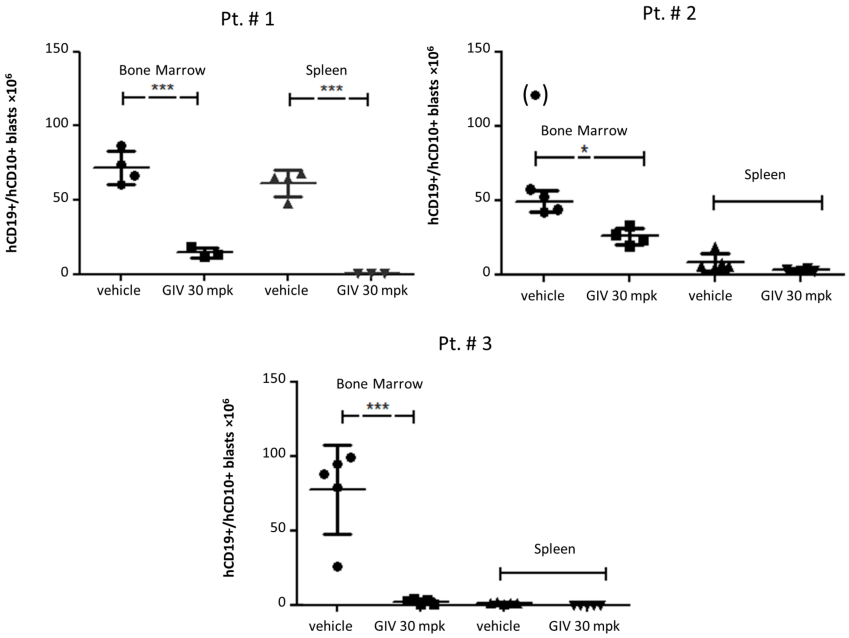

Figure 4. Efficacy of Givinostat in a xenograft model of *CRLF2* rearranged BCP-ALL.

Bone marrow and spleen blast counts at sacrifice in patient 1, 2, 3 xenograft models (3-5 mice per arm). Distribution of absolute blast count identified as human CD10/CD19 double positive cells with means and standard deviation are reported. One outlier in vehicle treated group (xenograft of patient 2), plotted in brackets, has been analyzed but excluded from the statistical analysis.

Givinostat augments the effect of chemotherapy in inhibiting proliferation and inducing apoptosis in *CRLF2* rearranged cell lines and xenograft blasts.

Having established the efficacy of Givinostat as single agent, we next evaluated its effect in combination with main chemotherapeutic drugs used in pediatric clinical protocols[30].

We measured the *in vitro* sensitivity of MHH-CALL4 and MUTZ5 cell lines to Methyl-prednisolone as monotherapy, both as anti-proliferative as well as apoptotic effects (Figure 5A and 5B, respectively). While MUTZ5 cells were sensitive to Methyl-prednisolone[31] (IC50 for cytotoxicity: 0.007ug/ml), MHH-CALL4 were only partially responsive to the drug, even at high doses (IC50 for cytotoxicity: 4.5ug/ml; even at 24ug/ml still 30% of cells are resistant). Indeed, Givinostat was able to sensitize MHH-CALL4 cells to Methylprednisolone with a synergic effect calculated using the Bliss formula (see supplemental methods).

Further, Givinostat was also able to synergize with the three drug regimen currently used in remission induction therapy: Vincristine, Dexamethasone and Asparaginase (VDA). At low dose, Givinostat (0.1µM) synergized with VDA to induce inhibition of proliferation and cell death in MHH-CALL4 cell line *in vitro* (Annexin V/Sytox assay: 62.5%±0.006 and 72.2%±0.009 live cells after 72 hours of treatment with VDA and Givinostat, respectively, if used as single drugs, versus 21.6%±0.003 live cells in combination ($p<0.001$). The observed effect of

the combination (expressed in percentage of live cells) was significantly lower than the expected one in case of additivity (45.2%±0.008; $p<0.001$). One representative experiment out of three is shown in fig 5 C-D. The same results were obtained with MUTZ5 cell line (Supplementary Figure 5).

We then confirmed these observations on xenograft blasts co-cultured *ex-vivo* on OP9 stroma. Although xenograft blasts demonstrated a decreased viability after 72 hours of culture even without drug treatment, as shown in Fig 5E we found a significantly strong cytotoxic activity of Givinostat in combination with both Methyl-prednisolone and VDA. The percentage of live cells after VDA treatment ranged from 6.27 to 35.33%, and significantly decreased to 1.37-4.30% with the combination. The same effect was observed for Methyl-prednisolone. After treatment with the single drug the percentage of live cells ranged from 5.17 to 39.10 *vs* 1 to 16.30% after combination with Givinostat. In particular, the effect of combination, evaluated by the Bliss formula, showed an additive effect for patients 1, 2, 3 and a synergic effect for patient 4, both for Givinostat plus Methyl-prednisolone and plus VDA.

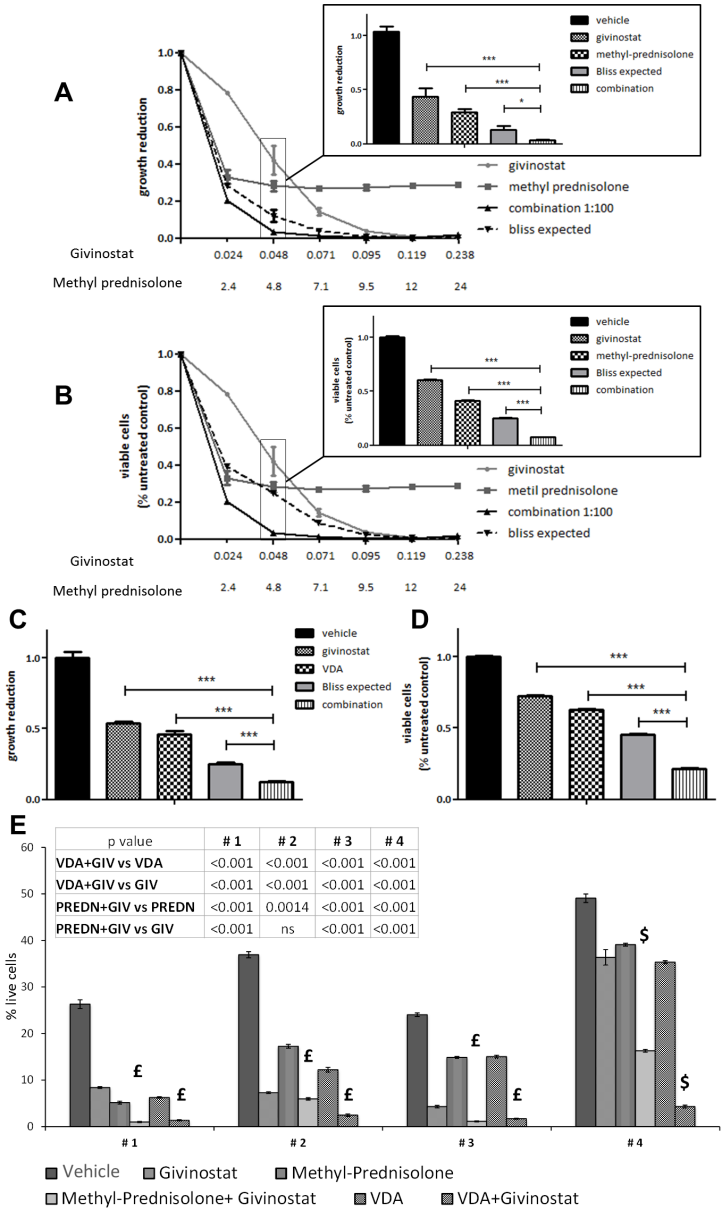

p value	# 1	# 2	# 3	# 4
VDA+GIV vs VDA	<0.001	<0.001	<0.001	<0.001
VDA+GIV vs GIV	<0.001	<0.001	<0.001	<0.001
PREDN+GIV vs PREDN	<0.001	0.0014	<0.001	<0.001
PREDN+GIV vs GIV	<0.001	ns	<0.001	<0.001

Figure 5. Effect of combination of Givinostat with conventional chemotherapy.

In vitro response of MHH-CALL4 cell line to 72 hours of treatment with Methyl-prednisolone and with Givinostat, alone or in combination, determined by proliferation (A) and apoptosis (Annexin/Sytox) assays (B). X axis: drug dose escalation expressed in µg/ml. Dotted lines indicate the expected effect of the drug combination calculated by the Bliss formula. The significance for the lowest dose of both drugs with the highest effect were shown in the black box in detail. Proliferation (C) and Annexin/Sytox assay (D) performed on MHH-CALL4 with Givinostat (0.1 µM) and VDA (Asparaginase 0.23 µg/mL; Dexametasone 0.01 µg/mL; Vincristine 0.001 µg/mL). The expected effect is represented by the grey column. (E) Effect of drug combination on xenograft blasts from patient 1 to 4 after 72 hours of treatment. Givinostat (0.1 µM) was combined with VDA (Asparaginase 0.12 µg/mL; Dexametasone 0.01 ug/ml; Vincristine 0.001 ug/ml) and Methyl-prednisolone (4.8 µg/mL). The percentage of viable cells are reported on Y axis. The £ represents additivity (Bliss formula: EV=AV) and the $ indicates synergy (EV<AV). The significant differences between conditions with their p-values are reported in the table.

DISCUSSION

In the present work we investigated the effect of Givinostat on pediatric BCP-ALL *CRLF2* rearranged cases. Givinostat is an epigenetic drug able to remodel chromatin and, as other HDAC inhibitors, it is known to have a global effect on epigenetic regulation of gene expression. We herewith focused on its effect on genes involved in the JAK/STAT pathway, which is activated in BCP-ALL *CRLF2* rearranged cases.

Notably, we observed the downmodulation of the activator of transcription *STAT5* and of its targets *cMYC* and *BCL2L1,* as already described in polycythemia vera and essential thrombocythemia, in which Givinostat is particularly active[20]. Its activity on *STAT5* was somehow expected since it was also described for other HDAC inhibitors such as Panobinostat in JAK2V617-driven diseases as well[32]. Differently from MPNs, in CRLF2 positive cases Givinostat was effective even in absence of JAK2 mutations, which are not always present in these patients. All these results highlight the potential for targeting 'undrugable' oncogenic transcription factors with epigenetic regulators involved in chromatin remodeling, since direct targeting of STAT proteins remains a great challenge. Interestingly, Givinostat downmodulated also the *CRLF2* gene itself and consequently it reduced the expression of the surface protein. This is particularly important in this subtype of ALL, since the overexpression of this receptor contributes to proliferation and survival processes. Furthermore, Givinostat was able to impair the signaling

network related to CRLF2, as it reduced the STAT5 phosphorylation level both at basal conditions and after TSLP stimulation.

Interestingly, the inhibition effect on the pathway involved different players at different levels of regulation, i.e. the expression of *PTPN1*, coding for a tyrosine phosphatase able to dephosphorylate and inactivate JAK2, was upregulated by the drug. Importantly, several other pathways driving proliferation and survival such as B-cell receptor signaling were downmodulated by the drug, indicating a broader effect of Givinostat in inducing apoptosis, not only by targeting JAK/STAT pathway but inducing a global change in tumor cell epigenome. This represents the main strength of this drug, which allows the targeting of cancer cells from different perspectives, thus lending it an advantage towards more specific therapies.

We verified the efficacy of Givinostat in inhibiting proliferation and inducing cell death of BCP-ALL *CRLF2*-rearranged cell lines at very low doses, with an IC50 similar or even lower than JAK2V617F-mutated SET2 cells, on which the effect of the drug on JAK/STAT signaling has been already demonstrated[24]. This dosage issue has an important clinical correlate, considering that the drug could be effective in patients *in vivo* using the same doses employed in MPN, already optimized and safe.

The cytotoxic effect was confirmed also on primary blasts from patients harboring *CRLF2* rearrangements. Notably, Givinostat efficiently killed blast cells by preserving the normal hematopoietic counterpart, as

demonstrated by CyTOF analyses. CyTOF represents a new generation single cell technology that overcomes the limitations of fluorescence-based flow cytometry[33] by using stable isotopes as reporters instead of fluorophores. This single cell analysis showed that the cellular population affected by Givinostat was represented by blasts with high expression of CRLF2, while the normal hematopoietic cells remain unaffected by the treatment.

Importantly, we have established the preclinical *in vivo* efficacy of Givinostat on xenograft models of three *CRLF2* rearranged patients. The drug markedly reduced the engraftment of leukemic blasts in the bone marrow of treated mice. The effect of reduction was also marked in the spleen for the patient that showed a high tumor burden also in this hematopoietic compartment.

Moreover, we demonstrated the efficacy of Givinostat in combination with other chemotherapeutics on cell lines and on blasts from *CRLF2* rearranged patients. Of note, the most responsive patient to Givinostat in combination with Methyl-prednisolone and VDA was a DS-ALL patient belonging to MRD high-risk group, refractory to the conventional therapy.

The strong effect of low doses of Givinostat in combination with current chemotherapy is intriguing because it elevates the potential of epigenetic therapies in pediatric ALLs and suggests a role for these therapies in subtypes of high risk ALL, like *CRLF2* rearranged BCP-ALL, for

which current cytotoxic chemotherapy yields suboptimal cure rates. Of note, in our cohort three out of five patients were DS-ALL, a subgroup of patients particularly suffering of therapy-related side effects[34]. Actually, some classes of HDAC inhibitors have been found to have a potent anti-leukemic effect in DS with acute megakarioblastic leukemia (DS-AMKL) by inducing apoptosis and suppressing the low basal level of autophagy, typical of cancer cells[35]. If confirmed in a larger cohort of DS-ALL patients the introduction of Givinostat in the standard therapeutic regimen could allow to reduce the doses of chemotherapeutic drugs and their related toxicity and morbidity without losing efficacy. Nevertheless, we cannot exclude that Givinostat is active in other subgroups and future studies could identify other patients who could benefit of the effect of this drug.

ACKNOWLEDGEMENTS

We thank Dr Andrea Ballerini for many helpful discussions. This project was supported by grants from the Associazione Italiana per la Ricerca sul Cancro (AIRC), from the parents' association "Insieme ad Andrea si può, ONLUS" and from the family of Alessandra Aloisi.

AUTHORSHIP CONTRIBUTIONS

A.M.S., J.S, L.T., M.V., G.F., M.B., C.B.,C.P. performed the experiments; A.M.S., J.S, L.T., C.P. analyzed the data; A.M.S., L.T., K.D, C.P. G.C. wrote the manuscript; G.F., K.D., G.G., L.H.M., G.P.N., A.B., G.TK. supervised the research; C.P. and G.C. designed the study and supervised the research.

AUTHORS' DISCLOSURES OF POTENTIAL CONFLICTS OF INTEREST

G.F. is an employees of Italfarmaco SpA.
G. P. N. and K.D. are employees of Fluidigm, Inc: Honoraria and Equity Owner respectively.
All other authors declare nothing to disclose.

REFERENCES

1. Hunger SP, Lu X, Devidas M, et al. Improved survival for children and adolescents with acute lymphoblastic leukemia between 1990 and 2005: A report from the children's oncology group. *J. Clin. Oncol.* 2012;30(14):1663–1669.
2. Russell LJ, Capasso M, Vater I, et al. Deregulated expression of cytokine receptor gene, CRLF2, is involved in lymphoid transformation in B-cell precursor acute lymphoblastic leukemia. *Blood*. 2009;114(13):2688–2698.
3. Chen I, Harvey RC, Mullighan CG, et al. Outcome modeling with CRLF2, IKZF1, JAK, and minimal residual disease in pediatric acute lymphoblastic leukemia: a Children's Oncology Group Study. *Blood*. 2012;119(15):3512–3523.
4. Harvey RC, Mullighan CG, Wang X, et al. Identification of novel cluster groups in pediatric high-risk B-precursor acute lymphoblastic leukemia with gene expression profiling : correlation with genome-wide DNA copy number alterations , clinical characteristics , and outcome Identification of nov. *Blood*. 2010;116(23):4874–4884.
5. Mullighan CG, Collins-underwood JR, Phillips LAA, et al. Rearrangement of CRLF2 in B-progenitor – and Down syndrome – associated acute lymphoblastic leukemia. *Nat. Genet.* 2009;41(11):1243–1246.
6. Hertzberg L, Vendramini E, Ganmore I, et al. Down syndrome acute lymphoblastic leukemia, a highly heterogeneous disease in which aberrant expression of CRLF2 is associated with mutated JAK2: A report from the International BFM Study Group. *Blood*. 2010;115(5):1006–1017.
7. Carpino N, Thierfelder WE, Chang M, et al. Absence of an Essential Role for Thymic Stromal Lymphopoietin Receptor in Murine B-Cell Development Absence of an Essential Role for Thymic Stromal Lymphopoietin Receptor in Murine B-Cell Development. *Mol. Cell. Biol.* 2004;24(6):2584–2592.
8. Tasian SK, Doral MY, Borowitz MJ, et al. Aberrant STAT5 and PI3K / mTOR pathway signaling occurs in human CRLF2 -rearranged B-precursor acute lymphoblastic leukemia. *Blood*. 2012;120(July):833–843.
9. Mullighan CG, Zhang J, Harvey RC, et al. JAK mutations in high-risk childhood acute lymphoblastic leukemia. *Proc. Natl. Acad. Sci. U. S. A.* 2009;106(23):9414–9418.
10. Yoda A, Yoda Y, Chiaretti S, et al. Functional screening identifies CRLF2 in precursor B-cell acute lymphoblastic leukemia. *Proc. Natl. Acad. Sci. U. S. A.* 2010;107(1):252–7.
11. Heim MH. The Jak-STAT pathway: cytokine signalling from the receptor to the nucleus. *J. Recept. Signal Transduct. Res.* 1999;19(1-4):75–120.
12. Baxter EJ, Scott LM, Campbell PJ, et al. Acquired mutation of the tyrosine kinase JAK2 in human myeloproliferative disorders. *Lancet*. 2005;365(9464):1054–1061.

13. Roberts KG, Morin RD, Zhang J, et al. Genetic Alterations Activating Kinase and Cytokine Receptor Signaling in High-Risk Acute Lymphoblastic Leukemia. *Cancer Cell*. 2012;22(2):153–166.
14. Weigert O, Lane AA, Bird L, et al. Genetic resistance to JAK2 enzymatic inhibitors is overcome by HSP90 inhibition. *J. Exp. Med.* 2012;209(2):259–73.
15. Maude S, Tasian S, Vincent T, et al. Targeting JAK2 and mtor in xenograft models of crlf2-overexpressing acute lymphoblastic leukemia (ALL). *Blood*. 2012;58(17):1014.
16. Maude SL, Dolai S, Delgado-Martin C, et al. Efficacy of JAK/STAT pathway inhibition in murine xenograft models of early T-cell precursor (ETP) acute lymphoblastic leukemia. *Blood*. 2015;125(11):1759–67.
17. Springuel L, Hornakova T, Losdyck E, et al. Cooperating JAK1 and JAK3 mutants increase resistance to JAK inhibitors. *Blood*. 2014;124(26):3924–3931.
18. Rambaldi A, Dellacasa CM, Finazzi G, et al. A pilot study of the Histone-Deacetylase inhibitor Givinostat in patients with JAK2V617F positive chronic myeloproliferative neoplasms. *Br. J. Haematol.* 2010;150(4):446–455.
19. Finazzi G, Vannucchi AM, Martinelli V, et al. A phase II study of Givinostat in combination with hydroxycarbamide in patients with polycythaemia vera unresponsive to hydroxycarbamide monotherapy. *Br. J. Haematol.* 2013;161(5):688–694.
20. Guerini V, Barbui V, Spinelli O, et al. The histone deacetylase inhibitor ITF2357 selectively targets cells bearing mutated JAK2(V617F). *Leukemia*. 2008;22(4):740–7.
21. Vojinovic J, Damjanov N, D'Urzo C, et al. Safety and efficacy of an oral histone deacetylase inhibitor in systemic-onset juvenile idiopathic arthritis. *Arthritis Rheum.* 2011;63(5):1452–1458.
22. Pinz S, Unser S, Buob D, et al. Deacetylase inhibitors repress STAT5-mediated transcription by interfering with bromodomain and extra-terminal (BET) protein function. *Nucleic Acids Res*. 2015;43(7):1–22.
23. Pinazza M, Borga C, Agnusdei V, et al. An immediate transcriptional signature associated with response to the histone deacetylase inhibitor Givinostat in T acute lymphoblastic leukemia xenografts. *Cell Death Dis.* 2016;6(1):e2047–12.
24. Amaru Calzada A, Todoerti K, Donadoni L, et al. The HDAC inhibitor Givinostat modulates the hematopoietic transcription factors NFE2 and C-MYB in JAK2 V617F myeloproliferative neoplasm cells. *Exp. Hematol.* 2012;40(8):634–645.
25. Krutzik PO, Nolan GP. Intracellular phospho-protein staining techniques for flow cytometry: monitoring single cell signaling events. *Cytometry. A*. 2003;55(2):61–70.
26. Bendall SC, Simonds EF, Qiu P, et al. Single-cell mass cytometry of differential immune and drug responses across a human hematopoietic continuum. *Science*. 2011;332(6030):687–96.
27. Amir ED, Davis KL, Tadmor MD, et al. viSNE enables visualization of high

dimensional single-cell data and reveals phenotypic heterogeneity of leukemia. *Nat. Biotechnol.* 2013;31(6):545–52.

28. Greco WR, Bravo G, Parsons JC. The search for synergy: a critical review from a response surface perspective. *Pharmacol. Rev.* 1995;47(2):331–385.
29. Bercovich D, Ganmore I, Scott LM, et al. Mutations of JAK2 in acute lymphoblastic leukaemias associated with Down ' s syndrome. *Lancet*. 2008;372(9648):1484–1492.
30. Conter V, Bartram CR, Valsecchi MG, et al. Molecular response to treatment redefines all prognostic factors in children and adolescents with B-cell precursor acute lymphoblastic leukemia: results in 3184 patients of the AIEOP-BFM ALL 2000 study. *Blood*. 2010;115(16):3206–3214.
31. Spijkers-Hagelstein J a P, Pinhanços SS, Schneider P, Pieters R, Stam RW. Chemical genomic screening identifies LY294002 as a modulator of glucocorticoid resistance in MLL-rearranged infant ALL. *Leukemia*. 2014;28(4):761–9.
32. Evrot E, Ebel N, Romanet V, et al. JAK1/2 and pan-deacetylase inhibitor combination therapy yields improved efficacy in preclinical mouse models of JAK2V617F-driven disease. *Clin. Cancer Res.* 2013;19(22):6230–6241.
33. Bjornson ZB, Nolan GP, Fantl WJ. Single-cell mass cytometry for analysis of immune system functional states. *Curr. Opin. Immunol.* 2013;25(4):484–494.
34. Izraeli S, Vora AJ, Zwaan M, Whitlock J. How I treat ALL in Down's syndrome : pathobiology and management. *Blood*. 2014;123(1):35–40.
35. Stankov M V, El Khatib M, Kumar Thakur B, et al. Histone deacetylase inhibitors induce apoptosis in myeloid leukemia by suppressing autophagy. *Leukemia*. 2014;28(3):577–88.

SUPPLEMENTARY METHODS

Patient samples

The analyzed patients were diagnosed and treated according to AIEOP-BFM ALL 2000 and 2009 protocols (NCT00613457 and NCT01117441) from 2005 to 2012.

BCP-ALL diagnosis was made according to standard cytomorphology, cytochemistry and immunophenotypic criteria. Immunophenotyping was carried out using APC conjugated anti-human CD10, FITC-conjugated anti-human CD19 (EBioscience, San Diego, California, USA) and PE-conjugated human CRLF2 (Biolegend, London,UK). Cells were collected on a FACSCanto II™ flow cytometer (BD, Becton Dickinson Biosciences, San Jose, California, USA) and analyses were performed with DIVA™ software. *CRLF2* overexpression and *P2RY8-CRLF2* fusion were analyzed as previously described[1]. Briefly, relative gene expression (indicated as fold change) was quantified by the 2-DDCt method. For *CRLF2* expression, the DDCts were calculated by subtracting to the DCt of each sample the median of the DCt of a published cohort of 464 BCP-ALL patients enrolled in Italy in the AIEOP-BFM ALL2000 study from February 2003 to July 2005[1]. Patients were considered *CRLF2* overexpressed when the relative gene expression was 20 fold-above the median[1]. The DDCts for *P2RY8-CRLF2* expression were calculated by subtracting to the DCt of each sample, the DCt of a selected positive patient external to this cohort[2]. Patients were further characterized for JAK2 alterations by HRM

technique[1] and for other BCP-ALL associated aberrations by Multiplex Ligation-dependent Probe Amplification (MLPA; SALSA MLPA P335-A3 ALL-IKZF1 probemix, MRC-Holland, Amsterdam, The Netherlands) according to the manufacturer's instruction[3,4].

Informed consent to participate in the study was obtained for all patients by parents or legal guardians.

Establishment of xenograft model

Primary leukemia cells from diagnostic bone marrow were injected (tail vain) into sublethally irradiated (125 rad) non-obese diabetic/severe combined immunodeficient mice (NOD.Cg-*Prkdc*^{scid} also termed NOD/SCID, Charles River Laboratories, Wilmington, MA, USA). Samples were injected at a dose of 7-10 x10^6 cell per mouse. Cells from bone marrow of successfully engrafted mice (more than 80% of human blasts in bone marrow) were re-injected (10^6 cells/mouse) to establish secondary or tertiary xenografts for treatment studies. Engraftment was determined by flow cytometric analysis of samples collected by bone marrow aspiration using antibodies against human CD10, CD19 and CRLF2 and, to exclude false positivity, mouse CD45.1 (Percp-Cy5.5-conjugated, EBioscience). For *ex vivo* studies, blasts were isolated from infiltrated bone marrow or spleens of primary and secondary mice (more than 80% BCP-ALL blasts). Cells were cultured on a confluent layer of OP9 stroma and kept in alpha-MEM medium supplemented with 20%

fetal bovine serum, 1% Glutamax (GIBCO® Life Technologies, Carlsbad, California, USA) and 1% penicillin/streptomycin at 37°C in humidified air with 5% CO_2[5]. Human recombinant TSLP (rh-TSLP, Immunotools, Friesoythe¸ Germany) was added in the medium at a concentration of 10 ng/ml.

Phosphoflow analysis of pSTAT5 levels

Cells were assessed for viability >75% by Trypan blu exclusion. After stimulation, cells were immediately fixed with paraformaldehyde (1.5%) and permeabilized with 90% ice-cold methanol.[6] Samples were than stained with Alexa-Fluor 488-conjugated anti-phospho-STAT5 Tyr 694 (BD Bioscience Franklin Lakes, NJ, USA) or isotype matched IgG and surface antigen-directed MoAbs (anti human CD10 and anti-mouse CD45.1). Cells were acquired on FACSCantoII™ flow cytometer. Data were collected and analyzed using DIVA™ software and Cytobank. Positivity threshold for phosphoprotein expression was established using isotype IgG-negative control. For Givinostat and vehicle treated samples, the levels of STAT5 phosphoprotein in response to rh-TSLP stimulus were normalized to the basal STAT5 phosphorylation levels for each cell line and patient for data display. For surface CRLF2 quantification, blasts were first gated for human CD10 expression and MFI values of CRLF2 positive population were evaluated.

Microarray analysis

RNA was extracted using TRIZOL reagent (Invitrogen, Life Technologies, Carlsbad, California, USA). RNA quality was assessed on an Agilent 2100 Bioanalyzer (Agilent Technologies, Waldbronn, Germany). Gene expression analysis was performed using the AffymetrixGeneChip Human Genome U133 Plus 2.0 array and the AffymetrixGeneChip 3' IVT PLUS reagent kit. From each sample 100 ng of RNA were converted in double-stranded cDNA and then labeled cRNA was generated by in vitro transcription. For the fragmentation 15 μg of purified cRNA were used. Hybridization, washing, staining and scanning protocols were performed following manufacturer's instructions. All data analysis was performed in R (http://www.R-project.org/ version 3.0.2) using Bioconductor and R packages. Probe level signals were converted to expression values using the robust multi-array averaging (RMA) algorithm[7]. Differentially expressed genes were identified using Significance Analysis of Microarray algorithm coded in the same R package[8]. In SAM, we estimate the number of false positive predictions (i.e., Fals e Discovery Rate, FDR) with 1000 permutations. To identify genes up- and down-regulated by Givinostat, we selected probe sets with FDR<0.05. Gene Ontology (GO) analysis was performed using DAVID version 6.7 (http://david.abcc.ncifcrf.gov/). Pathway analysis was carried out using Graphite (http://graphiteweb.bio.unipd.it/) that combines topological and multivariate pathway analysis with an efficient system of network

visualizations[9]. Gene set enrichment analysis (GSEA) was done comparing the expression profiles of treated versus control samples using the C2KEGG and C2cgp gene sets within the molecular signatures databases (MSigDB) collection[10]. The signal to noise metric and the gene set permutation were used to identify statistical enrichment of the selected gene sets in Givinostat versus DMSO treated cells.

RQ-PCR

Optimal primers and probes were selected using the Roche ProbeFinder software (https://www.roche-appliedscience.com/sis/rtpcr/upl). Genes analyzed included: *STAT5A*, *JAK2*, *IL7Rα*, *cMYC*, *BCL2L1*, *PTPN1* and the housekeeping *GUS* gene, tested as internal control. Each cDNA sample was tested in triplicate (Ct range between replicates <1.0). Differences in gene expression before and after treatment were statistically evaluated using the student t-test.

Combination assays and evaluation of synergy

The effect of each drug was expressed as the ratio of drug/vehicle treated sample. For each point, synergy or additivity was calculated using the Bliss independence model defined by the equation: $E_{xy}=E_x+E_y-(E_x x E_y)$, where ($E_{xy}$) is the additive effect of drugs x and y as predicted by their observed individual effects (E_x and E_y). Therefore E_{xy} represents the Expected value (EV) in case of additivity of the compounds, while the

Actual value (AV) indicates the real observed effect of the combination. Since in this issue the effect was evaluated as the reduction of proliferating cells/live cells, we considered both drugs additive when AV=EV, synergic: AV>EV and antagonists when AV<EV.

SUPPLEMENTARY RESULTS

Establishment of patient-derived ALL-xenografts

Diagnostic specimens from 5 patients were intravenously injected into immunodeficient mice and engraftment was determined measuring the percentage of human CD10+/CD19+/CRLF2+ blasts in the bone marrow by flow cytometry (See methods for full details). These 5 samples harbored the *CRLF2* rearrangement *P2RY8-CRLF2* fusion (*CRLF2r*) and 1 out of 5 harbored a *JAK2* mutation (*JAKm*) as listed in Table 1. The mutation consisted of a not formerly described insertion (L681-I682 insGL) in exon 16. All 5 samples successfully engrafted in NOD/SCID mice. The animals were sacrificed when they reached 80% of human blasts in bone marrow, and the recovered cells were then called primografts and used for *ex-vivo* analyses and for further serial transplantations.

Microarray analysis

As expected of an HDACi, Givinostat induced a drastic modification of the transcriptome resulting in distinct clustering between treated and untreated samples by unsupervised analysis (Figure 3A). Using SAM

(Significance Analysis of Microarrays) analysis, we identified 1331 unique genes (2068 probe sets) differentially expressed between control and treated samples with a FDR<0.05. In particular in treated samples, 541 were upregulated and 790 genes were downregulated when compared to the untreated controls as shown in the supervised analysis (Supplementary Figure 4A). According to Gene Ontology (GO) analysis, the 1331 genes were grouped into 6 main functional categories: phosphorylation, alternative splicing, SH2 domain (i.e. the protein phospho-tyrosine binding domain), actin-binding, ATP and cytoplasm (p-value<0.05and FDR< 0.05). Furthermore, gene set enrichment analysis (GSEA) demonstrated that Givinostat treated specimens were enriched for epigenetically silenced cancer genes, similarly upregulated with treatment with other HDAC inhibitors like 5-aza-2'-deoxycytidine (Aza-dC) and/or trichostatin A (TSA), supporting the action of the compound as an epigenetic modifier (Supplementary Figure 4B).

SUPPLEMENTARY REFERNCES

1. Palmi C, Vendramini E, Silvestri D, et al. Poor prognosis for P2RY8-CRLF2 fusion but not for CRLF2 over-expression in children with intermediate risk B-cell precursor acute lymphoblastic leukemia. *Leukemia*. 2012;26(10):2245-2253.

2. Bugarin C, Sarno J, Palmi C, et al. Fine Tuning of Surface CRLF2 Expression and Its Associated Signaling Profile in Childhood B Cell Precursor Acute Lymphoblastic Leukemia. *Haematologica*. 2015;100(6):e229-232.

3. Palmi C, Valsecchi MG, Longinotti G, et al. What is the relevance of Ikaros gene deletions as a prognostic marker in pediatric Philadelphia-negative

B-cell precursor acute lymphoblastic leukemia? *Haematologica*. 2013;98(8):1226-1231.

4. Palmi C, Lana T, Silvestri D, et al. Impact of IKZF1 deletions on IKZF1 expression and outcome in Philadelphia chromosome negative childhood BCP-ALL. Reply to "incidence and biological significance of IKZF1/Ikaros gene deletions in pediatric Philadelphia chromosome negative and Philadelphia chromosome positive B-cell precursor acute lymphoblastic leukemia". *Haematologica*. 2013;98(12):e164-165.

5. Cazzaniga V, Bugarin C, Bardini M, et al. LCK over-expression drives STAT5 oncogenic signaling in PAX5 translocated BCP-ALL patients. *Oncotarget*. 2015;6(3):1569-1581.

6. Kotecha N, Flores NJ, Irish JM, et al. Single-cell profiling identifies aberrant STAT5 activation in myeloid malignancies with specific clinical and biologic correlates. *Cancer Cell*. 2008;14(4):335-343.

7. Irizarry RA, Hobbs B, Collin F, et al. Exploration, normalization, and summaries of high density oligonucleotide array probe level data. *Biostatistics*. 2003;4(2):249-264.

8. Tusher VG, Tibshirani R, Chu G. Significance analysis of microarrays applied to the ionizing radiation response. *Proc Natl Acad Sci U S A*. 2001;98(9):5116-5121.

9. Sales G, Calura E, Cavalieri D, Romualdi C. graphite - a Bioconductor package to convert pathway topology to gene network. *BMC Bioinformatics*. 2012;13:20.

10. Subramanian A, Tamayo P, Mootha VK, et al. Gene set enrichment analysis: a knowledge-based approach for interpreting genome-wide expression profiles. *Proc Natl Acad Sci U S A*. 2005;102(43):15545-15550.

Supplementary Table 1

Complete panel of metal-conjugated antibodies used for CyTOF analyses.

Marker	Clustering	Location	Metal	Mass	Rationale
CD235	✓	S	In	113	Lineage
CD61	✓	S	In	113	Lineage
CD45	✓	S	In	115	B cell maturity
cPARP		I	La	139	Apoptosis
CD19	✓	S	Nd	142	B cell maturity
CD22		S	Nd	143	B cell maturity
CD79b		S	Nd	146	B cell maturity
CD20	✓	S	Sm	147	B cell maturity
CD34	✓	S	Nd	148	B cell maturity
CD179a		I	Sm	149	B cell maturity
Ki67		I	Sm	152	Cell fate
IgMi	✓	I	Eu	153	B cell maturity
Kappa, Lambda		S	Sm	154	B cell maturity
CD10	✓	S	Gd	156	B cell maturity
CD132		S	Gd	157	B cell maturity
CD179b		I	Gd	158	B cell maturity
CD24	✓	S	Gd	160	B cell maturity
TSLPR	✓	S	Dy	161	B cell maturity
CD127	✓	S	Dy	162	B cell maturity
CD43	✓	S	Er	167	B cell maturity
CD38	✓	S	Er	168	B cell maturity
CD58		S	Tm	169	B cell maturity
CD3	✓	S	Er	170	Lineage
CD16	✓	S	Yb	171	Lineage
CD33	✓	S	Yb	171	Lineage
HLA-DR		S	Yb	174	B cell maturity
IgMs	✓	S	Lu	175	B cell maturity
pCREB		I	Yb	176	p38 signaling
DNA			Ir	191/193	Detect cells
Cisplatin Viability			Pt	195	Apoptosis

Supplementary table 2

Numerical representation of the effect of Givinostat on the treated samples after CyTOF analysis

Number of events collected		Total live cells	CRLF2 high	CD45 high
Pt#2	Vehicle	22043	3663	8441
	Givinostat	14681	2593	1775
	Givinostat/vehicle	0.6660	0.7079	0.2103
Pt#3	Vehicle	22510	1552	9500
	Givinostat	16783	1819	1329
	Givinostat/vehicle	0.7456	1.1720	0.1399
Pt#4	Vehicle	31914	542	27574
	Givinostat	25050	590	11126
	Givinostat/vehicle	0.7849	1.0886	0.4035
Pt#5	Vehicle	27184	1304	3772
	Givinostat	17423	979	758
	Givinostat/vehicle	0.6409	0.7508	0.2010

Supplementary Table 3

Top 50 pathway differently modulated by Givinostat FDR<0.05

serial	Pathway	Pathway Genes	Mapped Genes
1	Natural killer cell mediated cytotoxicity	137	16
2	Osteoclast differentiation	123	16
3	Vascular smooth muscle contraction	113	16
4	Apoptosis	86	15
5	B cell receptor signaling pathway	73	15
6	Insulin signaling pathway	137	14
7	Oocyte meiosis	108	14
8	Cell cycle	124	13
9	Fc gamma R-mediated phagocytosis	95	13
10	HIF-1 signaling pathway	109	13
11	Hepatitis B	136	12
12	Leukocyte transendothelial migration	85	12
13	p53 signaling pathway	68	12
14	Circadian entrainment	96	11
15	Jak-STAT signaling pathway	99	11
16	Neurotrophin signaling pathway	116	11
17	Salivary secretion	48	11
18	Alzheimer's disease	49	10
19	Cholinergic synapse	95	10
20	Chronic myeloid leukemia	73	10
21	Dopaminergic synapse	124	10
22	Gap junction	89	10
23	Glioma	65	10
24	GnRH signaling pathway	85	10
25	Melanogenesis	101	10
26	Phosphatidylinositol signaling system	76	10
27	T cell receptor signaling pathway	98	10
28	Tight junction	118	10
29	Acute myeloid leukemia	57	9
30	Fc epsilon RI signaling pathway	62	9
31	Glutamatergic synapse	92	9
32	Glycerophospholipid metabolism	84	9
33	VEGF signaling pathway	67	9
34	Amoebiasis	46	8
35	Axon guidance	118	8
36	Chagas disease (American trypanosomiasis)	89	8
37	Epstein-Barr virus infection	83	8
38	ErbB signaling pathway	88	8
39	Gastric acid secretion	57	8
40	Long-term potentiation	70	8
41	NF-kappa B signaling pathway	80	8
42	Pancreatic cancer	69	8
43	PPAR signaling pathway	64	8
44	Progesterone-mediated oocyte maturation	80	8
45	Prostate cancer	87	8
46	Renal cell carcinoma	60	8
47	Small cell lung cancer	82	8
48	Wnt signaling pathway	144	8
49	Amphetamine addiction	64	7
50	Glycolysis / Gluconeogenesis	65	7

Supplementary Table 4

MFI of CRLF2 surface expression before and after treatment with Givinostat

median CRLF2	vehicle	Givinostat	F.C.	DS vehicle	DS Givinostat	paired t test
PT#1	6490.9	2013.3	3.1	2087.5	865.2	0.023
PT#2	4317.0	779.0	5.5			
PT#3	5415.6	2234.4	2.4			
PT#5	1629.0	512.0	3.2			

SUPPLEMENTARY FIGURES

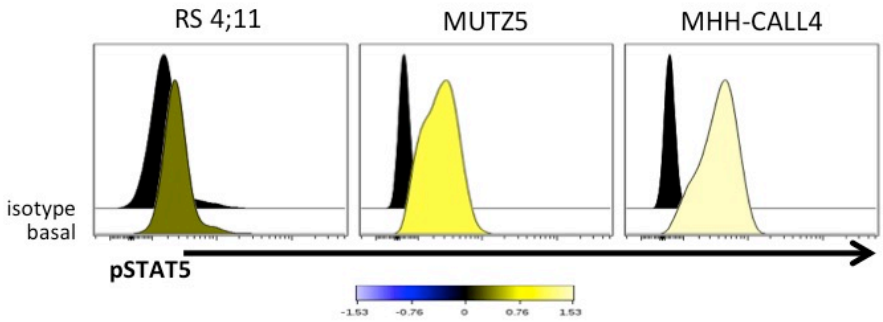

Supplementary Figure 1: Representation of basal STAT5 phosphorylation in different cell lines. RS4;11 (JAK2 wt) and CRLF2 rearranged/JAK mutated cell lines, MHH-CALL4 and MUTZ5 were analyzed. Data were represented as arch-sin ratio with first row (isotype). Due to JAK2 mutation the basal level of pSTAT5 is higher in MHH-CALL4 and MUTZ5 than RS4;11. The colorimetric depiction from blue to yellow reflects the intensity of the signal (blue low and yellow high).

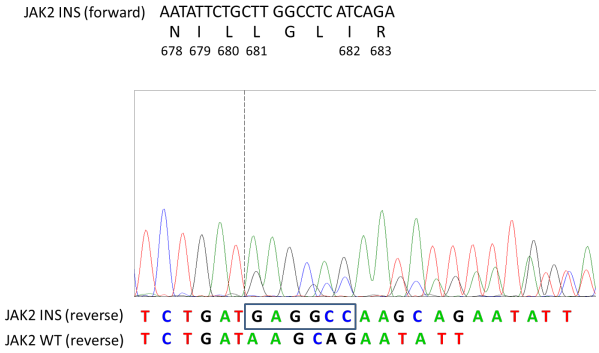

Supplementary Figure 2: The insertion of 6 nucleotides in frame in JAK2 sequence originate 2 new aminoacids (Glycine and Leucine) between Leucine 681 and Isoleucine 682. The insertion is in heterozygosis.

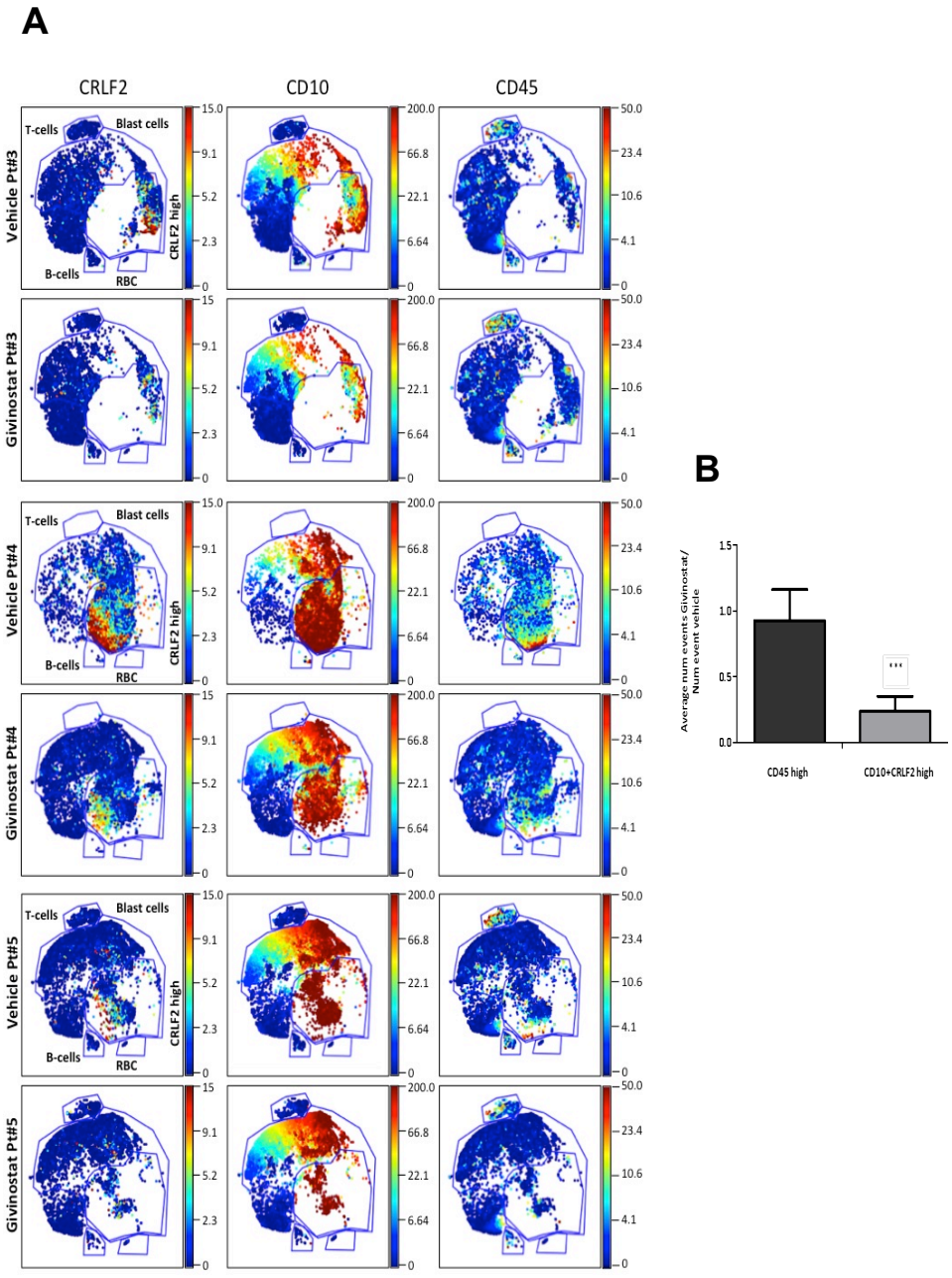
A
CRLF2
CD10
CD45
Vehicle Pt#3
Givinostat Pt#3
Vehicle Pt#4
Givinostat Pt#4
Vehicle Pt#5
Givinostat Pt#5
T-cells
Blast cells
B-cells
RBC
CRLF2 high
15.0
9.1
5.2
2.3
0
200.0
66.8
22.1
6.64
50.0
23.4
10.6
4.1
B
Average num events Givinostat/ Num event vehicle
1.5
1.0
0.5
0.0
***
CD45 high
CD10+CRLF2 high

Supplementary Figure 3: (A) Application of viSNE to leukemic bone marrow sample from patients 3,4,5 before and after treatment with Givinostat (0.2 µM for 24 hours). Each point in the viSNE map represents an individual cell and colorimetric depiction for each plot indicates the different level of expression of the considered marker in the cell population analyzed. Blue dots represents blasts negative for that antigen while positivity is indicated by a colorimetric progressive range from yellow to red. After treatment with Givinostat the number of dots belonging to high expressing CD10+CRLF2 high blasts diminished whereas, normal B cells, T cells and red blood cells (CD45 high) remained unaffected. (B): Histogram representing the modulation of different populations by Givinostat. Y axis: ratio between the number of Givinostat/vehicle treated cells; X axis: markers analyzed. Statistic are calculated using one sample T test.

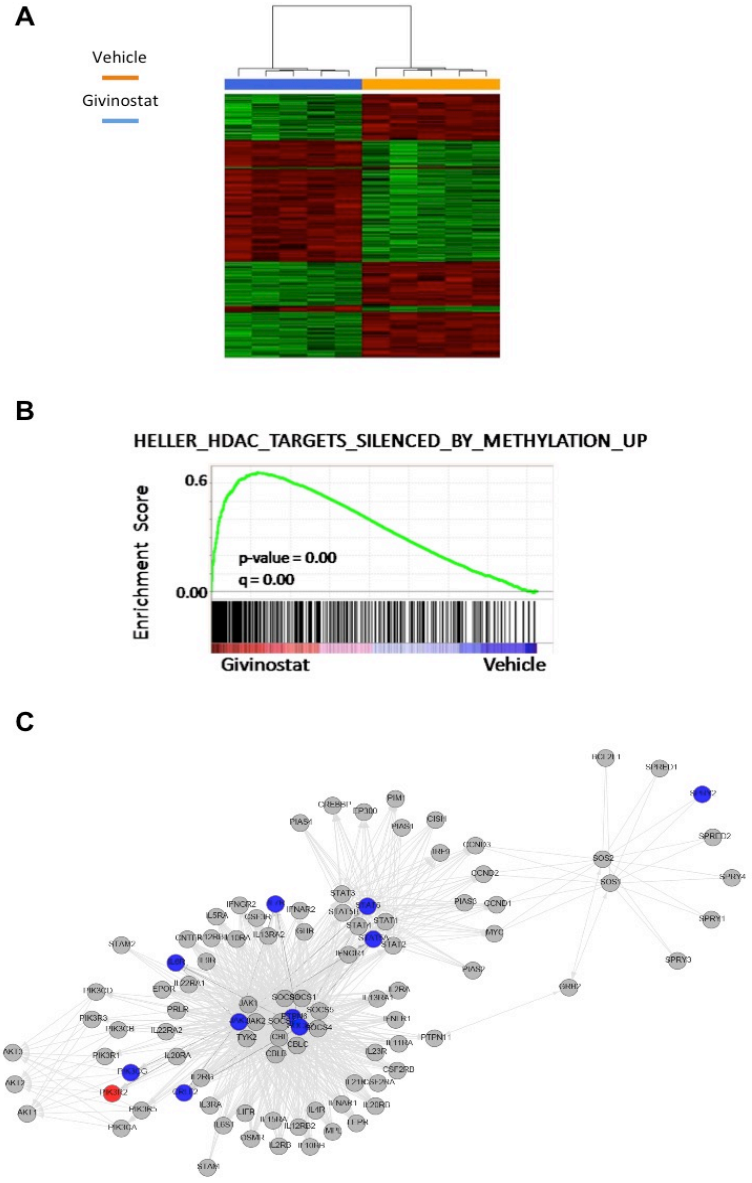

Supplementary Figure 4: (A) Unsupervised hierarchical clustering analysis using the 2068 probe sets differentially regulated with FDR< 0.05 according to SAM between Givinostat treated (blue) versus vehicle treated (orange) samples.

Down- and up-regulated genes are shown in the heat map in green and red, respectively. (B) GSEA plot showing the positive enrichment in the Givinostat treated samples for HDAC target genes (positive Normalized Enrichment Score, NES= 2.7727435). (C) Graphite network showing the genes enclosed in the KEGG JAK-STAT signaling pathway; genes down-regulated by Givinostat and included in the differentially regulated genes according to SAM are shown in blue. Genes up-regulated are shown in red.

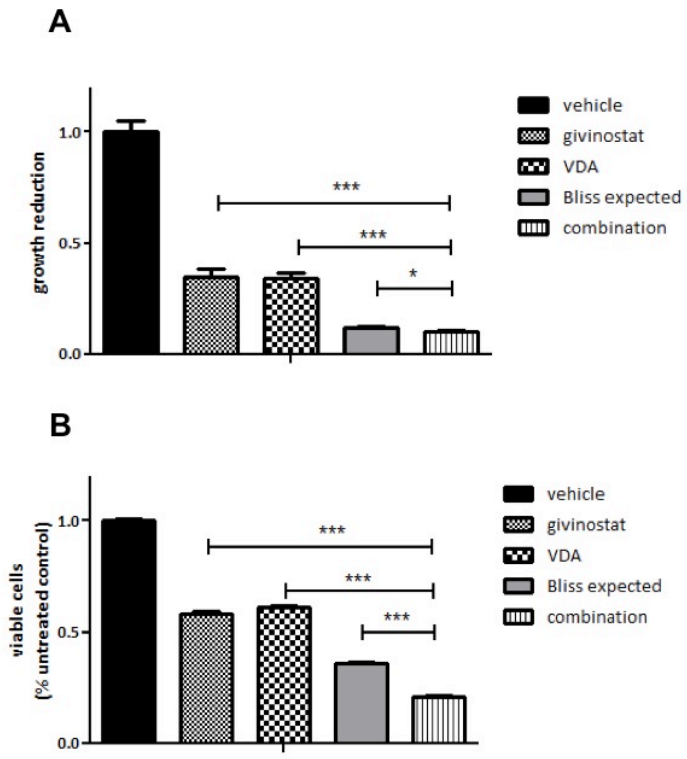

Supplementary Figure 5: Proliferation (A) and Annexin V/Sytox assay (D) performed on MUTZ5 cells in presence of Givinostat (0.1 µM) and VDA (Asparaginase 0.023 ug/ml; Dexametasone 0.001 ug/ml; Vincristine 0.0001 ug/ml) alone and in combination. The expected effect, calculated by Bliss formula, is represented by grey.

Chapter 5

Conclusions and future perspectives

In the present study we aimed to dissect the cell signaling and the functional relevance of deregulated pathways in the pathogenesis of childhood BCP-ALL.

We focused our interest on a specific subset of high-risk patients, having rearrangements in the *CRLF2* gene, which represents 7-10% of pediatric BCP-ALL[1,2], 50% of Ph-like ALL[3] and 50% of DS-ALL[4]. To date, it is known that *CRLF2* alterations, together with other Ph-like-related kinase alterations, are associated with a greater risk of relapse and inferior outcome in these ALL patients[5].

First, we herein demostrated the feasibility and reproducibility of a standardized flow cytometry-based protocol that allows the diagnostic screening of the *CRLF2* rearranged ALL patients that, in a next future, could be of interest for identification of patients that may benefit of targeted approaches. Since the *CRLF2* alterations are strictly correlated with a surface overexpression of the TSLPR subunit[6], we figure out if the TSLPR itself could represent a suitable marker easily detectable by FCM.

In a multi-centers study we analyzed a total of 421 consecutive diagnostic bone marrow samples from BCP-ALL children enrolled in six centers partecipating to the AIEOP-BFM-ALL-2009 trial. We were able to demonstrate that by applying the same analytical procedure, the detection of the TSLPR overexpressed patients could be easily performed by FCM at diagnosis of the disease.

Then, we investigated the concordance between the TSLPR detection by

FCM and the *CRLF2* transcript levels assessed as previuosly described[7] by real-time PCR, demonstrating complete concordance in the identification of true TSLPR-positive cases.

Finally, we concluded this first part of our research by examinating the functional readout of the *CRLF2* rearrangements in the context of intracellular signal networks involved in the leukemogenic process and, consistent with previuos published data[6], we detected a TSLP-induced activation of pSTAT5, prpS6, pAKT and p4EBP1 in the TSLPR positive patients. Interestingly, by a fine tune analysis we identify for the first time a subset of - otherwise undedetcbale - patients with a low TSLPR (under the level of standard FCM threshold) which displayed a moderate but significant activation of pSTAT5 and prpS6 different from that observed in the TSLPR negative patients.

We next further investigated the complexity of TSLPR-related signaling aiming at the identification of targetable molecules potentially useful in future clinical approaches.

For this purpose we applied to a cohort of 12 BCP-ALL samples (6 *CRLF2r* and 6 *CRLF2wt*) a new high dimensional single cell techonology called mass cytometry (or CyTOF). Taking advantage of the elevated numbers of parameters simultaneously measurable by CyTOF at single cell level, we demonstrated that in addition to the TSLP-induced pSTAT5 and prpS6 activation, the *CRLF2r* patients are characterized also by an activation of

pERK and pCREB pathways, suggesting cross-talk within JAK/STAT, PI3K/mTOR and RAS/MEK signaling networks.

Futhermore, single cell analysis allowed us to demostrate, for the first time, that the TSLP-induced phosphoproteins were co-expressed in a specific cell subset that exhibited also higher levels of Ki67, suggesting that the co-activation of these pathways occurs in dividing blast cells.

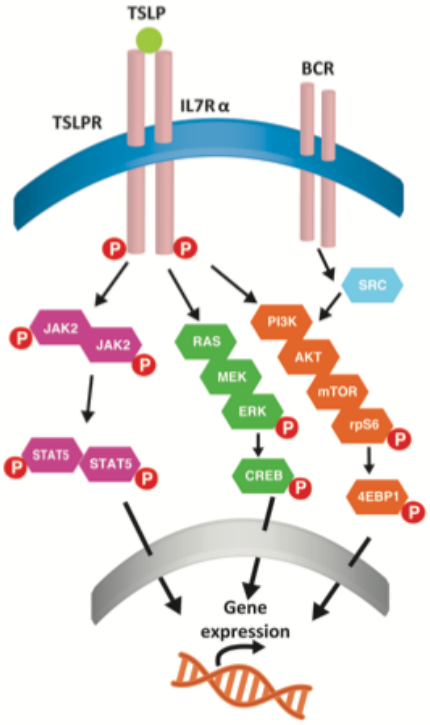

Figure 1. Schematic representation of TSLP-induced signaling pathway in *CRLF2r* BCP-ALLs

In the last years several studies have attempted the possibility to target diretcly the TSLPR in *CRLF2r* BCP-ALL by using different approaches, such as T cells engineered with a chimeric antigen receptor (CAR)[8], monoclonal antibodies[9,10] or biodegradable nanoparticles conjugated with antibody[11]. In our study we decided to test two anti-TSLPR mAbs, and compare their activity with those of the kinase inhibitors (KIs), Ruxolitinib, Dasatinib and NVP-BEZ235, which are currently already tested in other B-ALL subsets. CyTOF analysis revelead a strong inhibitory activity of the TSLPR-related signaling after the treatment with one of the two tested mAbs (A10 clone) which was even more effective than either Ruxolinitib or NVP-BEZ235. However, the most successful *in vitro* treatment, able to completely switch-off all the intracellular signals, was Dasatinib, an agent currently used in the treatment of Ph-positive ALL subset[12]. Interestingly both Dasatinib and A10 mAb were able also to blunt the prpS6 signaling from a particular cell subset unable to activate pSTAT5 under TSLP stimulation.

We next asked if the MRD chemo-resistant cells were still TSLPR positive and how they signal through the TSLP pathway; for this purpose we analyzed 3 additional *CRLF2r* patients at different time-points of treatment (day 8 and day 15 of remission-induction chemotherapy). We herein demostrated the persistence of the TSLPR expression in the MRD cells, which were characterized by basal activated prpS6 and pCREB as well as TSLP-induced pSTAT5 expression. Of note, A10 mAb and

Ruxolitinib were both able to inhibit cell signaling also in this chemo-resistant cells.

Upon this further demostration of the complexity of the network correlated with TSLPR (persistent in the MRD cells), we speculated that a combined rather than a single agent treatment might be more effective in eradicating these leukemia cells.

Therefore we tested all the above agents, either alone or in combination, on a IL3-independent/TSLP-dependent BaF3 CRLF2/IL7Rα expressing cell line, demostrating a strong synergic activity of Dasatinib with either Ruxolitinib or A10 mAb in inducing a pro-apoptotic effect. NVP-BEZ235 also showed a significant synergic activity in combination with either Ruxolitinib or A10 mAb, although this activity was less cytotoxic as compared to the Dasatinib-based combinations.

To test further possible therapeutic approaches, as demonstrated by Savino et al. (paper under revision), at the same time, we also investigated the efficacy of an epigenetic drug, the HDAC inhibitor Givinostat, since its capability to regulate the expressions of genes involved in the JAK/STAT pathway is already proved in myeloproliferative neoplasms (MPN) bearing *JAK2 V617F* mutation[13,14].

Overall, in this third part of the research we demonstrated the activity of Givinostat on STAT5 signaling in *CRLF2r* cells regardless of *JAK2* mutations. Interestingly, the Givinostat was able to downmodulate also the *CRLF2* gene itself and consequently the surface expression of the

TSLPR, thus inhibiting the TSLP-dependent pathway. Importantly, several additional pathways, driving proliferation and survival such as B-cell receptor signaling, were down-modulated by this drug, indicating a broader effect of Givinostat on blasts apoptosis inducing a global change in tumor cell epigenome. To test the functional read out of these epigentic changes we demostrated the efficacy and specificity of Givinostat in inhibiting proliferation and inducing cell death both in *CRLF2r* cell lines and patient derived xenografts (PDXs). Notably Givinostat was efficiently able to induce cell death at really low dosages and, from a CyTOF analysis, we demonstrated that its activity was specific for the leukemic cells, while preserving the normal hematopoietic counterparts. Moreover, we demonstrated the efficacy of Givinostat in combination with other chemotherapeutics on cell lines and primary blasts from *CRLF2r* patients. Finally we also tested this drug in a preclinical *in vivo* model of *CRLF2r* leukemia where Givinostat strongly reduced the engraftment of leukemic blasts in the bone marrow of treated mice.

Overall, our research provided novelties in the following contexts of *CRLF2r* BCP-ALL biology and management :

- FCM-based diagnostic screening;
- Single cell dissection and in vitro blockade of TSLP-dependent pathways by either KIs or mAbs at diagnosis and at early time-point of induction therapy;

- Epigenetic targeting approach.

In the near future, we would like to further extend the preliminar evidences regarding MRD *CRLF2r* cells and to validate the efficacy of promising KIs and anti-TSLPR mAb combinations in a PDX-*CRLF2r* model *in vivo* (already established in our laboratory).

In conclusion our data increase the current knowledge on the high-risk subgroup of BCP-ALL patients bearing *CRLF2* rearrangements, bringing up new possible therapeutic strategies that, together with the current chemotherpy regimens, could represent promising approaches to overcome the traetment failure frequently observed in these patients.

REFERENCES

1. Mullighan CG, Collins-Underwood JR, Phillips L a a, et al. Rearrangement of CRLF2 in B-progenitor- and Down syndrome-associated acute lymphoblastic leukemia. *Nat. Genet.* 2009;41(11):1243–6.
2. Roll JD, Reuther GW. CRLF2 and JAK2 in B-progenitor acute lymphoblastic leukemia: A novel association in oncogenesis. *Cancer Res.* 2010;70(19):7347–7352.
3. Roberts KG, Li Y, Payne-Turner D, et al. Targetable Kinase-Activating Lesions in Ph-like Acute Lymphoblastic Leukemia. *N. Engl. J. Med.* 2014;371(11):1005–1015.
4. Hertzberg L, Vendramini E, Ganmore I, et al. Down syndrome acute lymphoblastic leukemia, a highly heterogeneous disease in which aberrant expression of CRLF2 is associated with mutated JAK2: A report from the International BFM Study Group. *Blood*. 2010;115(5):1006–1017.
5. Loh ML, Zhang J, Harvey RC, et al. Tyrosine kinome sequencing of pediatric acute lymphoblastic leukemia : a report from the Children ' s Oncology Group TARGET Project. 2015;121(3):485–489.
6. Tasian SK, Doral MY, Borowitz MJ, et al. Aberrant STAT5 and PI3K/mTOR

pathway signaling occurs in human CRLF2-rearranged B-precursor acute lymphoblastic leukemia. *Blood*. 2012;120(4):833–842.

7. Palmi C, Vendramini E, Silvestri D, et al. Poor prognosis for P2RY8-CRLF2 fusion but not for CRLF2 over-expression in children with intermediate risk B-cell precursor acute lymphoblastic leukemia. *Leukemia*. 2012;26(10):2245–53.
8. Qin H, Cho M, Haso W, et al. Eradication of B-ALL using chimeric antigen receptor-expressing T cells targeting the TSLPR oncoprotein. *Blood*. 2015;126(5):629–639.
9. Borowski A, Vetter T, Kuepper M, et al. Expression analysis and specific blockade of the receptor for human thymic stromal lymphopoietin (TSLP) by novel antibodies to the human TSLPRα receptor chain. *Cytokine*. 2013;61(2):546–555.
10. Vetter T, Borowski A, Wohlmann A, et al. Blockade of thymic stromal lymphopoietin (TSLP) receptor inhibits TSLP-driven proliferation and signalling in lymphoblasts from a subset of B-precursor ALL patients. *Leuk. Res.* 2016;40:38–43.
11. Raghunathan R, Mahesula S, Kancharla K, et al. Anti-CRLF2 antibody-armored biodegradable nanoparticles for childhood B-ALL. *Part. Part. Syst. Charact.* 2013;30(4):355–364.
12. Gordon MS. M. S. Gordon, MD Dasatinib in Imatinib-Resistant Philadelphia Chromosome–Positive Leu- kemias. 2006;144–145.
13. Rambaldi A, Dellacasa CM, Finazzi G, et al. A pilot study of the Histone-Deacetylase inhibitor Givinostat in patients with JAK2V617F positive chronic myeloproliferative neoplasms. *Br. J. Haematol.* 2010;150(4):446–455.
14. Finazzi G, Vannucchi A, Martinelli V, et al. A phase II study of the HDAC inhibitor givinostat in combination with hydroxyurea in patients with polycythemia vera resistant to hydroxyurea monotherapy. *Br. J. Haematol.* 2013;161(5):688–94.

Appendix

Manuscript not included in the thesis

Single-Cell Developmental Classification of B-Cell Precursor Acute Lymphoblastic Leukemia at Diagnosis Reveals Developmentally Dependent Predictors of Relapse

Manuscript submitted

Zinaida Good,[1-4,*] **Jolanda Sarno**,[9,*] Astraea Jager,[1-2] Nikolay Samusik,[1-2] Nima Agaheepour,[1-2] Erin F. Simonds,[1-2,10] Leah White,[5] Norman J. Lacayo,[5] Wendy J. Fantl,[6] Giuseppe Gaipa,[9] Andrea Biondi,[9] Robert Tibshirani,[7-8] Sean Bendall,[3] Garry P. Nolan[1-2,§] and Kara L. Davis[1-2,5,§]

[1]Baxter Laboratory in Stem Cell Biology, [2]Department of Microbiology and Immunology, [3]Department of Pathology, [4]PhD Program in Immunology, [5]Department of Pediatrics, Division of Hematology/Oncology, [6]Departments of Obstetrics and Gynecology, [7]Departments of Statistics, [8]Department of Health Research and Policy, Stanford University, Stanford, CA 94305, USA. [9]M. Tettamanti Research Center, Pediatric Clinic University of Milano Bicocca, Monza, Italy. [10]Current address: Department of Neurology and Helen Diller Family Comprehensive Cancer Center, University of California San Francisco, San Francisco, CA 94158, USA.
*Co-first authors; [§]Co-senior authors

ABSTRACT

Single-cell studies in primary cancer samples hold promise to unravel intratumoral heterogeneity and uncover cell populations responsible for poor clinical outcomes. Yet, organizing this heterogeneity for true patient translation remains a significant challenge. B-cell precursor acute lymphoblastic leukemia (BCP-ALL) is characterized by the malignant expansion of B-lymphocyte progenitors in the bone marrow and relapse remains the leading cause of cancer-related mortality in children. We reasoned that single-cell study of BCP-ALL cells from *diagnostic* samples

would reveal hidden cell states associated with relapse and expose targets to augment therapy for patients at risk. Using single-cell mass cytometry, we measured expression of 40 proteins critical for B lymphopoiesis in 60 primary diagnostic BCP-ALL samples. To identify common cells states across diverse patients we built a single-cell developmental classifier to assign each leukemia cell to its closest match in normal B lymphopoiesis by defining an 11-protein cell-state signature for 15 developmental populations of B9 lymphocytes within the normal human marrow. We found that 97% of samples were enriched in populations spanning the pre-pro-B to pre-BI developmental transition, regardless of genetic background. Using a machine learning approach, we identified just 8 cellular features in these expanded populations at diagnosis sufficient to predict which patients would go on to relapse with 82% accuracy. This model, the Developmentally Dependent Predictor of Relapse (DDPR) identified presence of cells at the pro-BII to pre-BI transition characterized by high CD22 expression, basal activation of STAT5 and mTOR pathways, and lack of response to pre-B-cell receptor engagement to portend relapse. DDPR proved superior to the current relapse risk predictors (53-64% accuracy), performed well in an independent validation cohort (90% accuracy), and can work synergistically with existing risk predictors. Analysis of matched diagnosis-relapse pairs showed that DDPR features *pre-exist* at diagnosis and persist at relapse arguing that these cells are present at diagnosis

but resistant to therapy, providing rational targets for upfront treatment in BCP-ALL patients identified with DDPR. This study is the first to demonstrate the predictive value of single-cell 'omics' for patient stratification in a translational setting and is generally applicable to unravel the heterogeneity intrinsic to primary human cancers.